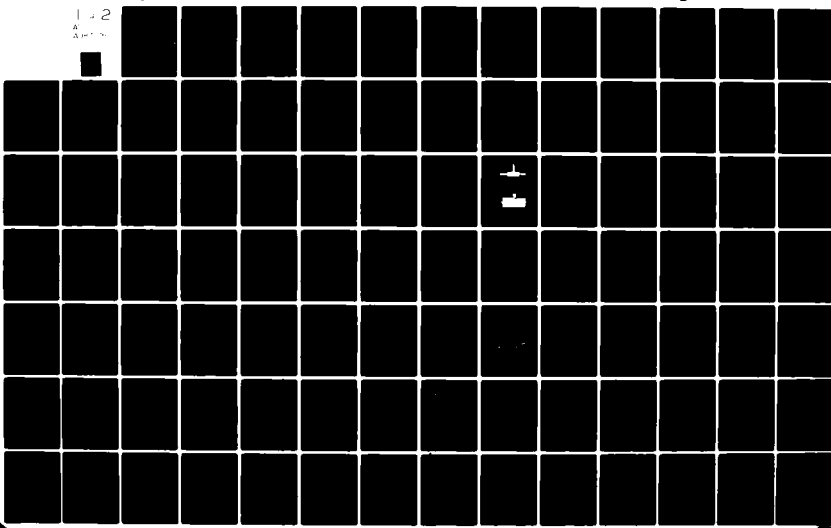
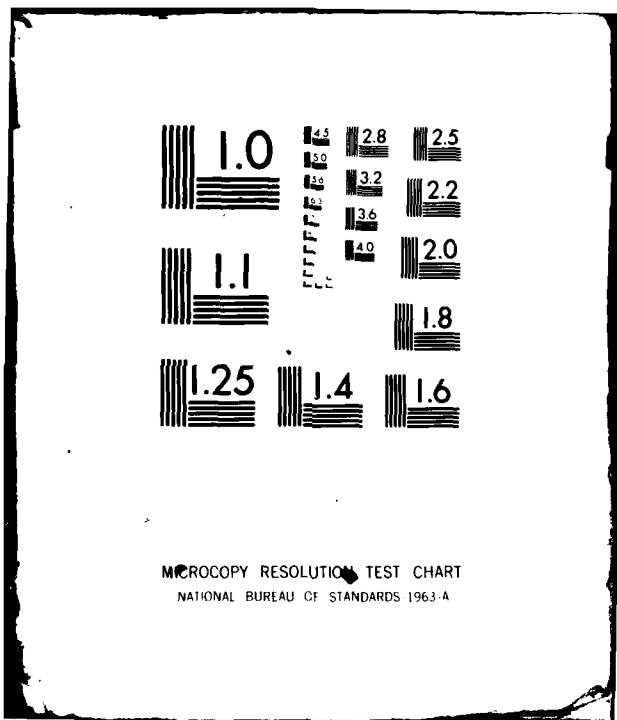


AD-A087 675

OFFICE NATIONAL D'EUDES ET DE RECHERCHES AEROSPATIALE--ETC F/G 22/2
SATELLITE SPACECRAFT CHARGING CONTROL MATERIALS. (U)
APR 80 B BENAISSE, L LEVY, A PAILOUS AFOSR-78-3704
UNCLASSIFIED ONERA/CERT/DERTS-CR-AF-05 AFWAL-TR-80-4029 NL

1 2
A
A
A





ADA 087675

AFWAL-TR-80-4029

LEVEL II

2
F1

SATELLITE SPACECRAFT CHARGING CONTROL MATERIALS

ONERA-CERT
DEPARTMENT OF STUDIES AND RESEARCH IN SPACE TECHNOLOGY
2 AVENUE EDOUARD BELIN, B.P. NO. 4025
31055 TOULOUSE CEDEC
FRANCE

APRIL 1980

STANDARD FORM
DTIC
ELECTED
AUG 7 1980
S C D

TECHNICAL REPORT AFWAL-TR-80-4029
Interim Report for period 1 September 1978 – 30 April 1979

Approved for public release; distribution unlimited.

FILE COPY
DDC

MATERIALS LABORATORY
AIR FORCE WRIGHT AERONAUTICAL LABORATORIES
AIR FORCE SYSTEMS COMMAND
WRIGHT-PATTERSON AIR FORCE BASE, OHIO 45433

80 7 31 022

NOTICE

When Government drawings, specifications, or other data are used for any purpose other than in connection with a definitely related Government procurement operation, the United States Government thereby incurs no responsibility nor any obligation whatsoever; and the fact that the government may have formulated, furnished, or in any way supplied the said drawings, specifications, or other data, is not to be regarded by implication or otherwise as in any manner licensing the holder or any other person or corporation, or conveying any rights or permission to manufacture, use, or sell any patented invention that may in any way be related thereto.

This report has been reviewed by the Office of Public Affairs (ASD/PA) and is releasable to the National Technical Information Service (NTIS). At NTIS, it will be available to the general public, including foreign nations.

This technical report has been reviewed and is approved for publication.

W. L. Lehn

W. L. Lehn
Project Engineer

W.C. Kessler

W. C. Kessler, Chief
Coatings & Thermal Protection
Materials Branch

FOR THE COMMANDER

P. D. Cherry

P. D. Cherry, Chief
Nonmetallic Materials Division

"If your address has changed, if you wish to be removed from our mailing list, or if the addressee is no longer employed by your organization please notify AFVAL/MLBE, W-PAFB, OH 45433 to help us maintain a current mailing list."

Copies of this report should not be returned unless return is required by security considerations, contractual obligations, or notice on a specific document.

SECURITY CLASSIFICATION OF THIS PAGE (When Data Entered)

17 REPORT DOCUMENTATION PAGE		READ INSTRUCTIONS BEFORE COMPLETING FORM
1. REPORT NUMBER AFVAL-TR-80-4629	2. GOVT ACCESSION NO.	3. RECIPIENT'S CATALOG NUMBER
4. TITLE (and Subtitle) Satellite Spacecraft Charging Control Materials		5. TYPE OF REPORT & PERIOD COVERED Interim Scientific Report 78 Sep 01 - 79 Apr 30
6. AUTHOR(s) B. Benaissa/L. Levy/A. Paillous/D. Sarrail		7. PERFORMING ORG. REPORT NUMBER ONERA/CERT/DERTS CR-AR-05 8. CONTRACT OR GRANT NUMBER(s) AFOSR-78-3704 Rev
9. PERFORMING ORGANIZATION NAME AND ADDRESS ONERA-CERT; Dept of Studies & Research in Space Tech; 2 Ave Edouard Belin, B.P.No. 4025;31055 Toulouse Cedex; France		10. PROGRAM ELEMENT, PROJECT, TASK AREA & WORK UNIT NUMBERS PE - 61101F Proj Tsk - 2422/01
11. CONTROLLING OFFICE NAME AND ADDRESS Air Force Wright Aeronautical Laboratories Materials Lab/MLBE Wright-Patterson AFB, OH 45433		12. REPORT DATE April 1980
13. MONITORING AGENCY NAME & ADDRESS (if different from Controlling Office) European Office of Aerospace Research and Development Box 14 FPO New York 09510		14. NUMBER OF PAGES 156
15. SECURITY CLASS. (of this report)		
16. DECLASSIFICATION/DOWNGRADING SCHEDULE		
17. DISTRIBUTION STATEMENT (of this Report) Approved for public release; distribution unlimited		
18. DISTRIBUTION STATEMENT (of the abstract entered in Block 20, if different from Report)		
19. SUPPLEMENTARY NOTES		
20. KEY WORDS (Continue on reverse side if necessary and identify by block number) Spacecraft Charging / Thermal Control Coatings / Conductive Adhesive / Conductive Coatings / Electron Irradiation / Geosynchronous Orbits		
21. ABSTRACT (Continue on reverse side if necessary and identify by block number) The feasibility of conductive adhesive technique for the electrical interconnection of ITO-coated second surface mirrors has been studied. The good electrostatic performance and the durability of components combining ITO coated aluminized Kapton and aluminum straps by means of a silver loaded silicone have been confirmed by a prequalification program.		

DD FORM 1 JAN 73 EDITION OF 1 NOV 65 IS OBSOLETE

SECURITY CLASSIFICATION OF THIS PAGE (When Data Entered) 313

DERTS.

SECURITY CLASSIFICATION OF THIS PAGE(When Data Entered)

Block 20:

→ The charge dissipation mechanisms for silica fabrics in a geosynchronous magnetic substorm environment have been studied by means of various sample configurations that have been tested under electron beam. Some recommendations have been given for a better use of silica fabrics as thermal control coatings in space.

SECURITY CLASSIFICATION OF THIS PAGE(When Data Entered)

PREFACE

ACKNOWLEDGEMENT

The authors gratefully acknowledge the active support of Mr. DAUPHIN and of people of MATERIALS SECTION of ESTEC who by their efforts and their previous large experience in the field of conductive adhesive did make possible the work on the adhesive bonding technique. S. J. BOSMA, F. LEVADOU and M. FROGATT have made a major contribution to all the work related to the prequalification programme.

Accession For	
NTIS GRA&I	<input checked="" type="checkbox"/>
DDC TAB	<input type="checkbox"/>
Unannounced	<input type="checkbox"/>
Justification _____	
By _____	
Distribution/ _____	
Availability Codes	
Dist	Available and/or special
A	

Section	TABLE OF CONTENTS	Page
I	INTRODUCTION	
	1 - 1 Background	1
	1 - 2 Approach	2
	1.2.1 The use of SSM coated with ITO	2
	1.2.2 The case of the composite quartz fabric/ FEP/Aluminum	3
II	TECHNIQUES USING CONDUCTIVE ADHESIVES FOR ELECTRICAL GROUNDING OF CONDUCTIVE SSM	4
	2 - 1 Introduction	4
	2 - 2 Development of a connection technique using conductive silicones	6
	2.2.1 Materials selected for the feasibility study	6
	2.2.2 Conductive adhesive preparation	7
	2.2.3 Design of a new tool for conductive adhesive curing	7
	2.2.4 Optimization of the curing conditions for RTV 566A + CHO Bond 1029 B adhesive	9
	2241 substrate preparation	9
	2242 aluminum foil tabs	9
	2243 priming	9
	2244 joint formation	9
	2245 resistance measurement	10
	2246 results	10
	2.2.5 Optimization of the curing conditions for conductive connections to be made on ITO- coated SSMs	11
	2.2.6 Electrical measurement of the contact resistance	11

Section	TABLE OF CONTENTS	Page
2 - 3	Prequalification of the conductive adhesive bonds	17
2.3.1	Purpose of the program	17
2.3.2	Preparation of samples	17
2321	materials	17
2322	preparation of the joints	18
2.3.3	Test sequence	21
2.3.4	Electrical resistance measurements	21
2341	background	21
2342	electrical contact resistance	23
2343	total electrical resistance	23
2344	sample conditioning	24
2345	test conditions	24
2346	applied current	24
2347	electrification time	24
2.3.5	Preliminary tests	27
2351	visual inspection	27
2352	in-air resistance measurement	27
2352-1	contact resistance	27
2352-2	total resistance	27
2353	in-vacuum resistance measurements	27
2353-1	test method	27
2353-2	test condition	29
2353-3	test results	29
2354	electron charging under scanning electron microscope	29
2354-1	test method	29
2354-2	test results	31
2355	optical microscope examination	31
2355-1	test method	31
2355-2	test results	31
2356	long term storage	33
2356-1	test method	33
2356-2	test results	33

Section	TABLE OF CONTENTS	Page
2.3.6	Chemical spray test	32
2361	test method	32
2362	test results	32
2362-1	electrical resistance	32
2362-2	visual inspection	35
2363	conclusions	35
2.3.7	Heat and Humidity test	35
2371	test method	35
2372	test results	35
2372-1	electrical resistance measurements	35
2372-2	visual inspection	36
2373	conclusions	36
2.3.8	Thermal cycling test	36
2381	test method	36
2382	test results	37
2382-1	electrical resistance measurements	37
2382-2	visual inspection	37
2383	conclusions	37
2.3.9	Acoustic test	37
2391	test method	37
2392	test results	38
2392-1	electrical resistance measurements	38
2392-2	visual inspection	38
2393	conclusions	38
2.3.10	Adhesion test	38
23101	test method	38
23102	test results	39
23103	conclusions	39

Section	TABLE OF CONTENTS	Page
2.3.11	Verification tests	39
23111	Background	39
23112	Contact resistance versus applied current test	41
23112-1	purpose of the test	41
23112-2	test method	41
23112-3	test results	41
23112-4	conclusion	43
23113	Long duration electrification test	43
23113-1	purpose of the test	43
23113-2	test method	43
23113-3	test result	44
23113-4	conclusion	44
23114	Electron charging under scanning electron microscope	44
23114-1	purpose of the test	44
23114-2	test method	45
23114-3	test results	45
23114-4	conclusions	45
2.3.12	Discussion of results	46
2 - 4	Electrostatic behaviour in a simulated substorm environment	47
2.4.1	Purpose of the experiment	47
2.4.2	Samples used in the test	47
2.4.3	Test facility	47
2.4.4	Test procedure	49
2.4.5	Results - TABLE	49
2 - 5	Final Conclusions	54

Section	TABLE OF CONTENTS	Page
III	SILICA FABRICS AND COMPOSITES	55
3 - 1	Introduction	57
3 - 2	The Electrostatic Charging Facility	58
3.2.1	General requirements for substorm simulation	58
3.2.2	Parameters of interest	58
3.2.3	The facility	60
3.2.4	The irradiation procedure	63
3 - 3	Sample configurations that have been studied	64
3.3.1	Scope	64
3.3.2	Silica fabric	64
3.3.3	Composite (quartz fabric/FEP/Alu)	69
3 - 4	Results	
3.4.1	Surface potential and currents in terms of time for samples the periphery of which is grounded	77
3.4.2	Evaluation of the various currents for samples the periphery of which was (or was not) grounded	77
3.4.3	Surface potential in terms of beam energy	92
3.4.4	Typical current recordings	92
3 - 5	Analysis	111
3.5.1	Background	111
3.5.2	Silica fabric behaviour	114
3521	surface potentials, leakage and secondary electron emission currents	114
3521-1	variation with time	114
3521-2	variation with the beam energy of steady state values of surface potentials leakage and secondary electron currents	117

Section	TABLE OF CONTENTS	Page
3522	Surface leakage current	117
3523	Arcing and discharging	119
3524	Remarks	122
3524-1	contamination and/or ageing	122
3524-2	visual inspection of the irradiated samples	122
3 - 6	Conclusions	123
3 - 7	Recommendations	124

IV CONCLUSIONS

Figures	TABLE OF FIGURES	Page
Figure 1	Cross-Sectional View of Joint Formation	8
Figure 2	Resistance Measurement	10
Figure 3	Sample Configuration for Resistance Measurement Method "A"	12
Figure 4	Sample Configuration for the Method "B"	13
Figure 5	Sample Configuration for the Method "C"	15
Figure 6	Sample Configuration for the Prequalification Programme	18
Figure 7	Measurement of the Total Resistance	24
Figure 8	Contact Resistance Measurements after Prequalification Tests	32
Figure 9	Total Resistance Measurements after Prequalification Tests	34
Figure 10	Test Results for Shear and Peel Systems	40
Figure 11	Contact Resistance Versus Applied Current	42
Figure 12	Sample Description	48
Figure 13	Schematic View of teh Sample Setting for Electron Irradiation	50
Figure 14	Front View of the Sample and Sample Holder for Electron Irradiations	51
Figure 15	Silica Fabric - FEP - Aluminum Foil Composite	56
Figure 16	Electron Energy Spectrum After Scattering through and Aluminum Foil	59
Figure 17	"Cedre" Substorm Simulation Facility	61
Figure 18 to Figure 24	Sample Configurations	65
Figure 25	5 keV Electron Irradiation	70
Figure 26	10keV Electron Irradiation	72
Figure 27	15keV Electron Irradiation	74
Figure 28	20keV Electron Irradiation	76
Figure 29	5 keV Electron Irradiation	78
Figure 30	10keV Electron Irradiation	80
Figure 31	15keV Electron Irradiation	82

Figures	TABLE OF FIGURES	Page
Figure 32	20keV Electron Irradiation	84
Figure 33 to Figure 37	Current Components	86
Figure 37		90
Figure 38	Surface Potential Versus Beam Energy	91
Figure 39 to Figure 49	Current Records	94
Figure 50	Surface Potential and $(I_L + I_C)$ Variations with Time	104
Figure 51	Secondary Electron Emission for FEP Teflon in Terms of Surface Potentail	111
Figure 52	δ Value in Term of Primary Beam Energy	112
Figure 53	Typical Recordings During Charging Phenomena	113

Table	TABLE OF TABLES	Page
Table 1	Test Sequence for the Prequalification Program	22
Table 2	Contact Resistance Measurements	26
Table 3	Total Resistance Measurements	28
Table 4	In Vacuum Resistances	30
Table 5	Test Results for Shear and Peel Systems	40
Table 6	Results Versus Electrification Time	44
Table 7	Procedure for the Electrostatic Test	52
Table 8	Behaviour of the ITO-Coated Kapton Grounded with a Conductive Adhesive in a Simulated Substorm Environment	53
Table 9	Surface Potential (in volts) Measurement after an 18 minute Irradiation	93
	Arcing Phenomena for the Configuration:	
Table 10	1 Layer Silica Fabric on Grounded Holder	105
Table 11	3 Layers Silica Fabric on Grounded Holder	106
Table 12	1 Layer Silica Fabric with FEP Film	107
Table 13	Composite Silica Fabric/FEP/Aluminum on Grounded Holder	108
Table 14	Composite Silica Fabric/FEP/Aluminum Over FEP	110

LIST OF PHOTOGRAPHS

Photograph 1	View showing ITO/Aluminised Kapton substrate with 3 straps bonded to it	20
Photograph 2	Close-up view of sample showing aluminum foil straps bonded to ITO/ aluminsed Kapton	20

SECTION I INTRODUCTION

1 - 1 Background

Anomalous spacecraft operation due to spacecraft charging and subsequent arcing and discharging is a problem experienced by satellites operating at synchronous orbit. The disruptions, anomalies, or even catastrophic damage to electronic subsystems and components caused by these discharges as well as the satellite thermal control materials degradation and contamination which may also result are of special concern to those systems which are expected to perform for long periods of time, seven to ten years, in synchronous orbit.

A variety of new non-charging satellite thermal control materials as well as electrical grounding techniques have been developed in the laboratory and applied to various charge prone satellite materials such as for instance thin film materials either metallized or coated with conductive transparent layers, and quartz fabrics. The performance of these materials has been evaluated in simple laboratory electron charging screening tests. Initially, these techniques provide effective electrical grounding of the metallized or conductive layer. Often after only relatively short times, either on the ground or on orbit, these grounding techniques fail, open electrically, as a result of vibration, corrosion, electrical or mechanical/thermal effects, loading and/or cycling and the materials are again subject to charging and subsequent chronic discharging.

Spacecraft system designers need more than simple conductive materials to effectively distribute and control spacecraft surface charging. To be practical, these conductive materials must be joined electrically (e.g. OSR mirror segment interconnects and MLI layer interconnects) and, in addition, there must be rugged and reliable methods of grounding these interconnected

arrays to a metallic substructure and/or to a charge dissipation point. Depending on the specific design, these interconnection and grounding schemes must be designed to handle the plasma currents at their expected densities. The main purpose of this program is to provide the "next step" beyond material development; that is, to combine into a simple "component" the material with appropriate interconnect/grounding systems and then to evaluate the performance, life expectancy, and durability of the combination.

1 - 2 APPROACH

The goal of this research and development was to combine new thermal control coatings (mainly flexible SSM coated with a conductive transparent oxide layer, and quartz fabrics) with various electrical bonding/grounding schemes in order to provide new charging control satellite "components". It was hoped that the proper use on board of such "components" would suppress the arcing and discharging phenomena. The work to be performed was divided into two main tasks.

1.2.1 The use of SSM coated with ITO

It is quite clear that the electrical interconnection and/or the electrical grounding of conductive coatings such as SSM coated with ITO will prevent any differential charging (above one volt) between adjacent parts of the satellite skin or between the skin and the frame. Consequently these electrical connections should suppress the arcing risk and the correlated anomalies.

The electrical connections seem to be achievable by means of conductive adhesive bonding techniques using conductive silver or other conductively pigmented/filled low outgassing silicones, polyurethanes or epoxies. Such techniques have been proved successfull for instance in order to electrically connect very thin layers of aluminum deposited on kapton.

Accordingly we proposed to assess the feasibility of the conductive adhesive technique on the SSM coated with ITO. As a first step a silver loaded silicone (RTV 566) would be used in order to benefit from the previous European experience on aluminized kapton that had been already summarized by a space prequalification. The silver loaded silicone would be applied with moderate temperature and pressure between the ITO layer and aluminum straps or on the edge of the sheets (connection film to film), or in holes and over the conducting surface (connection film to conductive substrate). If necessary, other conductive adhesives could have been tried (silicones, epoxies or polyurethane) the preference being given to the commercial products.

1.2.2 The case of the composite quartz fabric/ FEP/Aluminum

The behaviour of quartz fabrics under an electron beam bombardment simulating the geosynchronous magnetic substorm environment has been explained by a secondary emission conductivity (S.E.C.) where secondary electrons produced by the primary electron beam are thought to be a cloud of free charges within the dielectric material. If that is the case, the charging performance of the quartz fabric ought to be good only if this fabric is directly connected by its back face to a grounded metal plate.

The composite quartz fabric/FEP film/Aluminum, owing to the dielectric nature of the FEP teflon barrier between the pure quartz and the aluminum film, should not allow the charges to be dissipated even if the aluminum was grounded. However it was said that the behaviour of the composite was good under an electron beam bombardment (moderate potential surface, no discharges). As a first step such a behaviour ought to be verified and explained in such a way as to determine whether there was necessity to ground the aluminum layer. As a second step the interconnection and grounding techniques would be studied.

SECTION II

TECHNIQUES USING CONDUCTIVE ADHESIVES FOR ELECTRICAL GROUNDING OF CONDUCTIVE SSM

2 - 1 Introduction

Among the thermal control coatings that have been recently developed in order to provide a spacecraft charge control of satellites, flexible SSMs coated with thin transparent oxide films seem to be very promising. Some of them have been prepared in the United States by General Electric under USAF contract⁽¹⁾. Some others could be available soon from commercial sources. For instance SHELDHAL could provide some silvered FEP Teflon coated with ITO on the opposite side to silver⁽²⁾. BALZERS in Europe has already deposited for ESA similar transparent conductive layers on 3 mil aluminized FEP with outstanding, mechanical, optical and electrical properties⁽³⁾.

These various materials have been tested in the past under simulated substorm conditions^{(1) (3)} and have been shown to prevent space charging by electrons of 5 to 20 keV energy with 0.1 to 2 nA cm⁻² fluxes. Some mechanical bending tests have also been performed and have not indicated a decrease in the conductivity of the oxide layer that could suppress the charge dissipation.

However it is obvious that these materials must be used on board in conjunction with fixation, electrical interconnection and electrical grounding techniques that must effectively distribute and control surface charging. In other words, to be practical these

- (1) L.G. AMORE, A.E. EAGLES - Material and techniques for spacecraft static charge control - 1st Space charging technology conference Colorado Springs. October 1976
- (2) C.J. MAAg, private communication
- (3) A. PAILLOUS, Mise au point de matériaux combinant la qualité de réflecteurs solaires et une bonne conductibilité électrique. TOME 2 - Document CERT/DERTS - Rapport final sur Phase 2 du Contrat ESA/ESTEC 3184/N477/HP(SC)

conductive materials must be joined electrically and, in addition, there must be rugged and reliable methods of grounding these interconnected arrays to a metallic substructure and/or to a charge dissipation point. Depending on the specific design, these interconnection and grounding schemes must be designed to handle the plasma currents at their expected densities. The main purpose of this program is to provide the next step beyond material development, that is, to combine into a simple "component" the material with appropriate interconnect/grounding systems and then to evaluate the performance, life expectancy and durability of the combination.

Such electrical connections seem to be achievable by means of conductive adhesive bonding techniques using conductive silver or other conductively pigmented/filled low outgassing silicones or organic adhesives. These techniques were successfull for instance in order to electrically connect very thin layers of aluminum deposited on Kapton (4). In that case the connection by mechanical means such as bolts or rivets was not successfull due to the breaking of the very thin aluminum layer. The situation is worst for indium oxide and ITO layers on SSM because of the extreme thinness of these layers : some hundreds Angströms.

Accordingly it was decided to assess the feaseability of the conductive adhesive technique on the SSM coated with ITO in order to achieve electrical connections. Moreover it was decided to test the "component" (ITO-coated aluminized polymeric films + its interconnects) in a simulated substom environment and to follow a prequalification program.

(4) M.F. FROGATT - Grounding of thermal control films
CERT-DERTS/ESA Materials Workshop Toulouse 1977

2 - 2 DEVELOPMENT OF A CONNECTION TECHNIQUE USING CONDUCTIVE SILICONES

2.2.1 Materials selected for the feasibility study

As reported earlier, a previous practical experience had been acquired in Europe with a conductive adhesive preparation made of a silicone base RTV 566 filled with silver. This preparation had been used on the aluminized side of a Kapton film in order to provide a cheap and fiable electrical connection. Accordingly it was decided to use the same formulation of the adhesive for preliminary tests.

DERTS was provided with various ITO-coated FEP films of rather poor quality, by AFML / MBE . A preliminary evaluation of these conductive coatings was undertaken in order to select one of them for the feasibility study of the adhesive bonding technique . Results are briefly reported below.

ITO/FEP/Ag 838T - 27-1 and ITO/FEP/Ag 838T - 26-1

These coatings have a high solar absorptance that varies over the surface (from 0.12 to 0.18) ; the silver layer is severely scratched and does not cover the Teflon evenly.

These samples have a lower resistance near the edges and high resistance towards the center. Values are in the range 0.5 to 15 M Ω when measured with a probe consisting of two 1 cm wide copper electrodes at 1 cm distance of each other.

ITO/FEP Teflon/Ag (300Å ITO)

High solar absorptance, varies over the surface (0.11 to 0.34). Scratches on the silver layers. Low resistance towards the center (10 k Ω to values higher than 20 M Ω).

ITO/Kapton/Alu 838 K-1 and ITO/Kapton/Alu 838 K3

The optical properties are uniform (α_g 0.38 to 0.39). The resistance is low and uniform (0.5 to 5.0 k Ω).

ITO/Kapton/Alu (300Å ITO)

Shows various black spots at regular intervals probably originating from application of the In_2O_3 . The aluminized layer has a milky appearance in the centre of the sample.

Rather uniform electrical properties (15 to 60 $k\Omega$).

From these measurements and observations DERTS decided to carry out the prequalification program for the interconnections only with ITO/Kapton/Alu 838 samples. The remaining materials that seemed to be obsolete as from the present technology were only used in order to check the feasibility of the adhesive bonding techniques.

2.2.2 Conductive adhesive preparation

The main efforts were devoted to an RTV 566A + CHO BOND 1029 B formulation that seemed promising from previous works.

The trials showed that a convenient preparation was as follows:

- { RTV 566 A 100 parts by weight
- { CHO-bond 1029B 250 parts by weight
- thorough mixing, then addition to the mixture:
RTV 566 B catalyst 0.15 parts by weight
- further mixing ; degassing under vacuum
- application, curing.

2.2.3 Design of a new tool for conductive adhesive curing

Having had success with preliminary tests with the curing of conductive adhesive, it was necessary to be able to make joints and to reproduce them within closer resistance limits. The joints had to be realised by bonding an aluminum strip to the conducting layer.

A new tool was designed and developed. This tool has a heated probe, the pressure of which can be adjusted.

The tool is a WELLER WECP TEMTRONIK soldering station with the iron modified. A sketch of the heated head is given in FIGURE 1. The face of the hot end (Item 3) has a raised area 0.7 mm in height which, when pressed down to the level of the ceramic grip (Item 1), produced a load of 100 g. The stainless steel spring spanner (Item 2) is divided into 5 divisions. One division is equal to 20 g and one full revolution equals 100 g. The load is increased or decreased by rotating the spanner.

A temperature calibration has been performed, that allows a quick use of the soldering iron control console.

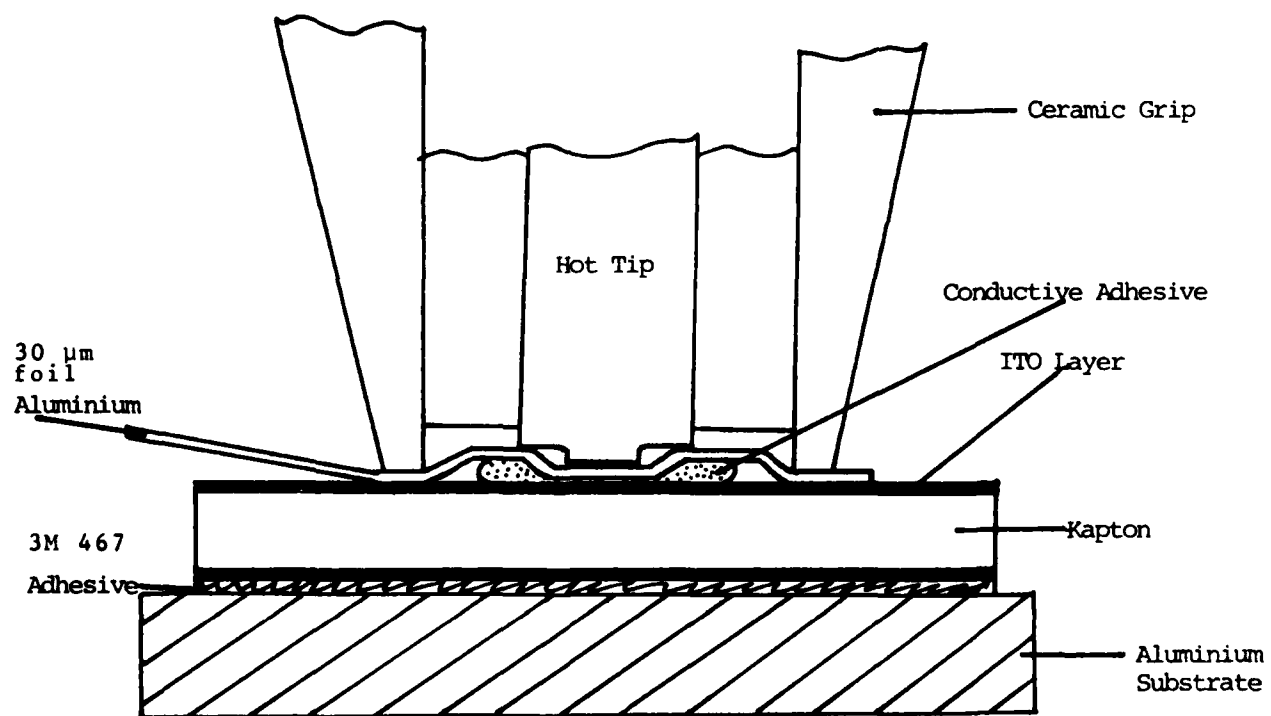


FIGURE 1 - CROSS-SECTIONAL VIEW OF JOINT FORMATION

2.2.4 Optimization of the curing conditions for the RTV 566A + CHO Bond 1029 B adhesive

In order to save ITO coated samples, aluminized Kapton was used for selection of the best conditions.

Ninety joints were made between aluminized Kapton and aluminum foil using various probe temperatures, probe loading and cure times. The conductive adhesive was prepared as indicated in Section 2.2.2

2241 Substrate preparation

80 mm x 20 mm pieces of Aluminized Kapton (25 micrometers thick) bonded with 3M 467 transfer tape to 1 mm aluminum plate of the same dimension.

2242 Aluminum foil tabs

16 μ m thick aluminum foil tabs of dimension 60 mm x 20 mm were carefully cut out.

2243 Priming

The substrates and foil tabs were carefully degreased by wiping with a Freon TF soaked Kimwipe. Dow Corning DC 1200 primer was carefully applied to the end of each tab to a distance of 20 mm from one end. Primer was applied to each end of the Al/Kapton substrate to a distance of 20 mm from the end.

2244 Joint Formation

A small amount of adhesive (see Section 2.2.2) was placed on the primed area of the aluminised Kapton. The primed aluminum foil was placed over it, and the heated tool, having already been set to the required load and temperature, was applied to the joint. The heat was applied for the required time and then the joint left to fully cure overnight. In all 90 joints were made on 45 substrates (2 to each substrate). Loads from 100 to 300 g were applied at temperatures of 50, 100 and 165°C. The duration of the application times were 1, 2 and 3 minutes.

The resistance of the joints were measured with the aid of a Hewlett Packard Digital Multimeter.

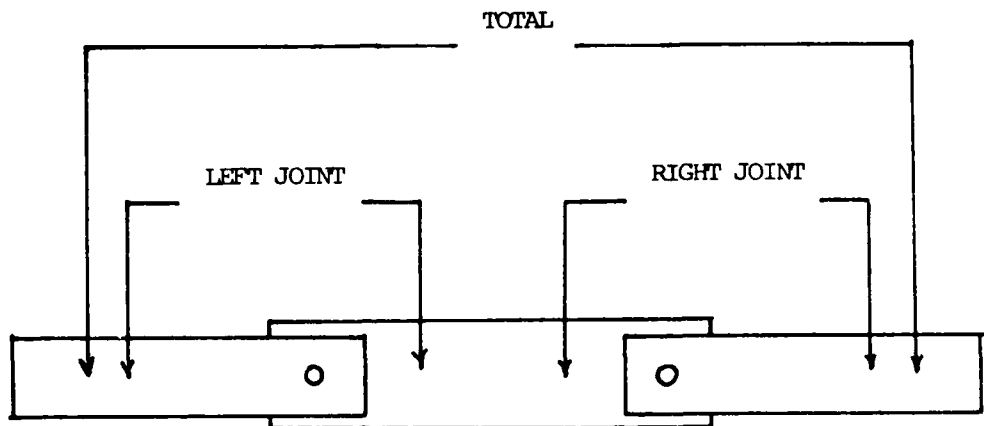


FIGURE 2 - RESISTANCE MEASUREMENT

The resistances were measured across each joint and across the total sample from tab to tab. (See FIGURE 2). To ensure that only the resistance of the joint was being measured, paper was placed between the Al/Kapton and aluminum foil to stop any other contact between the two adherents.

2246 Results

Out of a total of 90 joints, 73 were less than 10 ohms. Of the joints greater than 10 ohms, 11 came from those samples cured at 50°C, 4 from those cured at 100°C and 2 from the samples cured at 165°C. The most consistent resistances are obtained at 1 minute cure time and at any loading. The lowest resistances are obtained at 2 minutes cure time, and 200 and 250 g loadings. 1 minute at any of the 3 cure temperatures gives good results. A cure temperature of 165°C gives good results for all cure times.

One can say that 1 minute cure time at any of the cure temperatures and loadings will give acceptable resistances. To obtain the minimum resistance 2 minutes at 200 or 250 g loading and 100 or 165°C would seem the optimum settings for aluminum

foils (16 μm thick) applied to the aluminized side of an alum-inized Kapton (25 μm thick).

These statements were selected as the basis for the optimization of the electrical connections to be made with the ITO-coated samples.

2.2.5 Optimization of the curing conditions for conductive connections to be made on ITO-coated SSMs

The optimums settings are the followings:

- 200 g loading
- 2 minutes cure time
- 165°C hot end temperature (220° instrument console setting)

for a conductive adhesive prepared as described in Section 2.2.2.

The conditions were applied for all the samples prepared for the prequalification program (see below section 2.3) and for the electrostatic discharge tests (Section 2.4) with the ITO/Kapton/Alu 838 that was sent by AFML/MBE. Before application of the conductive adhesive, a Dow Corning DC 1200 primer had been applied on the ITO-coated Kapton as well as on the aluminum strap used for the connection.

2.2.6 Electrical measurement of the contact resistances

The most adequate parameter to determine the performance of a grounding point is the electrical contact resistance. A large variation of this parameter will indicate if a grounding point has the tendency to fail performance.

The measurement of the electrical contact resistance is difficult because a low ohmic contact (10-100 Ω) is applied to a material with a high ohmic resistance (k Ω to M Ω). Three methods have been evaluated which appeared capable of determining the

contact resistance in the high ohmic chain.

2261 METHOD A : time domain
reflectometry

Time Domain Reflectometry is a pulse reflection measurement technique. A pulse is sent continuously down a resistance chain. If a pulse encounters a step in the resistance the reflection travels back to the sending point, where it is compared in phase, time and amplitude with the original pulse. The comparison shows the resistance step as well as the value of the resistance.

This technique was applied on a sample configuration as shown in FIGURE 3. Since Time Domain Reflectometry relates time to distance, the finite rise time of the incident or reflected pulse limits the possible resolution of distance.

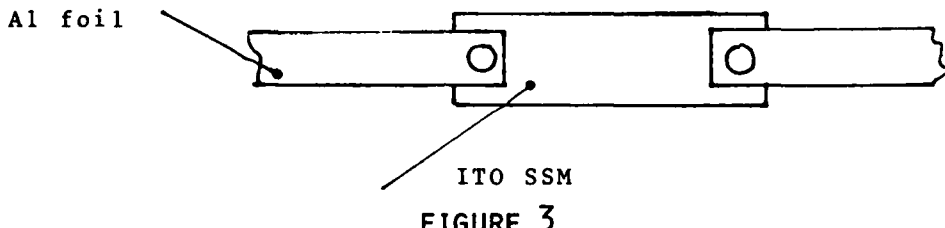


FIGURE 3

SAMPLE CONFIGURATION FOR RESISTANCE MEASUREMENT METHOD "A"

In the case of the test samples the transition from very low to high resistance is too large to allow for a reasonable resolution. The rise time of the equipment would have to be improved by a factor 100 to achieve meaningful results.

2262 METHOD B

This method consists of a combination of three resistance measurements by using three contacts, from which one single contact resistance is theoretically deduced and not directly measured.

FIGURE 4 shows the applied sample configuration.

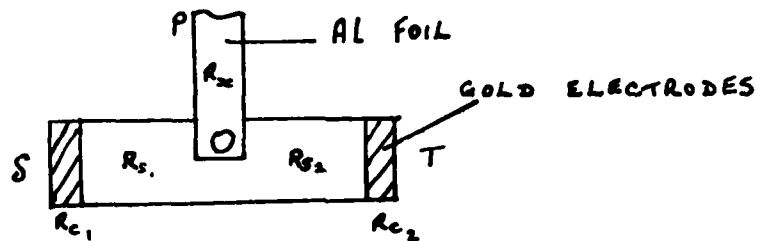


FIGURE 4 - SAMPLE CONFIGURATION FOR THE METHOD "B"

Two gold electrodes are vacuum deposited on the sample sides and the actual contact is situated in the centre.

The following resistance chains are measured:

$$R_{ps} = R_{c1} + R_x + R_{s1}$$

$$R_{pt} = R_{c2} + R_x + R_{s2}$$

$$R_{st} = R_{c1} + R_{c2} + R_{s1} + R_{s2}$$

$$\left. \begin{array}{l} \\ \\ \end{array} \right\} \rightarrow 2 R_x = R_{ps} + R_{pt} - R_{st}$$

R_{c1} = Contact resistance of first gold electrode

R_{c2} = Contact resistance of second gold electrode

R_x = Contact resistance of RTV 566 Bond

R_{s1} = Resistance of Indium Oxide Layer

R_{s2} = Resistance of Indium Oxide Layer

Because the electrical leads to the measuring apparatus were not removed during the three measurements, it was assumed that the contact resistances of the gold electrodes as well as the resistance of the indium layer would not change during the measurements.

The indium oxide layer shows however variations of hundreds of ohms during a measurement, which is only a few tenths of a per cent as compared to the actual resistance of several Mega-Ohms, but which is of the same order of magnitude as the contact resistance of the RTV.

It is not possible to deduce the contact resistance as the measurement error is of the same magnitude as the result. Sometimes it is even possible to find negative values.

2263 METHOD C

FIGURE 5 shows the sample configuration for the method which proved to be the most effective. The three contact principle is used to obtain the contact resistance of the centre electrode. At first, it was decided to apply gold deposited electrodes for the measurement, however there has been a difficulty with the adhesion of gold to ITO. The concept was changed so that all three electrodes are aluminum straps bonded with conductive adhesive. FIGURE 5 shows the electrical circuit applied.

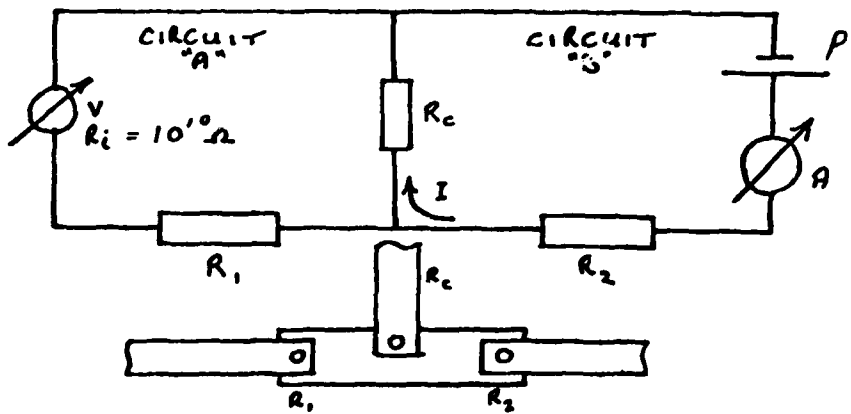


FIGURE 5 - SAMPLE CONFIGURATION FOR THE METHOD "C"

- P = Power supply
- A = Keithly Model 602 Electrometer (applied in Amperemeter Mode)
- V = Hewlett Packard Multimeter 3465 B (applied in Voltmeter Mode)
- R_i = Internal Resistance of Voltmeter = $10^{10} \Omega$
- R_1 = Contact Resistance of Left Electrode plus Resistance of ITO-Layer between Left and Centre Electrodes
- R_2 = Contact Resistance of Right Electrode plus Resistance of ITO Layer between Right and Center Electrodes.
- R_c = Contact Resistance of Centre Electrode.

The power supply and the amperemeter are connected to the centre and right electrodes. The right electrode functions only as a current conductor.

The voltmeter is connected between the centre and left electrodes.

The left electrode functions as a potential electrode: due to the internal resistance of the voltmeter the current passing through circuit "A" will be approximately a factor 1000 smaller than the current passing through circuit "B".

By adjusting the power supply in the circuit "B", the current through the contact resistance can be fixed. Circuit "A" is used to determine the voltage drop over the contact resistance. In this way the contact resistance can be deduced.

Based on this method a jig has been developped which ensures that the samples are measured under similar conditions of electrode pressure and sample positioning.

The results show that a nominal value for the contact resistance is 200 to 300 Ω for connections made by the conductive adhesive technique on ITO-coated Kapton. These values tend to be higher than the values for the same contact on the aluminum surface of an aluminized Kapton. This is not surprising as the contact resistance always includes a barrier layer of the substrate material. In the case of an aluminum substrate the contribution to the contact resistance will be very low, however for an indium oxide substrate the influence of the barrier layer will be dominating.

2 - 3 PREQUALIFICATION OF THE CONDUCTIVE ADHESIVE BONDS

2.3.1 Purpose of the programme

A study program was defined in order to check the stability under humidity, chemical spray, thermal cycling and vibrations of "components" prepared with the above mentioned method.

2.3.2 Preparation of samples

2321 Materials

a) Adhesive

RTV 566 silicone rubber produced by General Electric, USA

b) Primer

DC 1200 primer produced by Dow Corning, USA

c) Conductive_Powder

Cho-Bond 1029 B produced by Chomerics, USA

d) ITO-coated_aluminized_Kapton

This material was sent by AFML/MBE under reference ITO/Kapton/Alu 838. It is a 5 mil Kapton (du Pont de Nemours) with a 1000 Å layer of vacuum deposited aluminum by SHELDahl Northfield, Minnesota, USA.

On the Kapton side of this aluminized Kapton an ITO layer has been deposited by General Electric USA.

e) Aluminum_substrate

Aluminum alloy, 20x50x1 mm

f) Aluminum_Strap

Aluminum foil, 30 µm thick, 8 mm wide, produced by Carl Roth, Karlsruhe, Germany

g) Adhesive_transfer_tape

3M N° 467, produced by 3M Company, USA

2322 Preparation of the joints

a) Substrate Preparation

39 rectangular samples of aluminum alloy (20 x 50 x 1mm) were abraded with Scotch-Brite and degreased in Freon TF vapour. Aluminised Kapton of the same dimension is bonded to the aluminum substrate with 3M 467 transfer tape.

b) Aluminum straps

30 μm thick aluminum straps of dimensions 8 x 80 mm were prepared. Each sample was provided with three grounding straps according to the configuration shown in FIGURE 6.

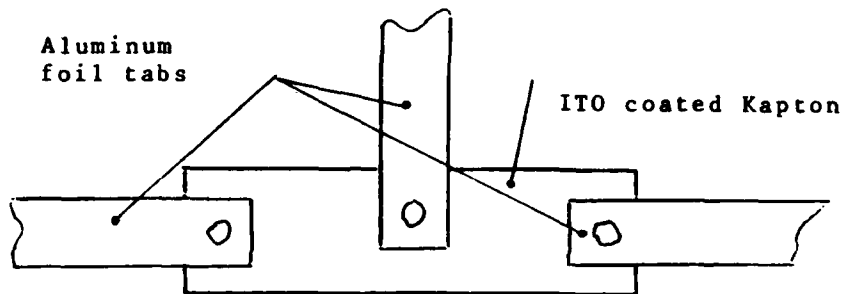


FIGURE 6

SAMPLE CONFIGURATION FOR THE PREQUALIFICATION PROGRAM

c) Priming

The straps were degreased by wiping with a Freon TF soaked Kimwipe. Dow Corning DC 1200 primer was applied to the end of each strap to a distance of 20 mm from one end. Primer was applied to each end of the aluminum Kapton substrate as well as in the middle of the samples.

d) Conductive Adhesive Preparation

The adhesive was prepared as follows:

RTV 566A - 100 parts by weight
CHO-Bond 1029B - 250 parts by weight

were mixed thoroughly and to the mixture was added:
RTV 566B catalyst- 0,15 parts by weight
After further mixing, the adhesive was degassed under vacuum.

e) Joint Formation

A small amount of the conductive adhesive was applied to the primed area of the ITO/Aluminised Kapton, the primed aluminum foil was placed over it and the heated tool applied over the joint. The tool was applied to the joint for a cure time of 2 minutes, with a hot tip temperature of 160°C and load of 200g, see FIGURE 1. These co-ordinates were found in previous investigations to be ideal for forming joints of low resistance (See Section 2.2.4 and 2.2.5).

A total of three joints were made on each of the 39 substrates. See photograph nos 1 and 2.



PHOTOGRAPH 1

View showing ITO/Aluminised Kapton substrate
with 3 straps bonded to it.



PHOTOGRAPH 2

Close-up view of sample showing aluminium
foil straps bonded to ITO/Aluminised Kapton
substrate.

2.3.3 Test sequence

The samples were submitted to the following prequalification tests :

- Chemical Spray Test
- Heat and Humidity Test
- Acoustic Test
- Thermal Cycling Test

The test parameters were :

- Electrical Contact Resistance
- Visual Inspection
- Adhesion Testing

Table I illustrates the sequence of tests and the manner in which the samples are divided to determine the influence of any one test. As an example samples 17 to 20 are submitted to chemical spray testing only, while samples 33 to 38 follow the entire test programme. This method identifies if one particular test or a combination of tests is detrimental to the material under evaluation.

In addition to the standard prequalification programme the material was submitted to several preliminary tests to determine its basic characteristics :

- In Vacuum Resistance
- Electrical Charging under Scanning Electron Microscope
- Inspection of the Sample Surface with an Optical Microscope
- Long Term Storage Effects

2.3.4 Electrical resistance measurements

2.3.4.1 Background

The purpose of the prequalification programme was to identify the reliability of the grounding configuration.

The most adequate parameter to determine the performance of a grounding point is the electrical contact resistance.

A large variation of this parameter will indicate if a grounding point has the tendency to fail performance.

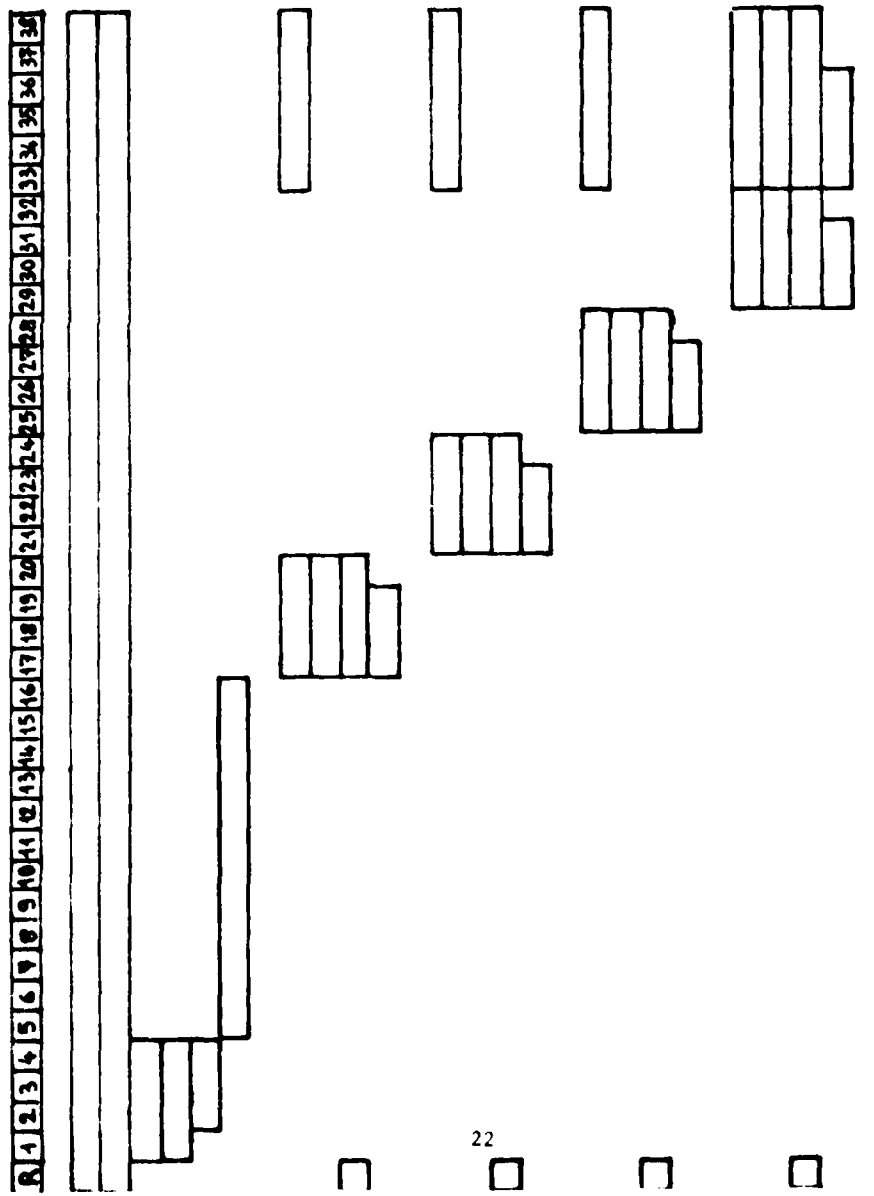


TABLE 1 - TEST SEQUENCE FOR THE PREQUALIFICATION PROGRAM

In the case of a grounding point on a highly conductive substrate material e.g. aluminum, it is sufficient to measure the total resistance of the grounding point and substrate, because a change of the contact resistance from the 10Ω -range to 100Ω -range will be easily detected as compared to the substrate resistance of a few milli-ohms.

For the case of a low ohmic contact ($10-100\Omega$ -range) on a substrate material with a high ohmic resistivity ($k\Omega-M\Omega$ -range), it is more difficult to identify the contact resistance.

This is the situation for the grounding configuration under evaluation. The Indium-Tin-Oxide layer shows variations of hundreds of ohms during a measurement, which is only a few tenths of a percent as compared to the actual resistance of several Mega-Ohms, but which is of the same order of magnitude as the contact resistance of the grounding point. For this particular grounding configuration the contact resistance will be defined as the combined resistances of the aluminum strap, conductive adhesive and the ITO-boundary layer at the contact point.

2342 Electrical contact resistance

Several methods had been evaluated which appeared capable of determining the contact resistance in a high ohmic chain: See Section 2.2.6.

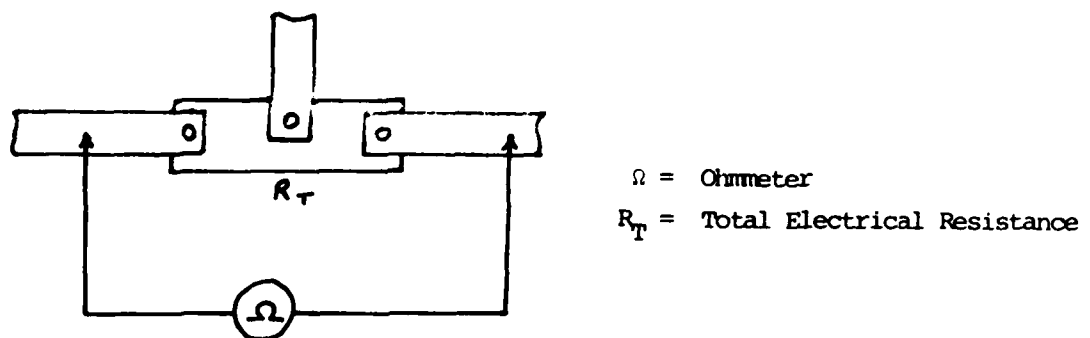
The most effective method that is described in Section 2263 was used here.

2343 Total Electrical resistance

After each subsequent test the total electrical resistance of each sample was measured with the Hewlett Packard Multimeter 3465 B applied in Ohm-meter mode.

The total electrical resistance is defined as the electrical resistance measured between left and right electrodes and includes contact resistance of left and right electrode as well as the resistance of the intermediate ITO layer.

FIGURE 7 shows the test method:



Ω = Ohmmeter

R_T = Total Electrical Resistance

FIGURE 7 - MEASUREMENT OF THE TOTAL RESISTANCE

2344 Sample conditioning

The samples were kept as a relative humidity of 65%-70% and a temperature of 18°C-20°C during 120 hours before commencing the test programme.

During the total programme samples were stored under these conditions when not submitted to a specific test.

2345 Test conditions

After each subsequent test, samples were stored during 48 hours under conditions similar to those stated in Section 2344 and then measured under these conditions.

2346 Applied current

For the measurement of the electrical contact resistance, the applied current was set at 10^{-5} A.

For the total electrical resistance, the ohmmeter reference current for the $20\text{ K}\Omega$ and $200\text{ K}\Omega$ ranges, which were most commonly used, is 10^{-5} A.

2347 Electrification Time

The electrification time for each measurement was set at 30 seconds, before the measurements value was read.

2348 Accuracy of the measurements

For the contact resistance, the read-out of the multimeter is ± 0.001 mV indicating that for a set current level of $(1.00 \pm 0.01) \times 10^{-5}$ A, the accuracy of the resistance measurement is $\pm 0.1 \Omega$.

For the total resistance measurement the read-out accuracy of the ohmmeter is $\pm K\Omega$ in the $20 K\Omega$ and $200 K\Omega$ -ranges.

TABLE 2 - CONTACT RESISTANCE MEASUREMENTS

Sample	Contact Resistance (Ω)					Remarks
	Initial Value in Air	After Spray Test	After Humidity Test	After Thermal Test	After Acoustic Test	
1	69					
2	104					
3	125					
4	244					
5	23	↑				
6	∞					
7	∞					
8	22					
9	32					
10	60					
11	214					
12	30					
13	220					
14	54					
15	50					
16	27					
17	90	38				
18	112	86				
19	106	360				
20	80	29				
21	29		29			
22	820	↑	471	↑		
23	77		74			
24	26		39			
25	68					52
26	40					29
27	43					16
28	153					67
29	30			28 K		
30	355			78 K ↓		
31	152			419		
32	204	↓		105 K ↓		
33	151	266	407	3 K	5 K	
34	57	51	90	160 K ↓	135 K	
35	56	41	50	170 ↓	337	
36	22	22	58	1 K	414	
37	72	83	106	4.5 K ↓	144	
38	41	24	69	261 ↑	274	
39	61	92	117	121	103	
R	102	32	39	44	18	

∞ : infinite value
 \uparrow : drift to higher value
 \downarrow : drift to lower value
 \ddagger : instable

2.3.5 Preliminary tests

2351 Visual inspection

During the entire test programme the visual inspection was performed with a "ZooM" type microscope at 30 x magnification. Special attention was given to the ITO-layer surrounding the grounding point for traces of cracks.

The initial inspection showed no major degradation.

2352 In-air resistance measurement

2352-1 contact resistance

The initial contact resistance of the majority of the samples showed a normal value between 20 and 400 Ω (see Table 2). Three samples (nrs. 5, 22, 32) were unstable, while two samples (nrs. 6, 7) had an infinite contact resistance indicating a faulty grounding point.

2352-2 total resistance

The initial total resistance of the samples varied from 2 to 30 $\text{K}\Omega$ (see Table 3). All samples showed relatively stable values.

2353 In-vacuum resistance measurement

2353-1

The contact resistance was measured according to the method described in § 2342 however with the jig installed in a vacuum chamber.

The measurement leads were passed through an electrical feedthrough, so that the contact resistance could be monitored during all phases of the test.

A turbo-molecular pump in combination with a primary pump provided a vacuum of better than 10^{-5} torr. The chamber pressure was monitored with a high vacuum gauge.

TABLE 3 - TOTAL RESISTANCE MEASUREMENTS

Sample	Total Resistance (KΩ)					Remarks
	Initial Value in Air	After Spray Test	After Humidity Test	After Thermal Test	After Acoustic Test	
1	7.46					
2	8.51					
3	16.88					
4	28.67					
5	4.77					
6	15.33					
7	22.75					
8	4.93					
9	2.44					
10	4.14					
11	20.33					
12	2.41					
13	2.38					
14	10.14					
15	2.45					
16	14.20					
17	3.28	4.83				
18	12.08	58.40				
19	8.62	21.28				
20	6.77	11.02				
21	3.85		4.19			
22	7.36		8.82			
23	3.16		3.49			
24	2.92		4.16			
25	6.77				25.05	
26	2.31				3.41	
27	3.88				5.71	
28	4.74				10.61	
29	4.39			3.59		
30	21.17			14.90		
31	2.80			2.66		
32	19.40			10.10		
33	15.45	41.69	31.21	11.53	16.30	
34	5.01	8.52	8.87	22.60	22.06	
35	2.33	3.21	2.85	7.36	5.55	
36	3.97	6.26	7.15	24.80	24.31	
37	2.85	3.84	3.47	4.52	4.20	
38	3.85	5.03	6.39	5.64	3.78	
39	13.82	20.72	35.01	36.52	41.77	
R	3.14	4.04	4.13	5.56	6.10	

2353-2 test conditions

The sample current was set at 10^{-5} A and remained applied during the total test sequence.

The test sequence was :

- Start Electrification Time
- In-Air Measurements during 10 minutes
- Start Pump-Down
- In-Vacuum Measurements until a Vacuum in the 10^{-5} torr Region is achieved
- Air Inlet
- In-Air Measurements during 10 minutes.

Sample nr. 1 remained in vacuum during 16 hours after 10^{-5} torr was reached to determine if there is a long term vacuum effect.

2353-3 test results

Test results are noted in Table 4 and indicate that there are no drastic variations of the contact resistance due to vacuum effects even after longer exposure periods.

Contact resistance tends to show a slight increase during the first minutes of pump-down, but decreases after approx. 10 minutes. Sometimes there are sudden variations of the resistance value. Both phenomena are believed to be caused by bubbling of the sample surface due to trapped air between the aluminised Kapton and the aluminium substrate.

After air-inlet the contact resistance does not vary considerably from the last value measured in vacuum.

2354 Electron charging under scanning electron microscope

2354-1 test method

A sample was installed in the sample compartment of a scanning electron microscope.

The samples substrate was insulated from the sample holder but the top ITO-layer was grounded to the holder by means of the central grounding strap. By this method it could be

TABLE 4 - IN VACUUM RESISTANCES

t (min)	Sample 1		Sample 2		Sample 3		Sample 4	
	R (Ω^C)	P (torr)						
0	95	air	242	air	550	air	681	air
3	95	air	246	air	552	air	683	air
6	97	air	247	air	553	air	685	air
10	99	air	247	air	555	air	685	air
Start Pump-Down								
13	130	8×10^{-3}	217	9×10^{-3}	562	8×10^{-3}	680	8×10^{-3}
16	143	1×10^{-3}	233	8×10^{-4}	574	8×10^{-4}	692	8×10^{-4}
20	138	5×10^{-4}	185	3×10^{-4}	557	4×10^{-4}	673	4×10^{-4}
23	137	2.4×10^{-4}	186	2.2×10^{-4}	555	2.8×10^{-4}	671	2.8×10^{-4}
26	137	2.0×10^{-4}	178	1.9×10^{-4}	547	2.0×10^{-4}	672	2.2×10^{-4}
30	135	1.6×10^{-4}	176	1.6×10^{-4}	539	1.5×10^{-4}	653	1.6×10^{-4}
33	152	1.2×10^{-4}	177	1.3×10^{-4}	537	1.3×10^{-4}	651	1.3×10^{-4}
36	162	1.0×10^{-4}	175	1.0×10^{-4}	537	1.0×10^{-4}	650	1.1×10^{-4}
40	165	9×10^{-5}	175	8×10^{-5}	540	8×10^{-5}	650	9×10^{-5}
43	167	8×10^{-5}	155	7×10^{-5}	538	8×10^{-5}	653	8×10^{-5}
46	165	8×10^{-5}	156	7×10^{-5}	540	8×10^{-5}	652	8×10^{-5}
50	170	7×10^{-5}	156	6×10^{-5}	539	7×10^{-5}	650	7×10^{-5}
Air Inlet								
53	166	7×10^{-5}	157	air	530	air	652	air
56	165	7×10^{-5}	159	air	534	air	654	air
60	167	7×10^{-5}	162	air	535	air	657	air
90	170	6×10^{-5}						
16 hrs.	166	2×10^{-5}						
Air Inlet								
3	174	air						
6	178	air						
10	181	air						

t = Electrification Time

R = Contact Resistance

 P_V^C = Pressure in Vacuum Chamber

determined if the grounding point had sufficient conductance to leak the incident electron flux on the ITO surface to ground.

The incident electron beam could be set at energy levels of up to 30 KeV and flux levels of up to 10^{-3} A.

Charging and subsequent discharging of the sample could be monitored by abrupt changes of the sample leakage current as well as sudden increases in the intensity of the electron image of the sample on the microscope screen.

2354-2 test results

Samples 1 to 3 showed no evidence of charging or discharging. Sample 4 showed several micro-discharges immediately after electron irradiation commenced, but these were soon followed by a "quiet" period.

Indications are that local charging can take place due to insufficient current paths in the conductive adhesive - ITO boundary. The micro-discharges probably create new current paths which have sufficient conductance to avoid recharging of the ITO-surface.

2355 Optical microscope examination

2355-1 test method

A Reichert Projection Microscope was applied in Interferometer Mode using the Normarski Technique. This technique allows a better visualisation of cracks, but - due to the polarized light - the vertical defects are far more emphasized than the horizontal ones.

The magnification utilized was x 120.

2355-2 test results

The ITO-layer surrounding the grounding points was carefully examined.

No major cracks could be identified for any of the samples.

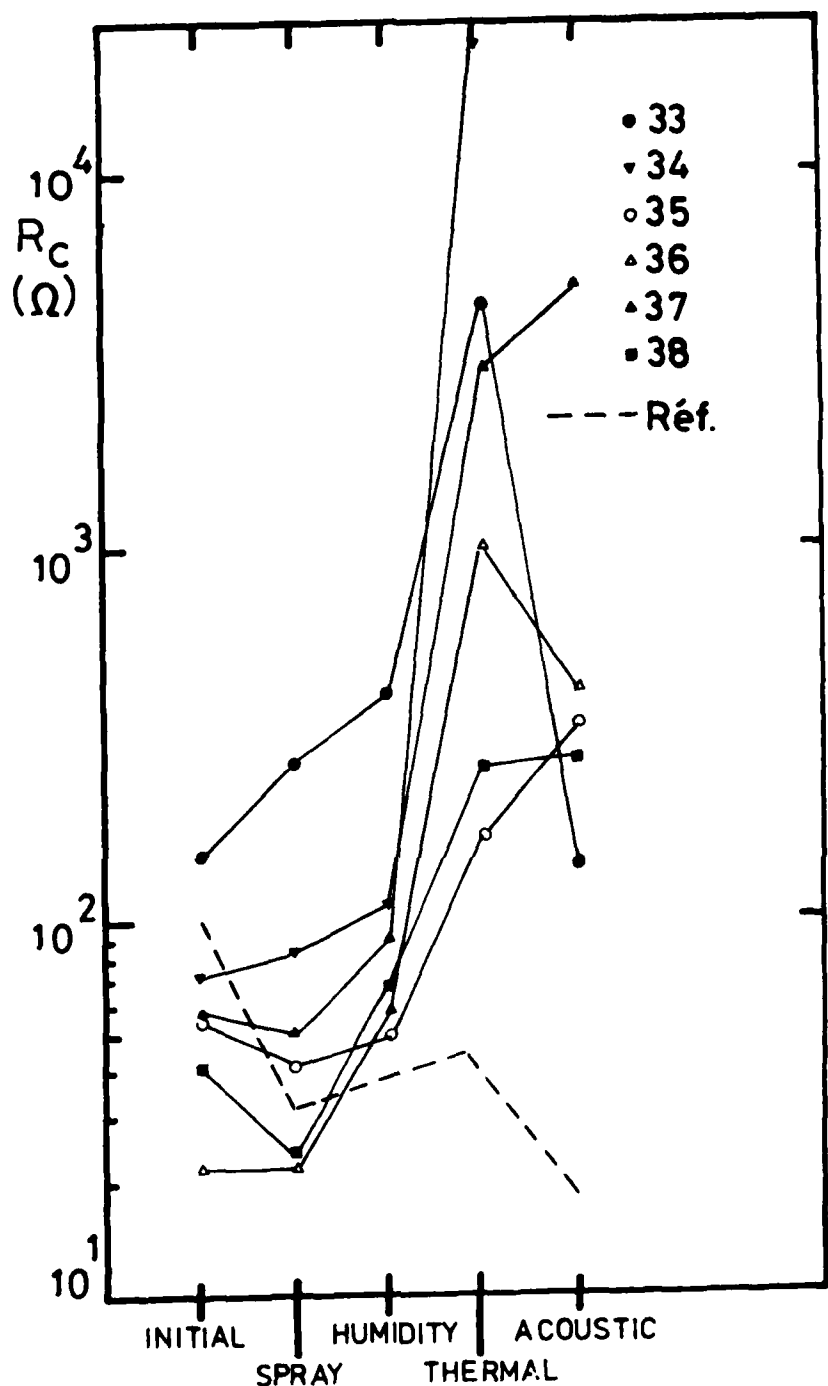


FIGURE 8
CONTACT RESISTANCE MEASUREMENTS AFTER PREQUALIFICATION TESTS

2356 Long term storage

2356-1 test method

A long term storage at a relative humidity of 55%-70% and a temperature of 18°C-20°C will be used for samples 5 to 16. Samples 5 to 8 will be measured after 6 months, 9 to 12 after 1 year and 13 to 16 after 18 months.

2356-2 test results

No results are available as the test is still under continuation.

2.3.6. Chemical spray test

2361 Test method

The samples were sprayed for one minute with Iso-Propyl alcohol at room temperature.

2362 Test results

2362-1 electrical resistance measurements

(Tables 2,3, Figures 8, 9)

- Contact resistance

The measured values did not indicate a preference of the contact resistance to follow an increasing or a declining trend.

The contact resistance showed arbitrary variations and although two samples had a relatively large increase (nrs. 10 and 33), these were still within acceptable limits.

- Total resistance

The total resistance of the samples showed an increase of the values by a factor 2 to 4.

The contact resistance of the centre electrodes did not show a tendency to increase, which one can assume is

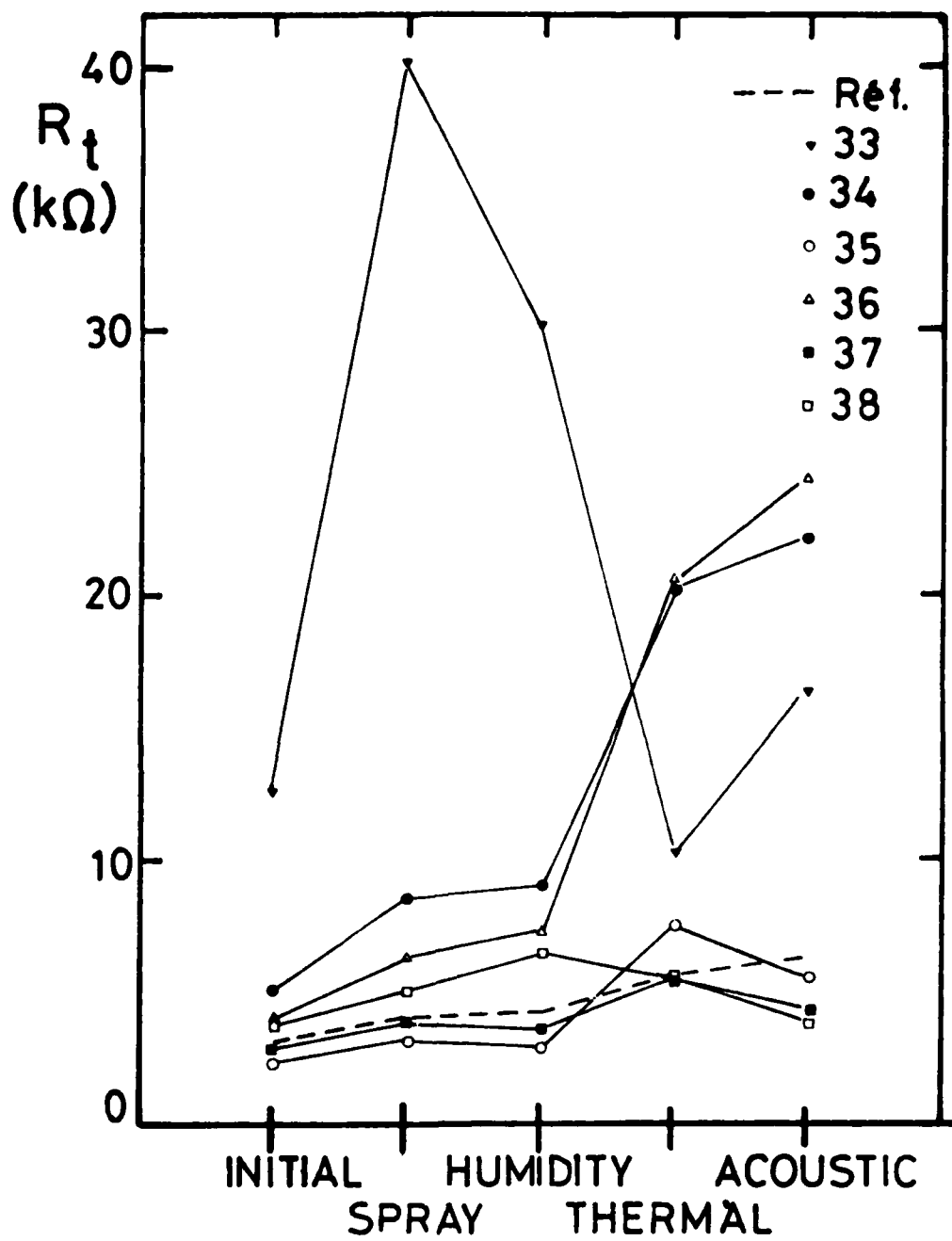


FIGURE 9
TOTAL RESISTANCE MEASUREMENTS AFTER PREQUALIFICATION
TESTS

also true for the side electrodes.

In this case the increase of the total resistance is mainly due to an increase of the resistivity of the ITO-layer.

The conclusion is not surprising as the conductance through the ITO layer is mainly a surface phenomena and the spraying with iso-propyl alcohol will create impurities in the surface path.

2362-2 visual inspection

No degradation of the sample top surface was observed.

2363 Conclusions

No major variation of the electrical grounding point was observed. The ITO-layer of the substrate material showed an increase of resistivity.

2.3.7. Heat and humidity test

2371 Test method

The samples were submitted to 7 days in the humidity chamber at a temperature of 50°C and relative humidity of 95%.

2372 Test results

2372-1 electrical resistance measurements

(Tables 2, 3, Figures 8, 9)

- Contact resistance

Samples nr 21 to 24 which were submitted to humidity testing only, showed constant values, except for nr 22. This sample had however been unstable during initial measurement, so that the variation is not due to the humidity test.

Samples nr 33 to 38 which are submitted to all tests, have an increasing trend, but within acceptable limits.

- Total resistance

The total resistance of the samples nr 21 to 24 showed a small increase.

The resistance values of samples nr 33 to 38 showed no major increase compared to the values after chemical spray testing. The decrease of sample nr 33 is more likely due to mechanical effects than to humidity testing.

Apparently the humidity affects the ITO-layer if chemical spray test has not been performed before.

In the case of chemical treatment before, the surface of the ITO has already been impurified and the effect of humidity is not accumulated.

2372-2 visual inspection

No degradation of the sample top surface was observed.

2373 Conclusions

No major variation of the electrical grounding point was observed. Samples which had been through chemical spray before showed a slight increase in contact resistance.

Humidity affects the ITO layer of the substrate material and causes an increase of ITO-resistivity.

2.3.8. Thermal cycling test

2381 Test method

The test was performed according to ESA specification PSS-11/ QRM-04T. The samples were submitted to 100 cycles between $+100^{\circ}\text{C}$ $\pm 5^{\circ}\text{C}$ and $-150^{\circ}\text{C} \pm 5^{\circ}\text{C}$ at a change rate of $10^{\circ}\text{C} \pm 2^{\circ}\text{C}$ per minute, with dwell times of 5 minutes \pm 5 minutes under vacuum.

2382 Test results

2382-1 Electrical resistance measurements

(Tables 2 and 3, Figures 8 and 9)

- Contact resistance

The contact resistance of all samples increased, 7 out of 10 samples had resistance values in the k Ω -range.

It is evident that the variation of the contact resistance due to thermal cycling is much more significant than for the previous tests.

- Total resistance

The total resistance of the samples which were only submitted to thermal cycling had lower values after testing compared to the initial values.

The samples which had been through all previous tests showed four samples with an increased resistance and two with a lower resistance, so that a general trend is difficult to identify.

2382-2 visual inspection

No degradation of the sample top surface was observed.

2383 Conclusions

Thermal cycling causes a significant increase of the electrical contact resistance.

The surface resistivity of the ITO-layer decreases after thermal cycling, however if the sample has passed all previous tests it is difficult to conclude any trend for the ITO-layer.

2.3.9 Acoustic test

2391 Test method

The test was performed according to ESA specification EV-01-1-1

in the LING RCM 192 Acoustic Reverberation Chamber (See

2392 Test results

2392-1 Electrical resistance measurements

(Tables 2,3 Figures 8,9)

- Contact resistance

The contact resistance of the samples which were only submitted to acoustic testing, decreased for the samples which had passed all previous tests, two out of five samples (nrs. 36, 37) showed a significant lower value than after thermal cycling. Indications are that the contact resistance could recover after the effects of thermal cycling.

- Total resistance

The total resistance of the samples which were only submitted to acoustic testing, increased. This increase is caused by a higher resistivity of the ITO-layer. For the samples which had passed all previous tests, the total resistance showed a general trend to decrease, except for sample 33.

2392-2 visual inspection

No degradation of the sample top surface was observed.

2393 Conclusions

No major variation of the electrical grounding points was observed. Some samples which had been through the previous tests showed a recovery of the electrical contact resistance, but this is probably not a characteristic which is specifically caused by the acoustic test.

2.3.10 Adhesion test

23101 Test method

The tests were performed using an Instron Tensile Test Machine at a cross-head speed of 0,2 cm/min.

The two opposite grounding straps of each sample were submitted to a shear test and the central strap to a 90° peel test.

(See FIGURE 10)

23102 Results

They are given in TABLE 5

23103 Conclusions

As a result of the shear test, the aluminium strap of one the grounding points tore for each sample. The result indicates that the bond strength of the system aluminium strap-conductive glue-ITO-layer is higher than the strength of the aluminium strap itself.

As a result of the 90° peel test, the aluminium strap was separated from the conductive adhesive. The major part of the conductive adhesive remained bonded to the ITO-layer, but a sufficient layer was removed with the strap to indicate that the bonding strength of the glue to the aluminium is adequate.

No major variations of the adhesion characteristics were identified for a sample after a particular test or the combination of all tests, which implies that the mechanical reliability of the bond is high.

2.3.11 Verification tests

2.3.11.1 Bacground

Some of the phenomena which were a result of the prequalification programme, were not completely understood. It was decided to perform specific tests to verify the behaviour of the samples. In particular it was necessary to determine if the samples could recover from the effects of thermal cycling.

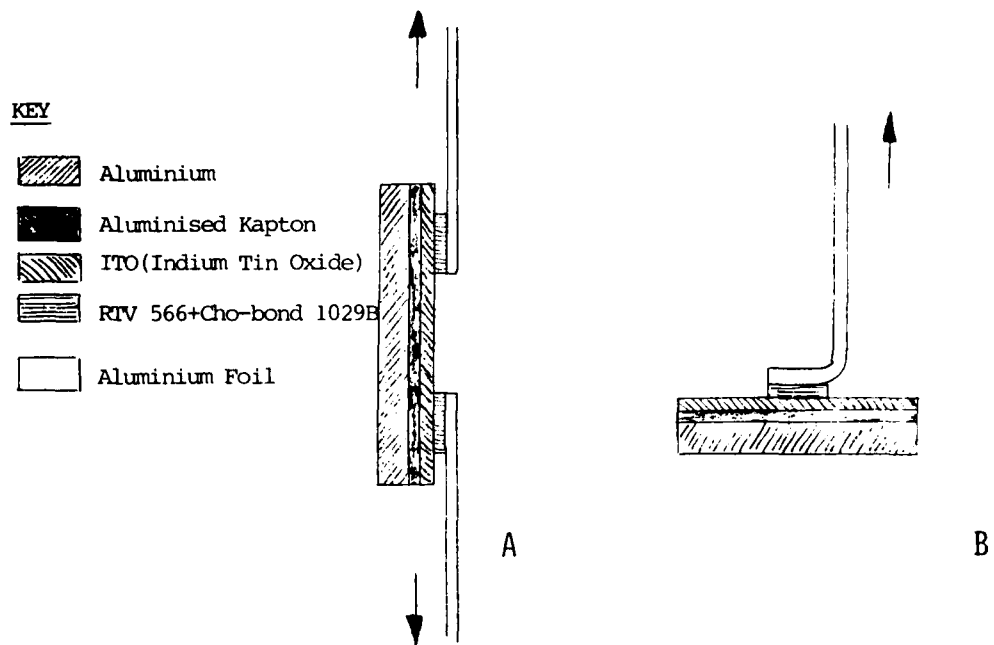


FIGURE 10 - Schematic showing test configurations : a) shear test
b) 90° peel test

TABLE 5 - TEST RESULTS FOR SHEAR AND PEEL SYSTEMS

SAMPLE No.	SHEAR TEST		90° PEEL TEST	
	Break Load	Failure Position	Pull off Load	Failure Position
A2	1240 gms	in Al foil	330 gms	Adhesive-in RTV566
A3	1400 "	"	305 "	"
A4	1450 "	"	218 "	"
A7	1740 "	"	290 "	"
A17	1690 "	"	287 "	"
A18	1380 "	"	255 "	"
A19	1460 "	"	210 "	"
A22	1480 "	"	280 "	"
A23	1560 "	"	308 "	"
A25	1290 "	"	308 "	"
A26	1560 "	"	210 "	"
A27	1320 "	"	340 "	"
A29	1150 "	"	220 "	"
A30	1505 "	"	270 "	"
A31	1455 "	"	282 "	"
A33	1080 "	"	270 "	"
A34	1440 "	"	309 "	"
A35	1140 "	"	265 "	"
A36	1320 "	"	258 "	"

23112 Contact Resistance Versus Applied Current Test

23112-1 Purpose of the test

To determine if an increase of the electrical current load through the grounding point would create more current paths and subsequently result into a lower contact resistance. The results of this test would indicate if micro-discharges could modify the contact resistance of a grounding point to an extent that further charging of the ITO-surface is avoided.

23112-2 test method

The contact resistance was measured according to the method described in Par. 2.3.4

The applied current was set at the initial level and remained at this level for 30 secs. after which the voltage drop over the contact resistance was noted. The current was then increased to the second step and the same procedure followed.

The current values were 0.5×10^{-7} , 1.0×10^{-7} , 0.5×10^{-6} , 1.0×10^{-6} , 0.5×10^{-5} , 1.0×10^{-5} , 0.5×10^{-4} , 1.0×10^{-4} , 0.5×10^{-3} , 1.0×10^{-3} , 0.5×10^{-2} , 1.0×10^{-2} A. followed by the same sequence back to the initial value.

23112-3 test results

Test results are illustrated in Fig. 11. All three samples showed an initial increase of contact resistance until a maximum value was reached, followed by a decline for higher current levels.

For the downward sequence the same curve characteristic was followed, except for the fact that the total curve was shifted towards lower resistance values.

The same pattern was followed by all three samples tested, independant of the initial resistance value.

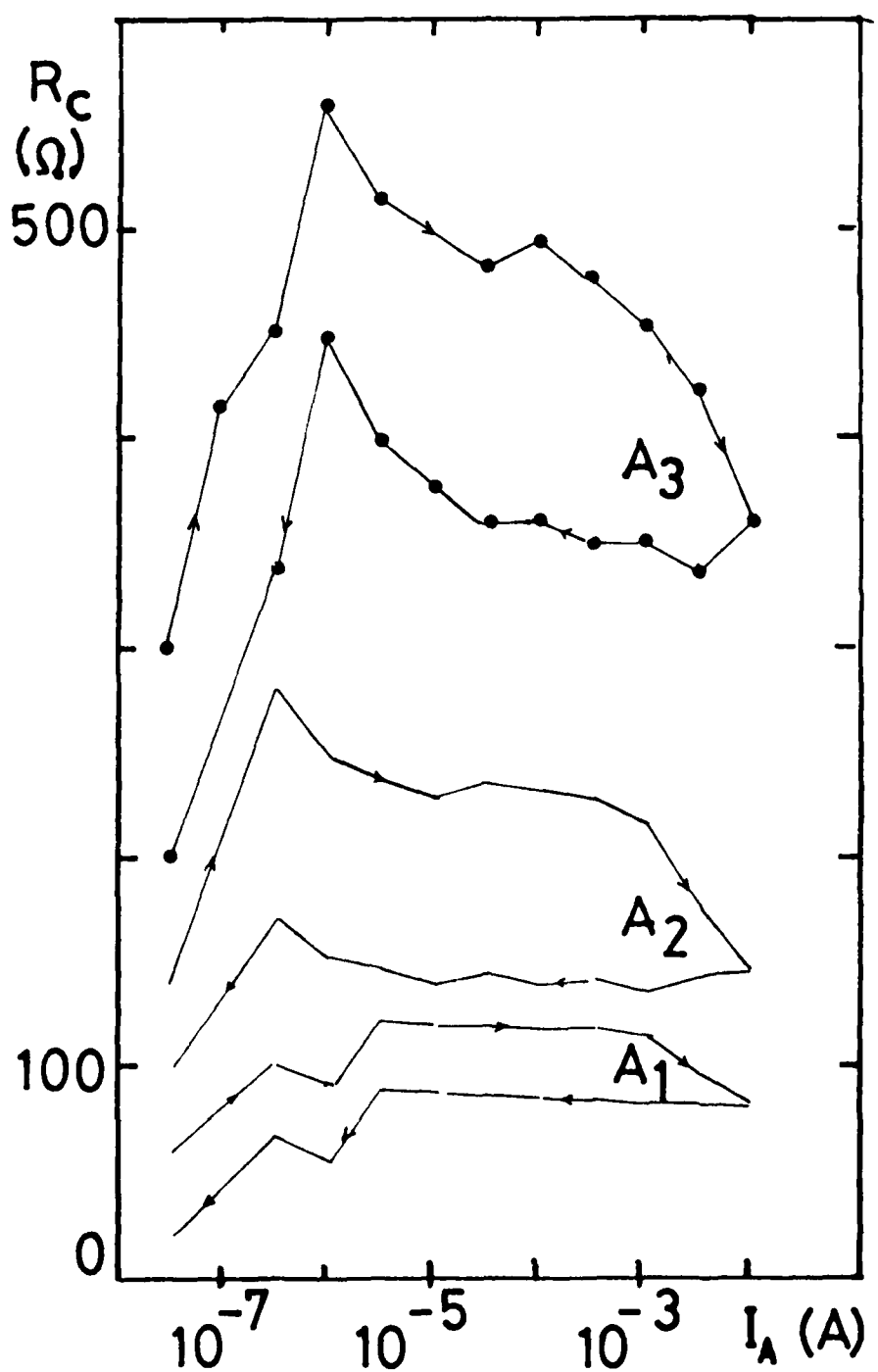


FIGURE 11
CONTACT RESISTANCE VERSUS APPLIED CURRENT

At the 1.0×10^{-5} Ampère level the contact resistance values were :

Sample	Up-Direction	Down-Direction
A1	119 Ω	86 Ω
A2	229 Ω	140 Ω
A3	484 Ω	359 Ω

The samples did not immediately return to their initial values of contact resistance. Resistance measurements 24 and 48 hours after the test, showed a slow increase of contact resistance.

23112-4 conclusion

If a grounding point does not initially have sufficient conductivity, local charging of the ITO surface can occur, the subsequent micro-discharges will create new current paths and lower the contact resistance to an extent that further charging is avoided.

23113 Long duration electrification test

23113-1 purpose of the test

To determine if the samples which had been through thermal cycling would recover to low contact resistance values if submitted to longer electrification times.

The results of the test would indicate if samples would behave adequately in a substorm environment, where there is a continuous electron flow through the material.

23113-2 test method

The contact resistance was measured according to the method described in Par. 2342

The samples were submitted to an applied current of 1.0×10^{-5} A during 2 hours.

23113-3 test results

The results are noted in Table 6.

TABLE 6 - RESULTS VERSUS ELECTRIFICATION TIME

t (min)	R _C (Ω)		
	Sample 30	Sample 31	Sample 32
0	56 K	582	6 K
5	37 K	479	5 K
20	15 K	306	2 K
40	5 K	251	1.5 K
60	3 K	206	1 K
90	1.3 K	152	580
120	51	131	492

23113-4 conclusion

All three samples show a significant decrease of contact resistance with electrification time.

Apparently the contact point can recover from the effects of thermal cycling.

23114 Electron charging under scanning electron microscope

23114-1 purpose of the test

It was decided to repeat the test for samples, which had been through one of the prequalification tests.

By this method it could be determined if one of the prequalification tests has detrimental effects on the behaviour of the grounding point under electron irradiation.

23114-2 test method

See Par. 23541

23114-3 test results

The following samples were tested :

Sample 17 : Chemical Spray Test

Sample 21 : Heat and Humidity Test

Sample 29 : Thermal Cycling Test.

Sample 17 showed several micro-discharges immediately after electron irradiation commenced, these were soon followed by a "quiet" period.

Samples 21 and 29 showed no evidence of charging or discharging.

23114-4 conclusions

Even though thermal cycling had increased the contact resistance of sample 29 to the K Ω -range, the sample did not discharge under electron irradiation.

The discharging of sample 17 is not apparent as the contact resistance after chemical spray was low, however it is not evident if the bubbling of the sample due to trapped air during pump-down of the S.E.M. sample compartment affects the contact resistance.

2.3.12 Discussion of results

In general it can be stated that the grounding points passed the prequalification programme except for thermal cycling.

The exact mechanism which causes the increase in contact resistance after thermal cycling is not well understood. The resistivity of the ITO-layer does not increase. However this adhesive formulation had been prequalified before on a thin aluminum substrate (5) and passed the thermal cycling test. Furthermore the mechanical stability of the bond after thermal cycling is excellent.

The only plausible conclusion is that a barrier layer is formed between the ITO-layer and the conductive adhesive during thermal cycling. This would explain why the sample recovers after longer electrification time.

The impact of the increased contact resistance on the performance of the grounding point is debatable. In particular as the grounding configuration shows no tendency to charge under electron irradiation and even shows recovery effects in standard laboratory conditions.

It is questionable if an extremely low contact resistance is required for the grounding of substrate material with resistivity in the $K\Omega$ to $M\Omega$ -region.

Even with contact resistances in the $K\Omega$ -range the incident electron flux of $10^{-9} A cm^{-2}$ in a substorm environment would be leaked to ground without significant charging.

A test panel of ITO coated aluminised Kapton with four conductive adhesive bonded grounding straps followed the prequalification programme and was submitted to simulated substorm environment. Results are given in Section 2-4.

(5) J. BOSMA, M. FROGATT, G. GOURMELON - "Evaluation of a conductive adhesive system for the grounding of aluminized Kapton tape, ESAM STM - 204 juin 1978

2 - 4 ELECTROSTATIC BEHAVIOUR IN A SIMULATED SUBSTORM ENVIRONMENT

2.4.1 Purpose of the experiments

The aim of this test was to determine the electrostatic behaviour in a simulated substorm environment for a component (ITO coated aluminized Kapton with its interconnects) before and after a prequalification program.

2.4.2 Samples used in the test

Two samples were prepared at the same time. A sketch is given in FIGURE 12. Each sample carries four aluminum strips (8 mm wide, 30 μ m thick) that were fixed on the ITO coated side of a Kapton SSM (ITO/Kapton/Alu 838 K1 sent by AFML/MBE) with the conductive adhesive, following the procedure described at section 2.3.2.

One of these samples (sample A) was stored in normal laboratory conditions for about 7 months.

The other one (sample B) was used in the prequalification program described Section 2.3 and went through the chemical spray, heat and humidity and thermal cycling steps. Due to a lack of time, the acoustic test was not performed on sample B.

Both samples were exposed in identical conditions to a simulated substorm environment in order to evaluate their performance.

2.4.3 Test facility

The CEDRE facility was used in its configuration MELEZE that allows the secondary emission to be measured (for more details see Section 3.2). The samples were irradiated in a high vacuum $3 \cdot 10^{-6}$ Torr) obtained by a turbomolecular pumping unit. The electron beam was delivered by an electron gun giving energies in the range 4 keV to 25 keV. The uniformity of irradiation (better than 10 percent) was obtained at the sample level by means of a scattering foil made of aluminum 1.5 micrometer thick.

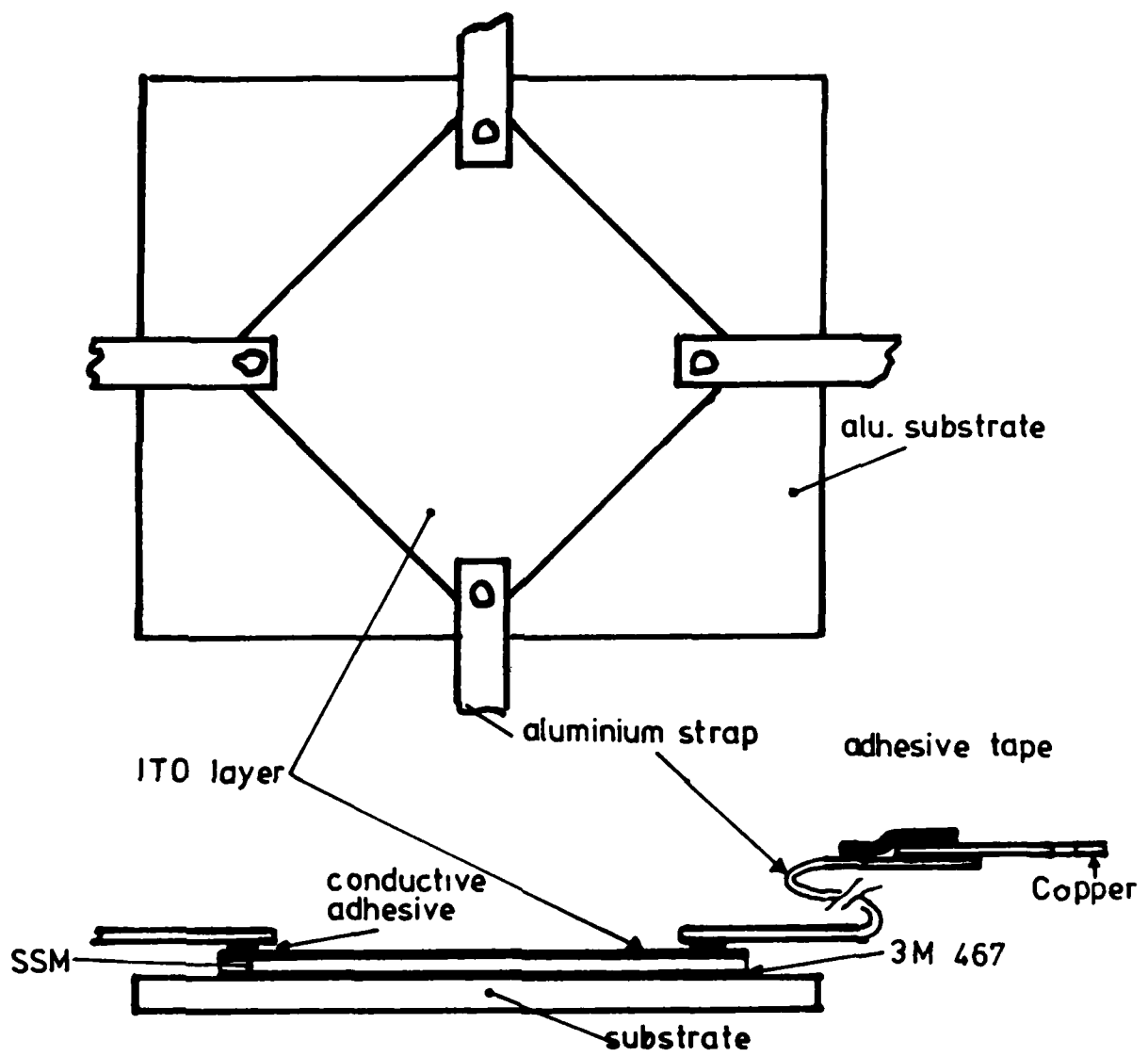


FIGURE 12 - SAMPLE DESCRIPTION

The sample under investigation is fixed onto an aluminum plate grounded through a nanoammeter (Keithley 616 electrometer). Each of the four aluminum straps can be connected with a feed-through to an ammeter. The secondary emission of the sample is measured with the collecting hemicylinder (See FIGURE 13).

The surface potential is measured with a capacitive potential probe that faces the samples and that is moved in a parallel direction to them. This measure is performed about 20 seconds after the stopping of irradiation. The sample holder must be rotated in order to allow the potential measurements.

Only a 6cm diameter surface was irradiated in the central part of both samples. This 6cm diameter was delimited by means of a grounded mask (FIGURE 14). It was not possible to prevent the electron irradiation of a part of the aluminum connections (about 4 cm^2).

2.4.4 Test procedure

The procedure that has been followed is given in TABLE 7. Three electrical currents are continuously recorded under electron irradiation. I_{sec} is the collected secondary emission. I_{surf} is the total current that is collected on the four aluminum strips. $I_L + I_c$ is the current that is collected on the sample holder. (See FIGURE 13).

2.4.5 Results - TABLE 8 summarizes the results

Both samples perform very well under the simulated sub-storm environment. No charge build up has been noticed and no breakdown has been evidenced. However, the secondary emission as well as the leakage current seem slightly higher for the sample that has been exposed to the prequalification program. But the total surface current (that is collected by the aluminum strips bonded with the conductive adhesive on the ITO) is still very high in the sample that has been aged. It is important to note that the surface current increases with the electron energy in the range that has been studied.

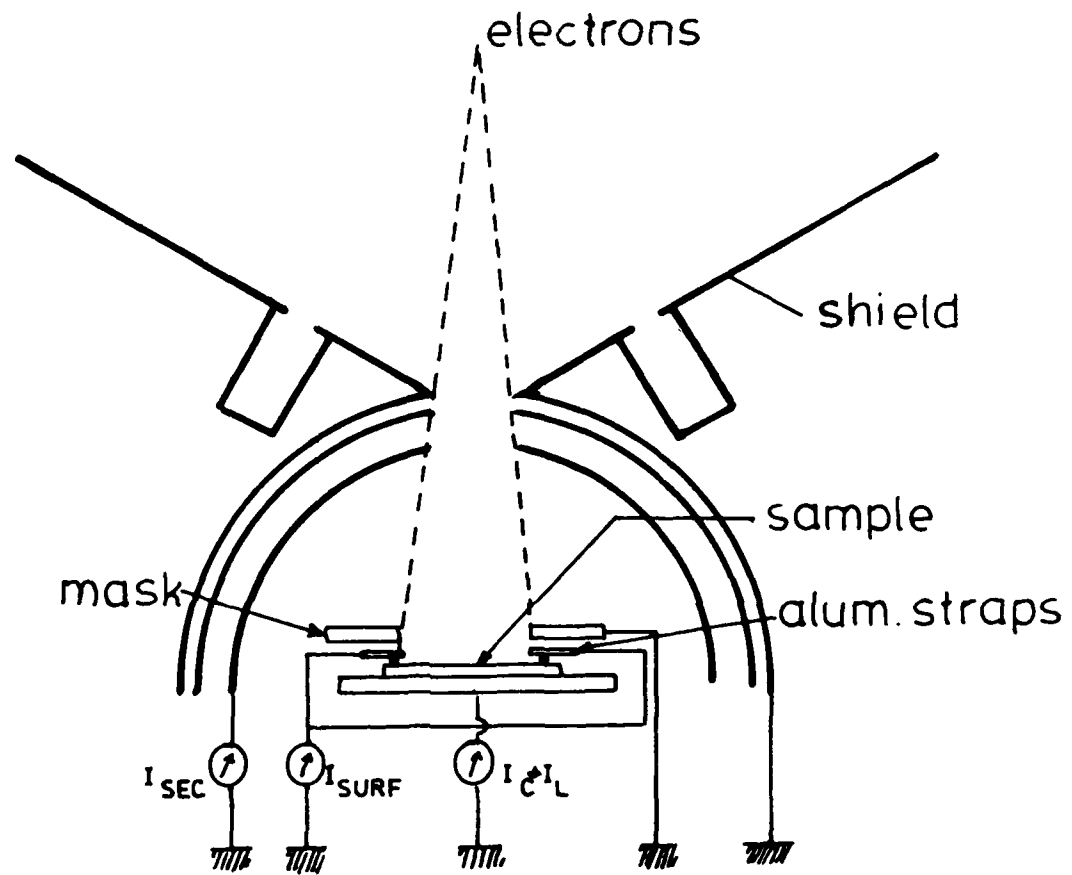


FIGURE 13
SCHEMATIC VIEW OF THE SAMPLE SETTING FOR
ELECTRON IRRADIATION

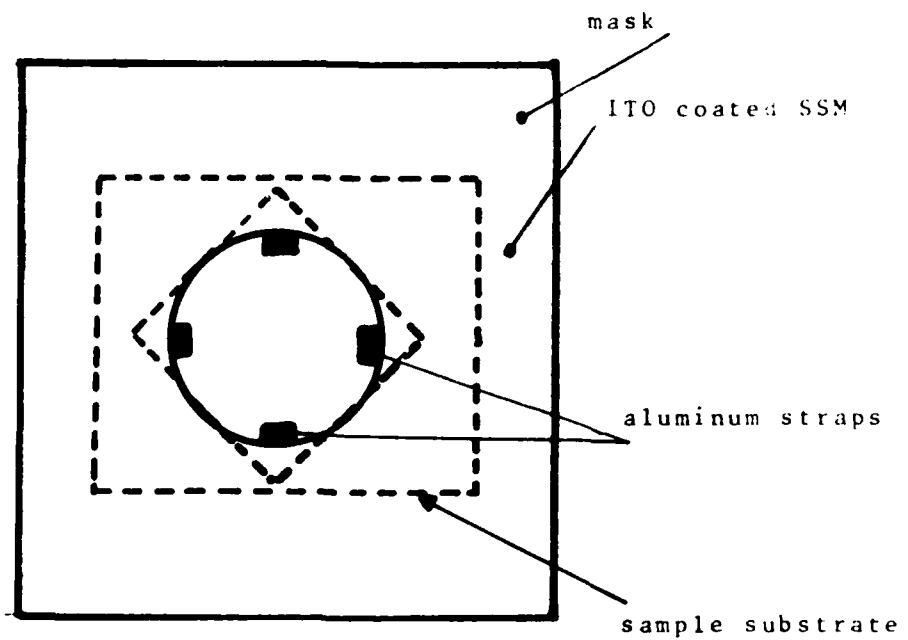


FIGURE 14
FRONT VIEW OF THE SAMPLE AND SAMPLE HOLDER
FOR ELECTRON IRRADIATIONS

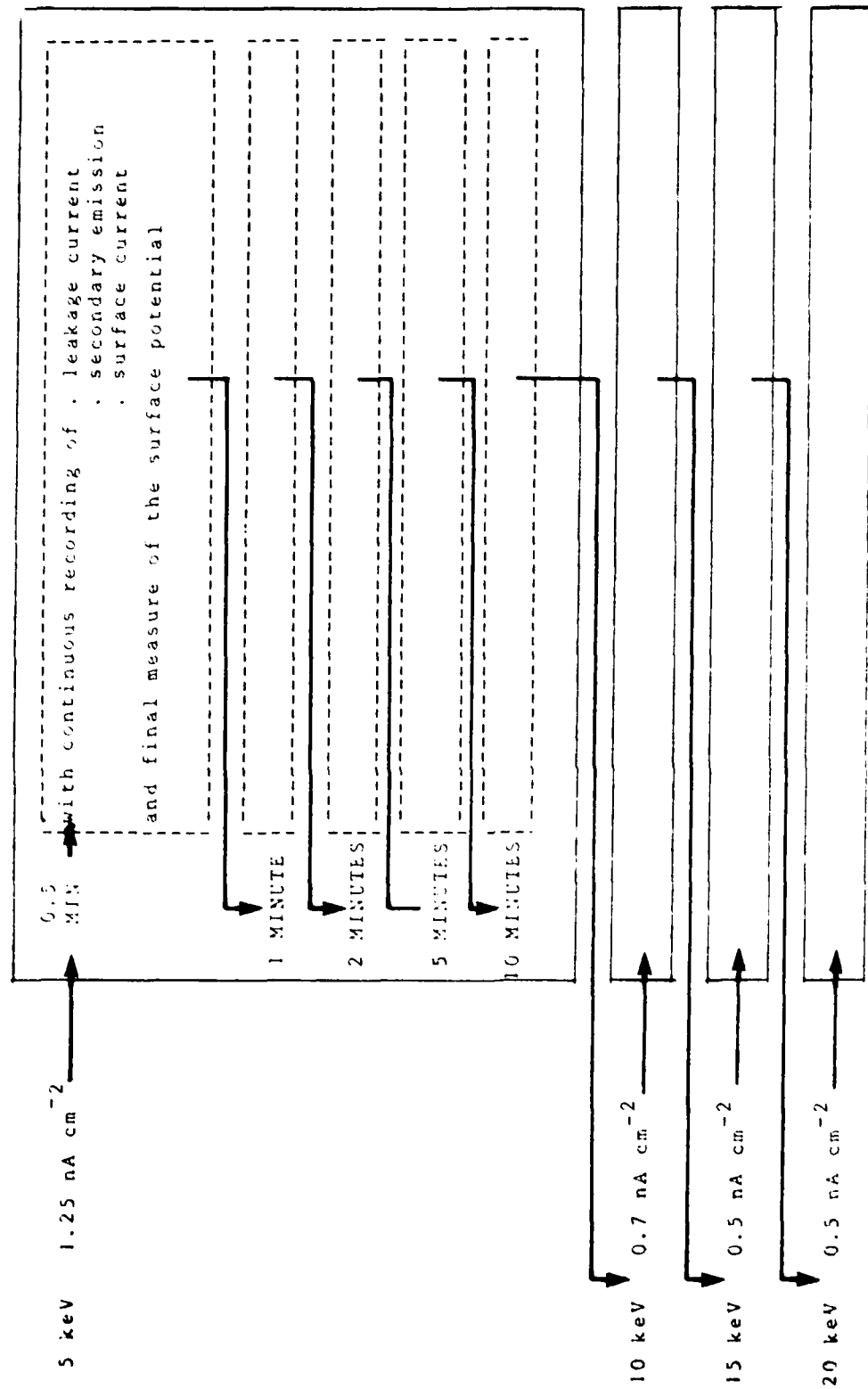


TABLE 7 - PROCEDURE FOR THE ELECTROSTATIC TEST

		BEAM ENERGY / INTENSITY					
		5 keV 1.25 nA cm ⁻²	10 keV 0.7 nA cm ⁻²	15 keV 0.5 nA cm ⁻²	20 keV 0.5 nA cm ⁻²		
V (volts)	< 10	< 10	< 10	< 10	< 10		
I _C + I _L (nA)	0.5	0.2	0.08	0.08	0.08		
I _{surf} (nA)	10.5	11.5	11	11	11		
I _{sec} (nA)	12	4	2.5	2.5	2.5		
Breakdowns	no	no	no	no	no		
V (volts)	< 10	< 10	< 10	< 10	< 10		
I _C + I _L (nA)	1	1.1	1.2	1.2	1.2		
I _{surf} (nA)	4	5.5	9	9	9		
I _{sec} (nA)	16	8	2.5	2.5	2.5		
Breakdowns	no	no	no	no	no		

TABLE 3 - BEHAVIOUR OF THE ITO-COATED KAPTON GROUNDED WITH A CONDUCTIVE
ADHESIVE IN A SIMULATED SUBSTORM ENVIRONMENT

2 - 5 FINAL CONCLUSIONS

It can be stated that an indium-tin-oxide coated aluminised Kapton material grounded with an aluminum strap bonded by means of a conductive adhesive is prequalified for use on application satellites.

For scientific satellites there is some reserve as the increase in contact resistance after thermal cycling could cause surface potentials to exceed the 1-Volt electrostatic cleanliness requirement for short periods of time. Further investigation of the exact mechanism which causes increases after thermal cycling would be required to determine if a 1-Volt potential level can be obtained.

Preliminary tests (not reported here) with other flexible SSM coated with conductive transparent layers have shown that similar electrical connections could be achieved with the same conductive adhesive and aluminum straps.

Other grounding means such as connection film-to-film with a common conductive adhesive fringe or connection film-to-metal substrate using the same adhesive in holes and over the oxide surface, could be considered with reasonable chance of succeeding.

SECTION III
SILICA FABRICS AND COMPOSITES

3 - 1 Introduction

Silica fabrics have been proposed for use as passive thermal control coatings that do not support charge build up under electron beam bombardment at energies to at least 30 keV with associated current density in excess of 30 nA cm^{-2} (6).

Such an excellent behaviour under simulated substorm conditions, has been explained (7) by a secondary emission conductivity (SEC) where secondary electrons produced by the primary electron beam are thought to be a cloud of free charges in the voids between the silica fibers within the dielectric material. If that is the case, the charging performance of the quartz fabric ought to be good only if this fabric is directly connected by its back face to a grounded metal plate.

However for space application, it is generally necessary to bond the fabric to a spacecraft structure. An adhesive could be used, but its migration through the voids between the silica fibers could lead to unstable optical properties under space radiation. A composite structure has been proposed that would solve this problem of outgassing (6). The composite is obtained by laminating at 280°C the quartz fabric with a FEP film and an aluminum

(6) A.E. EAGLES et al: Fabric coatings - A new technique for spacecraft passive temperature control - AIAA paper 65-668 AIAA 10th Thermoph. Conf. Denver, Colorado, May 1975

(7) V.J. Belanger, A.E. EAGLES: Secondary emission conductivity of high purity silice fabrics - Proceedings Spacecraft charging technol. Conf. Colorado Spring, October 1976

foil : FIGURE 15. Bonding of the laminate to the spacecraft

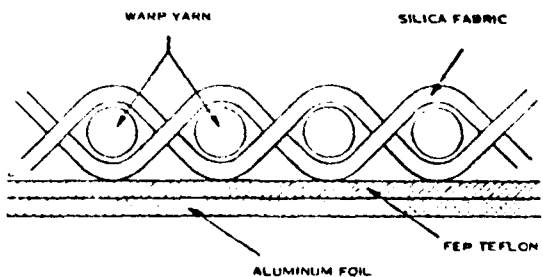


FIGURE 15
SILICA FABRIC - FEP - ALUMINUM FOIL COMPOSITE
(after (6))

structure can be accomplished with adhesives without the problem of the adhesive migration through the fabric. Moreover the overall optical properties are better for the composite due to the reflecting aluminum surface.

The composite quartz fabric/FEP film/Aluminum, owing to the dielectric nature of the FEP Teflon barrier between the silica fibers and the aluminum film should not allow the electric charges to be dissipated under substorm conditions even if the aluminum was grounded. Unexpectedly it was said ⁽⁸⁾ that the behaviour of the composite was good under electron beam bombardment (moderate potential surface, no sudden discharges) without special grounding techniques.

It was decided to verify such a behaviour and, if necessary, to explain it in such a way as to determine whether there is a necessity to ground the aluminum layer or the edges of the silica fabric when one uses the composite structure on board a spacecraft. In this particular case, the interconnection and grounding techniques should be studied.

(8) N.J. STEVENS, F.D. BIRCOPEC, J.V. STASKUS, R.A. BLEEN, S.J. NARCISO - Testing of typical spacecraft materials in a simulated substorm environment - Proc. 1st Spacecraft charging Technol. Conf. Colorado Springs, october 1976

Various comparative tests were programmed in order to evaluate the charging performance of diverse configurations all including silica fabrics with or without electrical grounding.

The DERTS substorm simulation facility called "CEDRE" was used for all the experiments. It was modified in order to provide direct measurements of the secondary emission and of the surface current together with measurements of surface potentials and leakage currents.

3.2.3.1 ELECTROSTATIC CHARGING FACILITY

3.2.4 General requirements for substorm simulation

Electrostatic testing of coatings requires adequate substorm environment simulation and associated instrumentation for characterization of the induced effects.

Simulation of the electrons of the plasma can be achieved by means of quasi-monoenergetic electrons in the 5 to 25 keV energy range and fluxes up to 10 nA/cm^2 . These electrons can be produced by the scattering of a focused beam delivered by an electron gun and directed to an aluminum thin foil. The transmitted beam is enlarged enough to irradiate a $(200 \times 200) \text{ mm}^2$ surface with a good homogeneity.

Due to scattering the transmitted beam is no longer monoenergetic. Its energy spectrum has been measured for various incident energies and foil thicknesses. FIGURE 16 shows the energy spectrum for an incident primary energy of 18 keV. This spectrum is widened in the range of the low energies compared to the direct primary beam spectrum.

Simulation necessitates also possibility of illuminating the irradiated samples with ultra-violet light (sun light simulation), performance of irradiation under vacuum at controlled temperature.

The simulation chamber used at DERTS is founded upon the afor-mentioned structure.

3.2.2. Parameters of interest

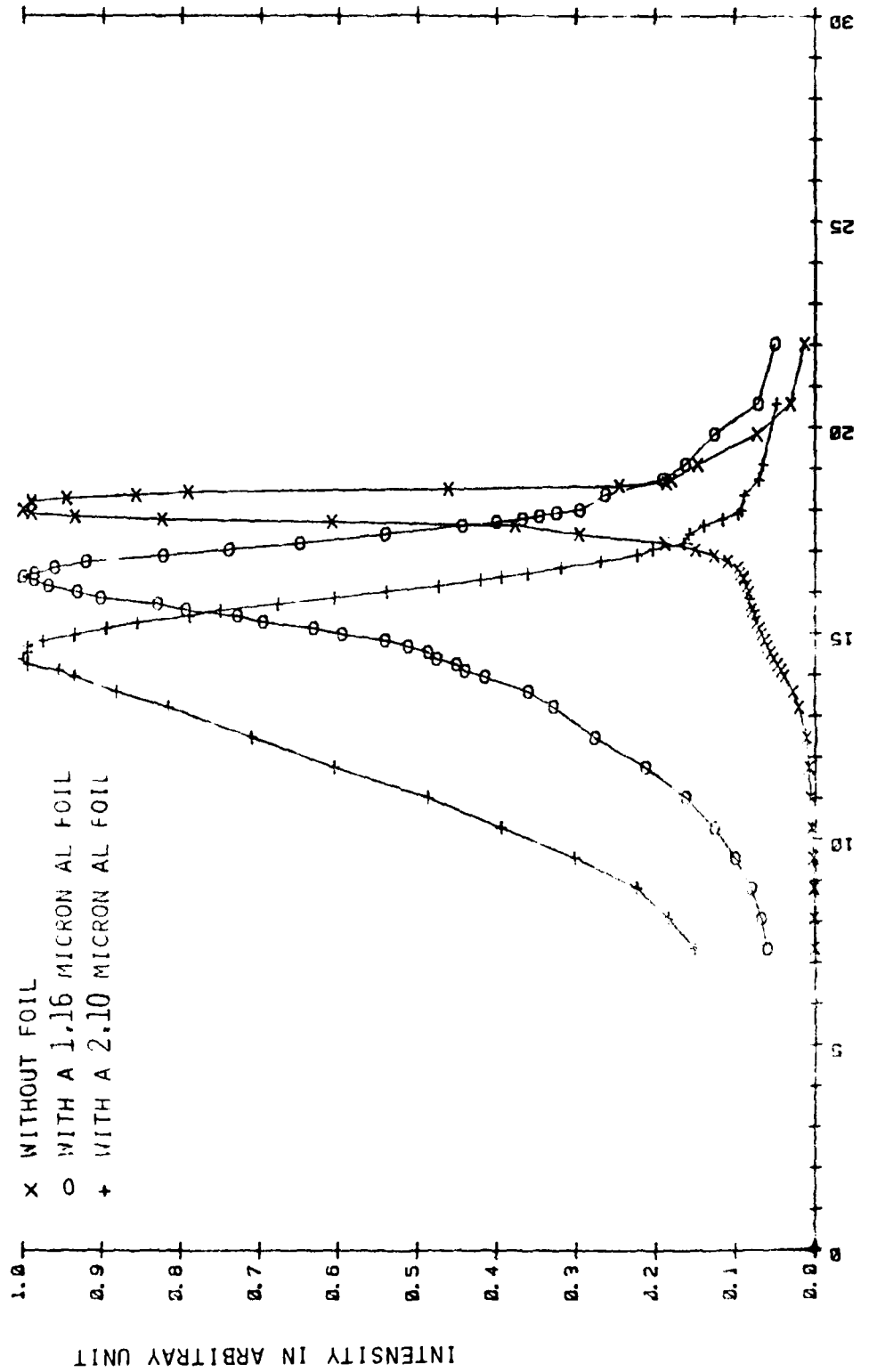
The main expected informations are the following :

- surface potentials or surface potential profiles
- volume leakage currents (or sample-to-holder currents)
- secondary emission currents

THIS PAGE IS BEST QUALITY PRACTICABLE
FROM COPY FURNISHED TO DDC

SCATTERED ELECTRONS SPECTRUM

INCOMING ENERGY = 18.0 KEV



ELECTRON ENERGY SPECTRUM AFTER SCATTERING THROUGH AN ALUMINUM FOIL

FIGURE 16

- breakdown (*) currents (shape and magnitude of the current pulse generated by sudden discharging)
- visual inspection and photography of samples under electron irradiation (localization of arcing).

3.2.3 The facility

FIGURE 17 is a schematic view of the "CEDRE" (Chambre pour l'Etude Des Revêtements sous Electrons) facility used to assess the electrostatic behaviour of dielectric coatings in simulated geosynchronous substorm environment.

General structure of the vacuum chamber is cylindrical. Turbomolecular pumping units allow the chamber and the electron gun to be operated at pressure levels less than $5 \cdot 10^{-5}$ Torr. The electron gun (SAMES manufacturer) works in the range 4 to 25 keV with fluxes at the sample level up to 10 nA cm^{-2} . An aluminum foil 1,2 μm thick is used in order to scatter the electrons.

The sample holder is made up of 4 plates (200×200) mm^2 each maintained at fixed temperature with a circulating fluid. This holder is fixed onto a rotating shaft allowing the presentation of any of the four plates in front of the energetic electron beam. In normal conditions, two faces can receive samples, the two others being used as Faraday cup holder, energy and surface potential measurement calibration systems.

Two samples of (200×200) mm^2 can be tested without opening the chamber so as to perform comparative tests on them. The irradiated area is restricted at the sample level to a 60 mm diameter circle, by use of collimating openings, if it is wished.

(*) The word "breakdown" will be generally used in the next sections. It does not refer to an actual dielectric breakdown closely related to the electric strength of an insulator. It is only related to disruptive phenomena that occur in particular conditions involving the macroscopic and even microscopic structure of the total assembly under test.

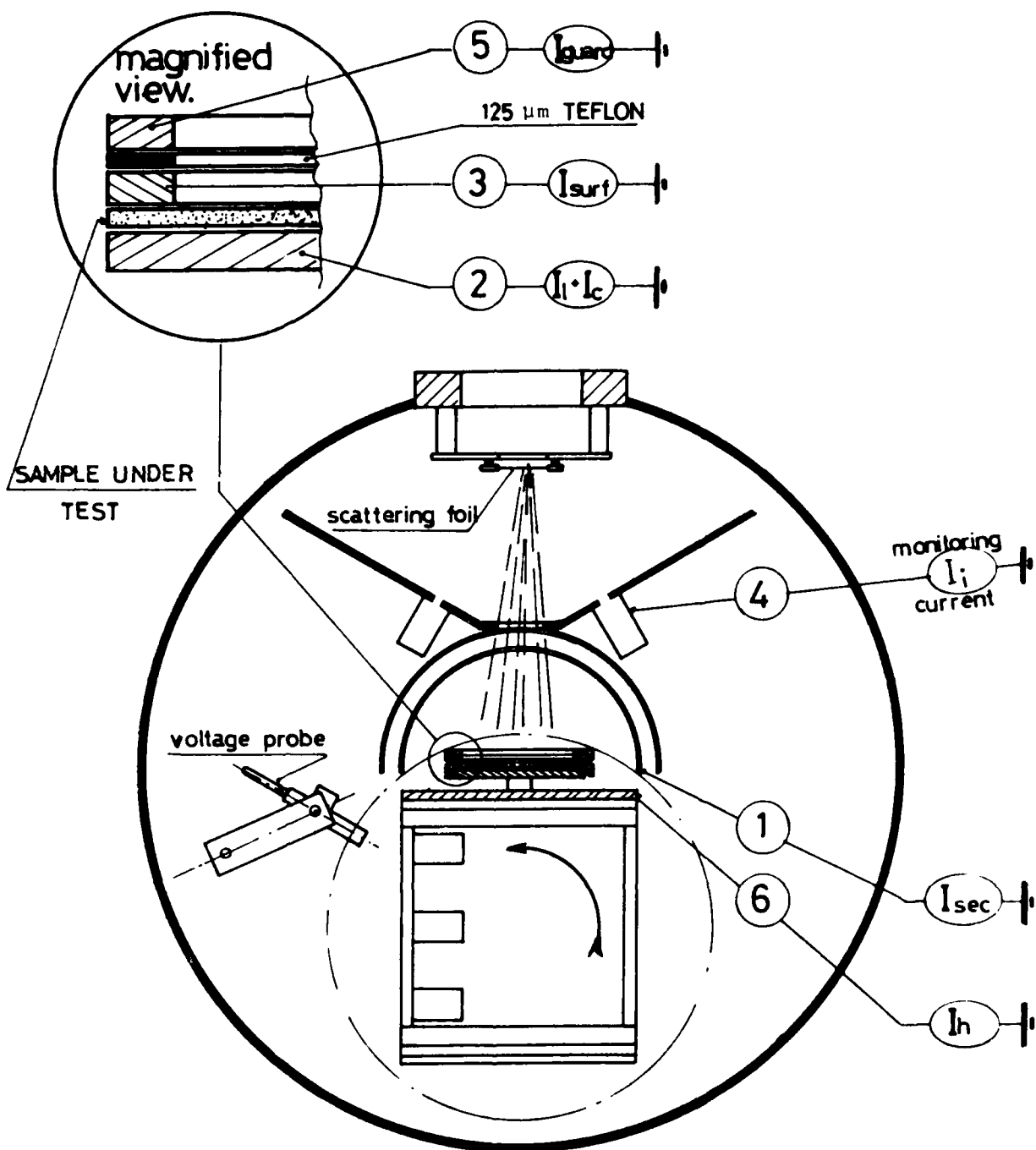


FIGURE 17
"CEDRE" SUBSTORM SIMULATION FACILITY

The surface potential is measured by a potential probe held by a mechanical scanner. An electronic instrumentation is fed by the signal emitted by the probe and moves with it under vacuum. A potentiometer system yields its vertical position and allows recording on a X-Y plotter the surface potential profile of the electrically charged coating.

The secondary electrons can be measured together with the backscattered electrons by means of a collecting hemispheric electrode ① surrounding the irradiated area (see FIGURE 17) (*).

The fixation system of the sample allows measurement of the surface leakage current on a circular ring ③ lying on the sample surface but out of the irradiated area. A guard circular ring ⑤ electrically insulated from the ring ③ by a 125 micro-meter thick FEP film covers the whole ring ③ .[Note that in case of measurements using electrodes ③ et ⑤ , the sample under irradiation is grounded by its periphery. However it is possible to disconnect from ground the rings ③ and ⑤ in order to provide a sample grounding only by its back face. These two possibilities were always used for the experiment we will describe below.]

The coating is fixed onto a metallic plate ② which is grounded to earth by means of a nanoammeter giving the volume leakage current plus the capacitor charging current. ④ , ③ and ⑤ are also grounded by means of other nanoammeters. All the currents are simultaneously recorded.

Two fixed Faraday cups ④ are used to continuously monitor the electron flux during the irradiation.

Under certain circumstances, a current measured on a metallic plate ⑥ next the sample but set back from the sample surface needs also to be measured.

(*) When this collecting hemisphere is used, the facility is said to be used in "MELEZE" configuration. This collecting electrode was specially designed for the work that is reported hereunder.

3.2.4 The irradiation procedure

before starting the irradiation, the mobile Faraday cups are placed facing the beam which is set to the desired values of energy and intensity. When the beam is set to its correct value, the information on Faraday cups ④ are read so as to monitor the irradiation later.

Then the beam is stopped by a mechanical shutter powered by a motor. The sample is placed facing the beam (by rotating the shaft of the holder). All the current values issued from ①, ②, ③, ④, ⑤, respectively secondary emission current, I_{sec} / leakage + charging current, $I_L + I_C$ / surface leakage current, I_{surf} / current collecting on the guard, I_g / current collected on the holder, I_H as well as the monitoring irradiation current I_i are recorded versus the time. The irradiation is started by opening the shutter.

After fixed duration times of irradiation (0.5, 1, 2, 5 and 10 minutes) the irradiation is stopped and the surface potential is measured after the sample holder was rotated and placed in front of the potential probe.

Both samples on the holder were tested in the same conditions of energy and intensity before selection of new conditions of energy and intensity. Four energy levels were used : 5, 10, 15 and 20 keV with intensities of 1.25, 0.7, 0.5 and 0.5 nA cm^{-2} respectively.

The test procedure is the same that is given in TABLE 7.

At the end of each irradiation stage and before starting the next, the samples were totally discharged by irradiating them with low energy electrons.

3 - 3 SAMPLE CONFIGURATIONS THAT HAVE BEEN STUDIED

3.3.1 Scope

Secondary emission, volume leakage current and surface leakage current are the three ways electrons are likely to escape from an irradiated dielectric coating and therefore to contribute to lower its surface potential.

To determine the relative importance these three discharging processes take in the setting of surface potential is of prime importance. As a matter of fact such a knowledge could help to fix the best directions for use in order to lower the surface potential value and to suppress the arcing risks.

So, it was the main purpose to evaluate and to understand the electrostatic behaviour of silica fabrics and of composites such as quartz fabric /FEP/Alu since the intermediate FEP layer could be thought to act as a barrier limiting the "volume" leakage current" of these composites.

On the other hand, the behaviour of such a composite when layered on a dielectric material (for instance, an adhesive) is a subject in which spacecraft system designers are greatly interested since it could lead to a practical possible application.

This statement led us to the various study configurations here under described.

3.3.2 Silica fabric

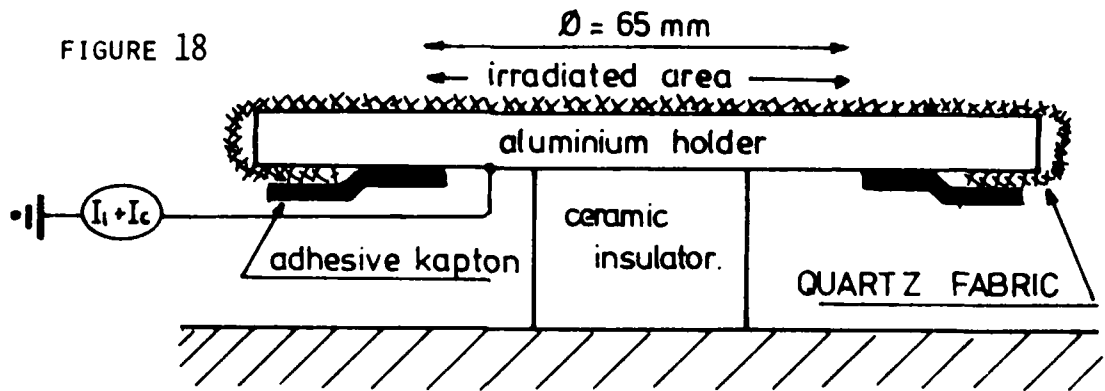
The material we have used, was sent by AFML/MBE. It is a quartz fabric heat cleaned at 800° for 3 hours.

5 different settings were used. They are described here under. They were progressively modified as we started collecting first results. Most of the work that will be reported is however related to settings 3.3.2 a and 3.3.2 b since comparative tests were extensively performed with the same settings using the composite silica fabric/FEP/Aluminum instead of the quartz fabric

3.3.2. α

QUARTZ FABRIC on aluminum holder and attached with kapton tape at the holder back side.

FIGURE 18

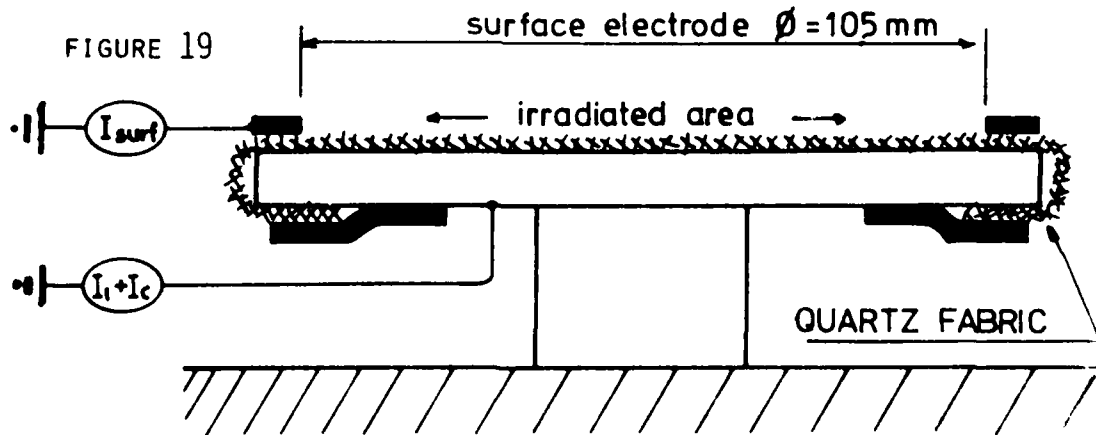


3.3.2. β

QUARTZ FABRIC on aluminum holder (with a circular ring used as a surface leakage current collector electrode).

This ring was put after we found that the surface potential profile measured with the setting 3.3.2 α presented very sharp variations. The aim was to maintain the fabric in close contact with the aluminum plate all over its surface. Additionally it was used to collect surface currents. (Actually the new potential profiles were found to be more flat).

FIGURE 19



QUARTZ FABRIC on aluminum holder with two circular rings.

The lower ring is used as in 3.2.3.8 as a surface leakage electrode.

The upper ring (insulated from the lower) is used as a guard electrode to prevent the surface leakage electrode from receiving secondary electron emitted by the sample or reemitted by the hemispheric electrode. A small current, not always negligible compared to the surface leakage current was measured.

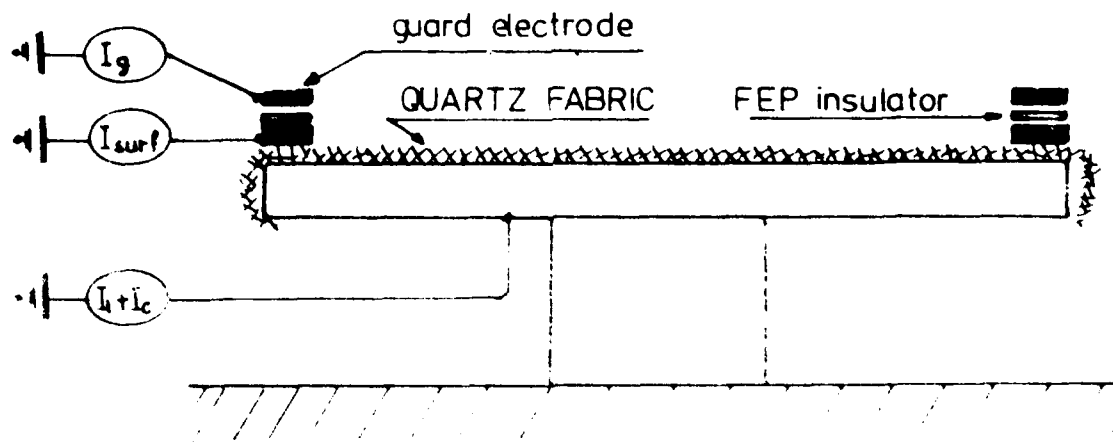


FIGURE 20

QUARZ FABRIC on aluminum holder with two circular rings is in 3.3.2 a but the inner diameter of the rings is the same (very slightly higher) as the diameter of the irradiated area.

The leading idea was that the surface conductivity of the irradiated area could be much higher than the one of the non irradiated area and gave rise to surface leakage currents much more important. (This was not corroborated by the experiment we performed).

This setting was used for irradiation of one layer or three layers of the silica fabric as well as for irradiation of the composite quartz fabric FEP-Aluminum (See Section 3.3.3 a)

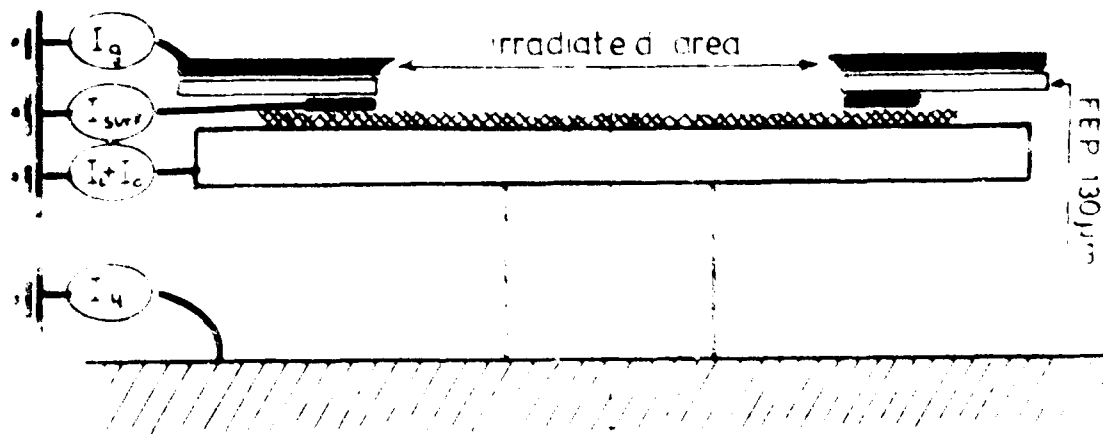


FIGURE 21

In addition of the currents I_{surf} , $I_c + I_c$, I_g , (see measurement of the current I_g collected on a plate next to the sample) it is not possible

3.3.2 b

QUARTZ FABRICS on FEP on aluminum holder with two circular rings as in 3.3.2 a. A 50 micrometers thick FEP film layered between the fabric and the aluminum holder is supposed to be equivalent to any non conductive adhesive used to apply the fabric on any spacecraft conducting surface. The same setting was equally used with the composite instead of the quartz fabric (See setting 3.3.3.b)

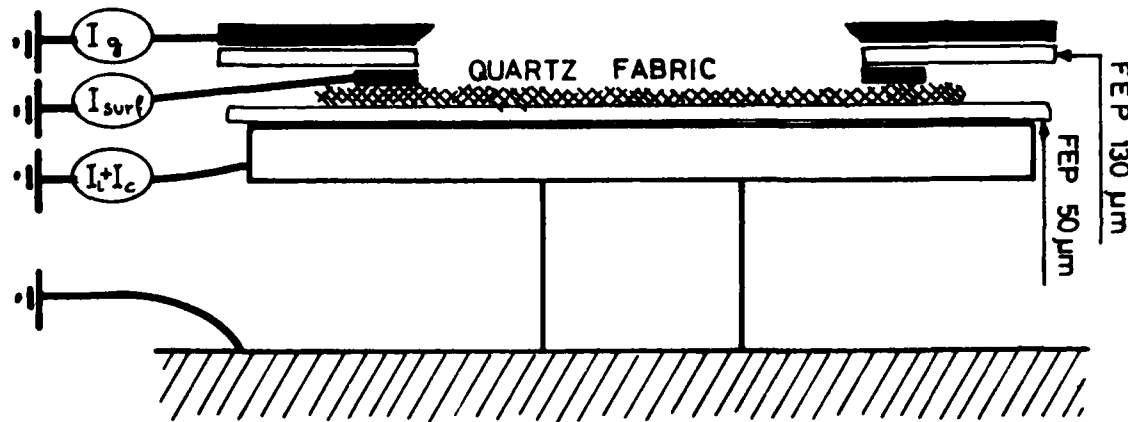


FIGURE 22

3.3.3. Composite (QUARTZ FABRIC/FEP/ALU)

The material we have used was sent by AFML/MBE. It is a laminate 581 Astroquartz/FEP/Aluminum.

As said just above, two different settings were used.

3.3.3. a

Composite on aluminum holder with two circular rings as in 3.3.2 a. The aluminum back layer of the composite is in electrical contact with the aluminum holder. (FIGURE 23)

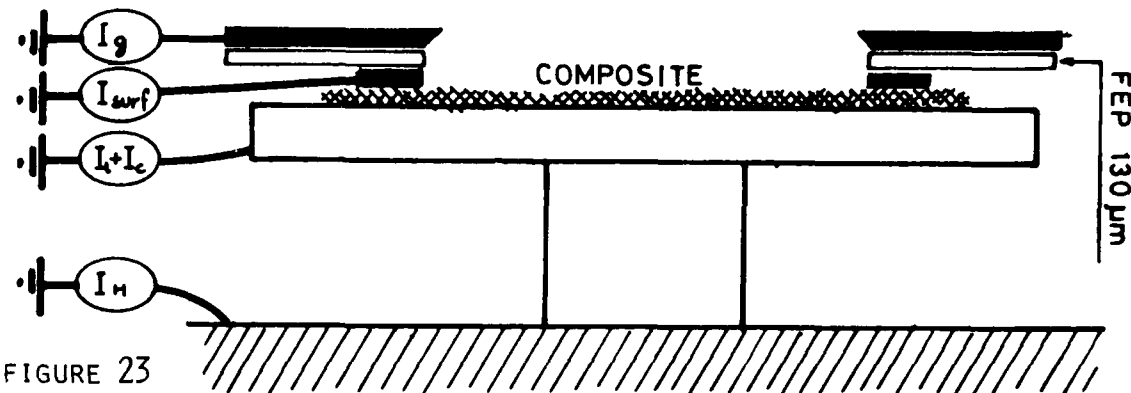


FIGURE 23

3.3.3. b

Composite on FEP on aluminum holder with two circular rings. The aluminum layer is let floating in this study configuration that uses a 50 micrometer thick FEP film (FIGURE 24)

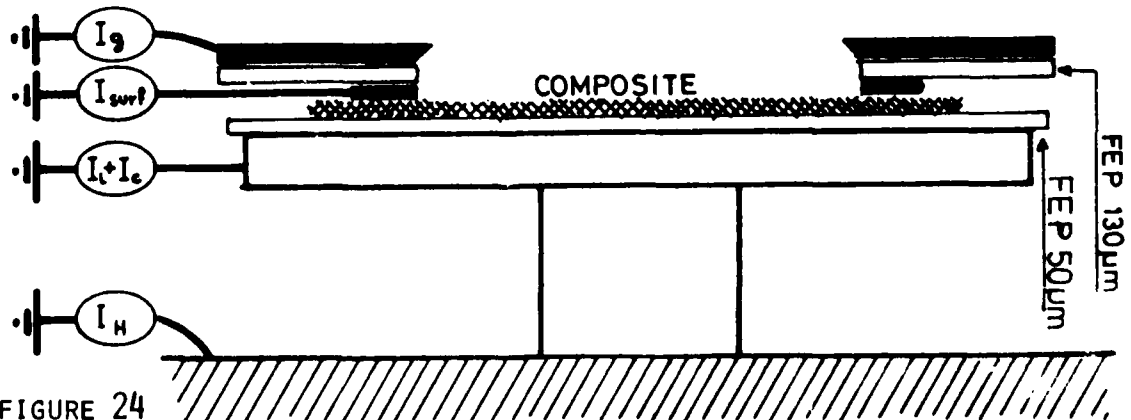


FIGURE 24

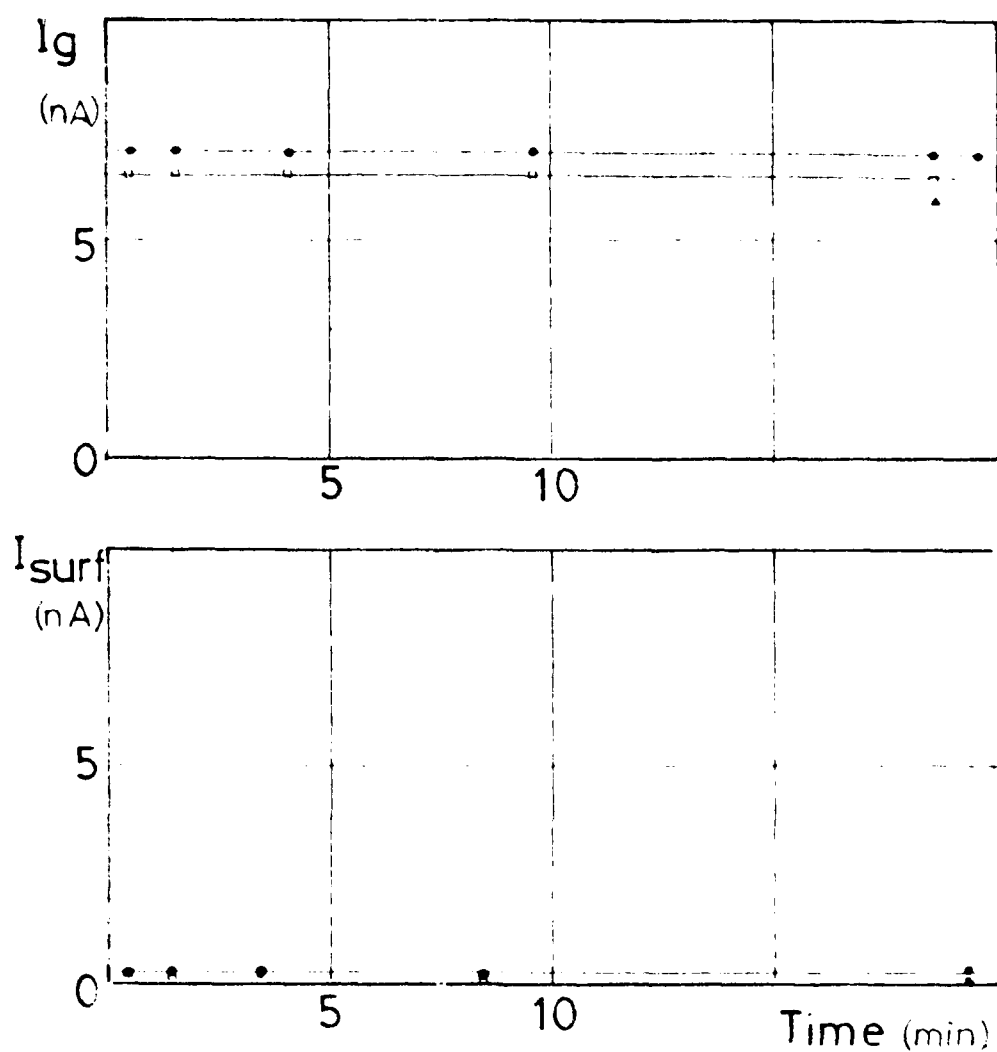


FIGURE 25

5 KEV ELECTRON IRRADIATION (1.25 nA cm^{-2})

- SILICA FABRIC (1 LAYER)
- SILICA FABRIC (3 LAYERS)
- ▲ SILICA FABRIC (1 LAYER) OVER FFF FILM

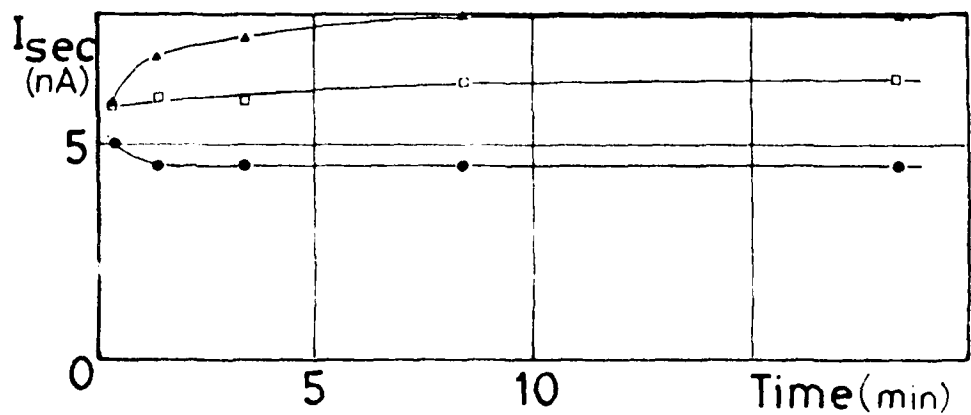
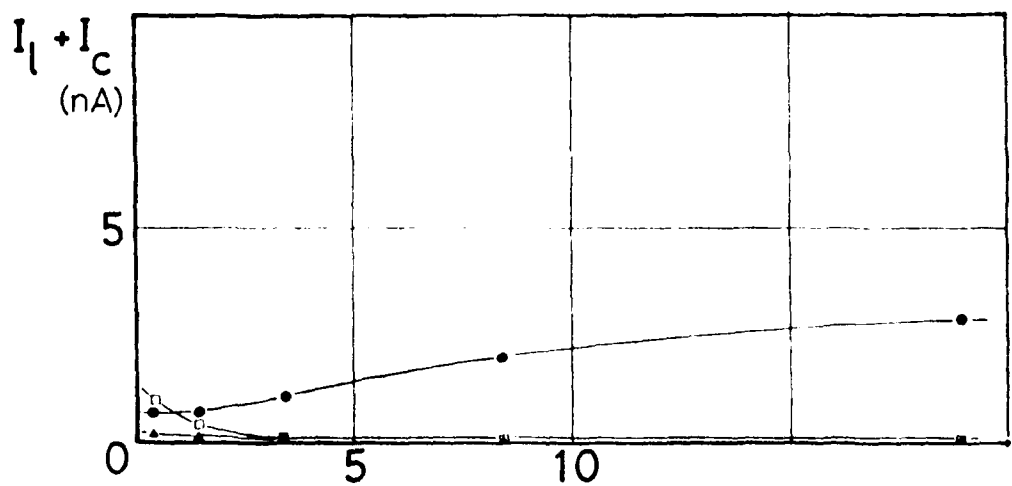
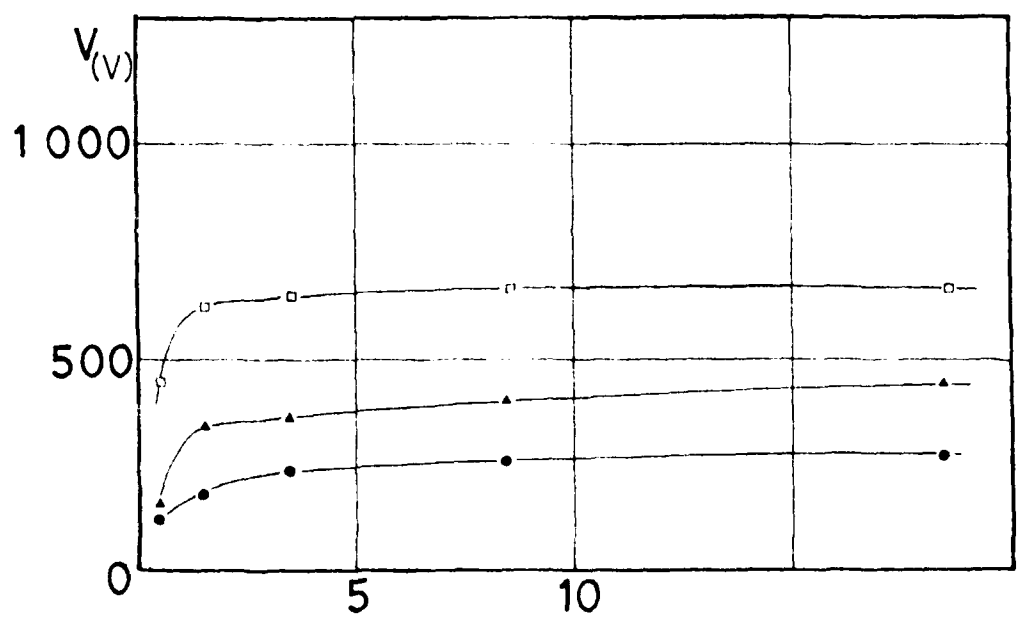
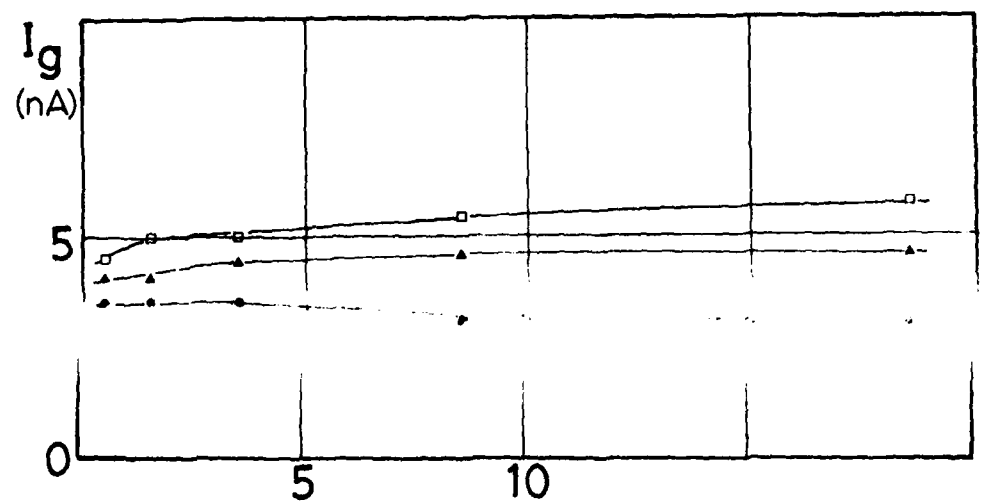
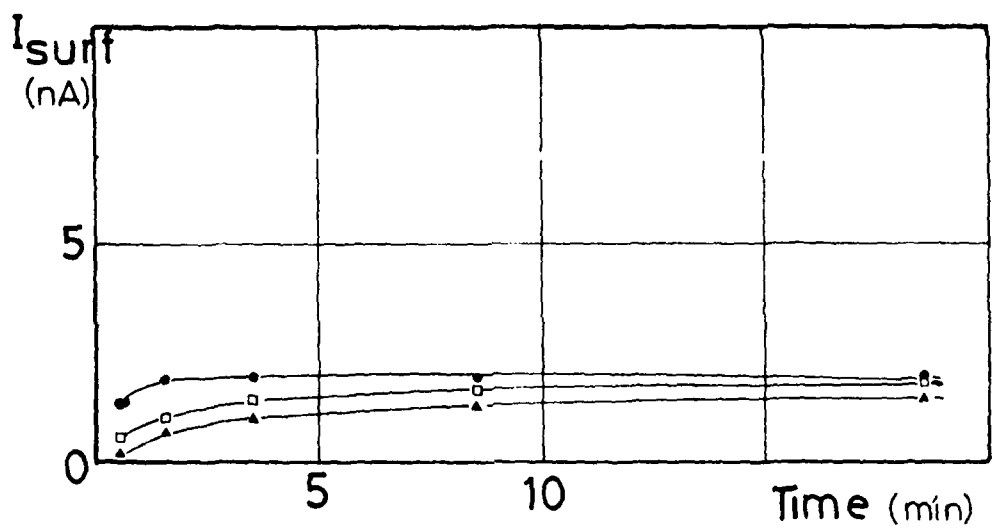


FIGURE 26



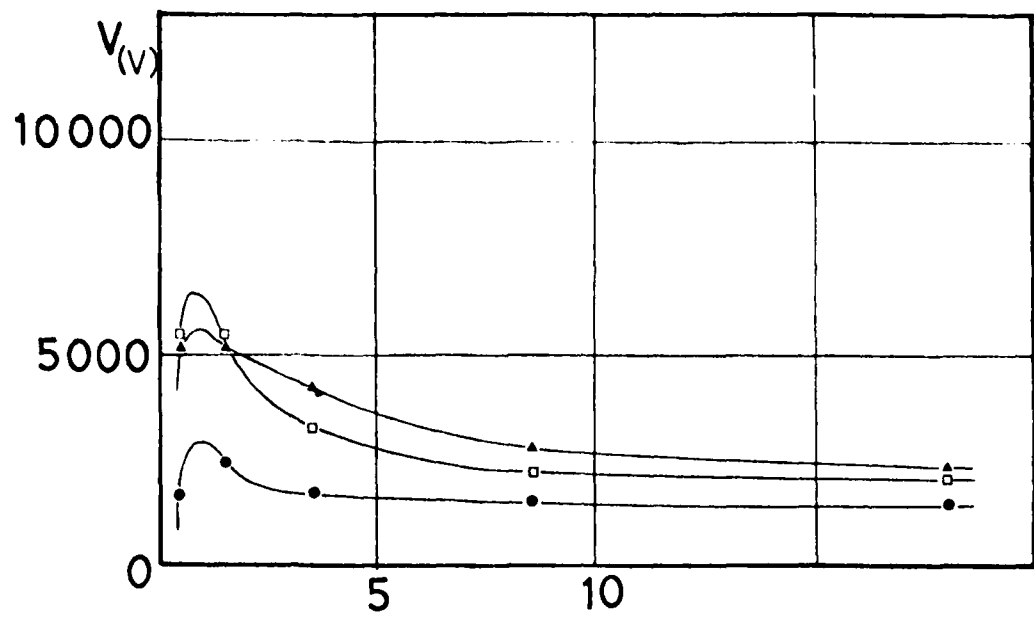
(D)



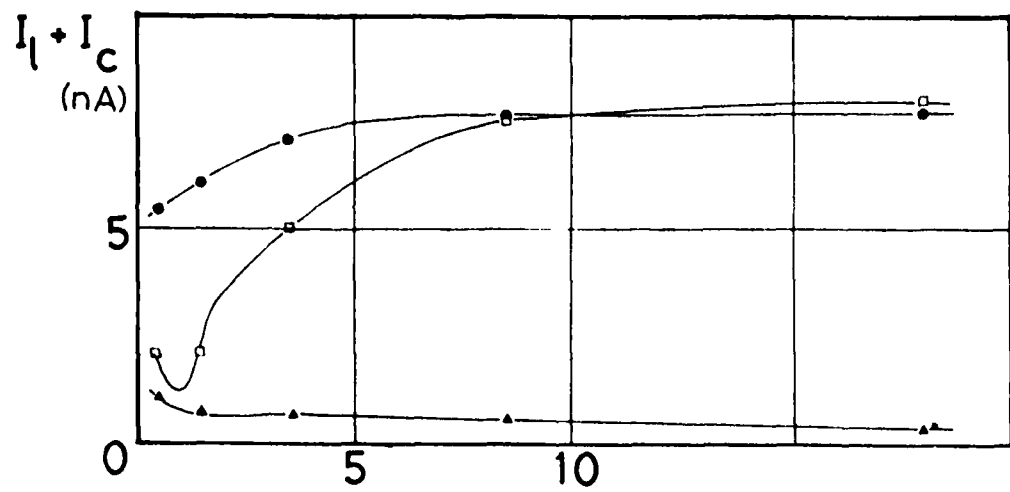
(E)

FIGURE 26
10 KEV ELECTRON IRRADIATION ($0.7, \text{ nA CM}^{-2}$)

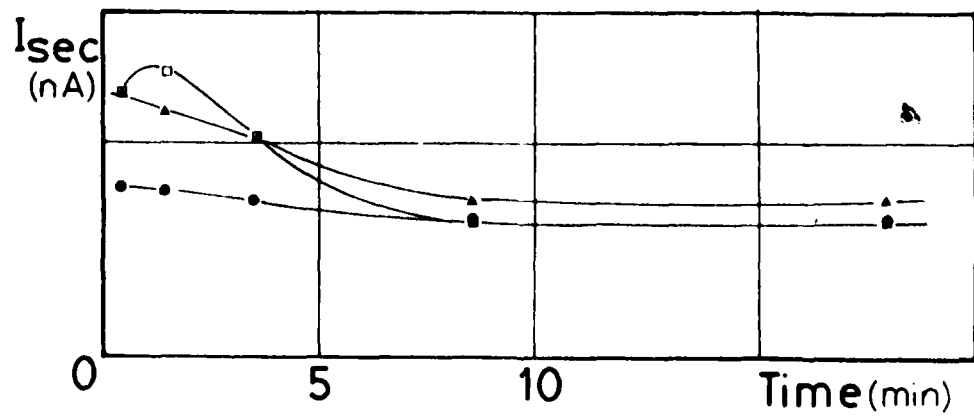
- SILICA FABRIC (1 LAYER)
- SILICA FABRIC (3 LAYERS)
- ▲ SILICA FABRIC (1 LAYER) OVER FEP FILM



(A)



(B)



(C)

FIGURE 27

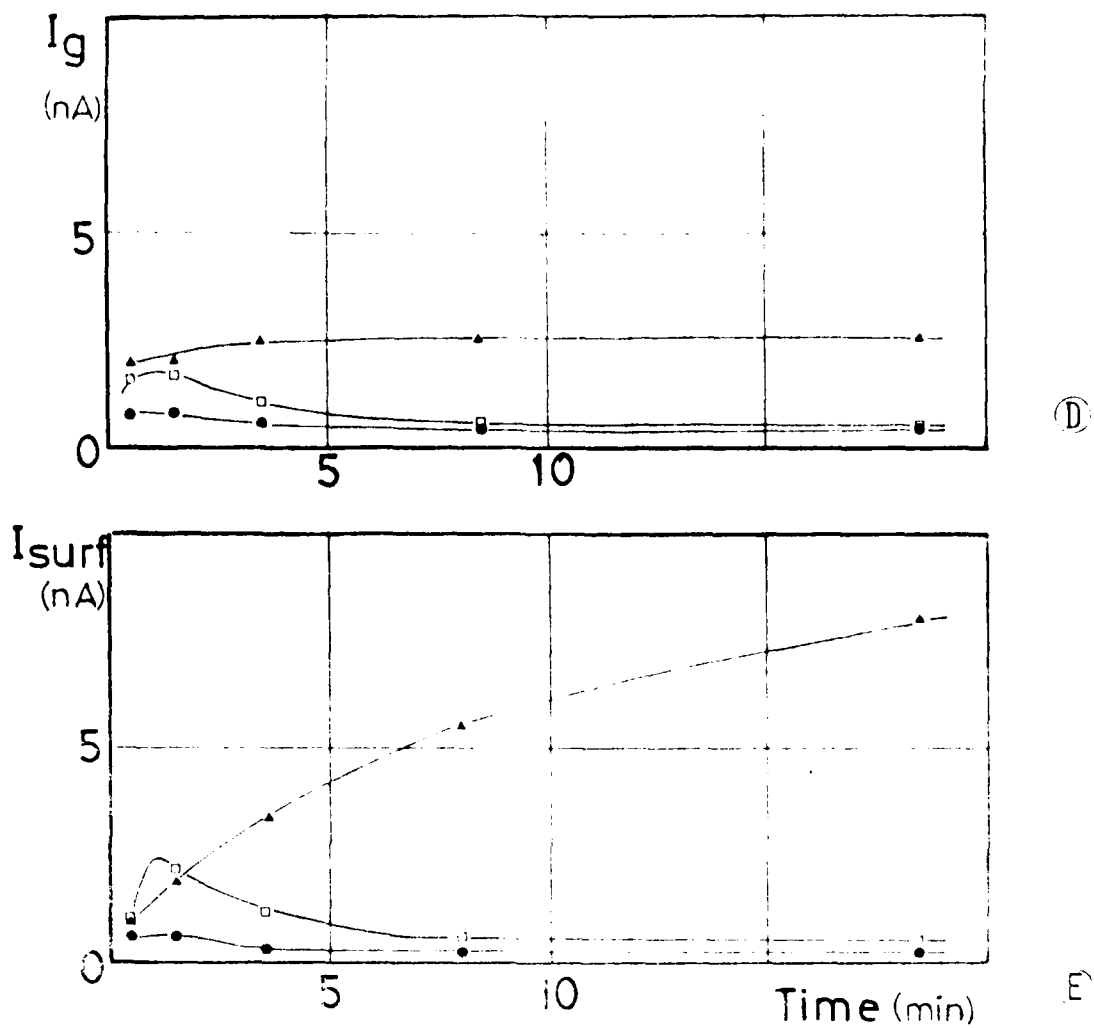
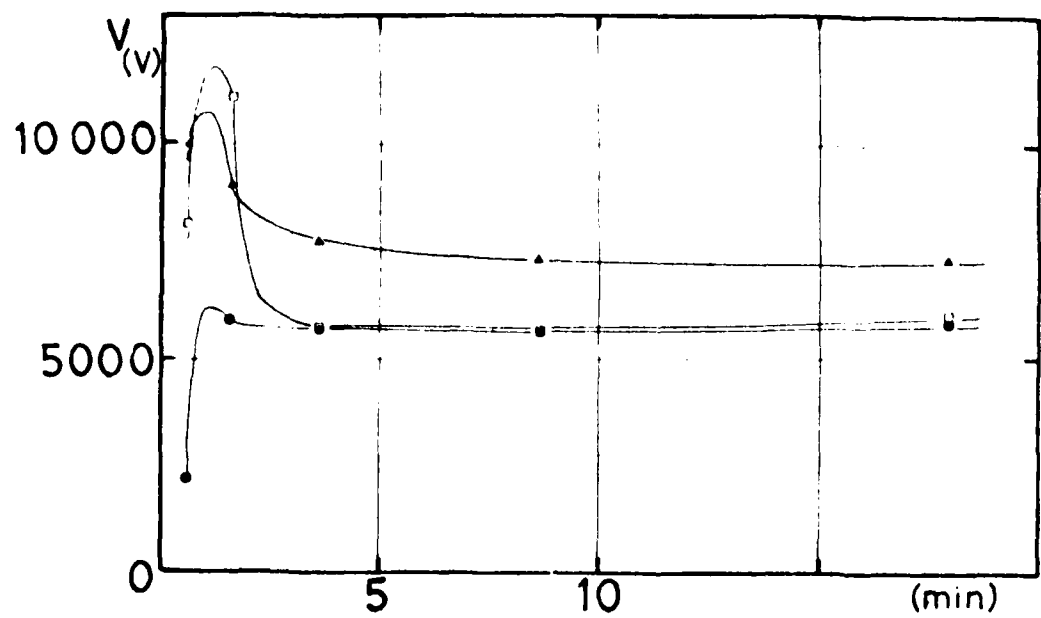


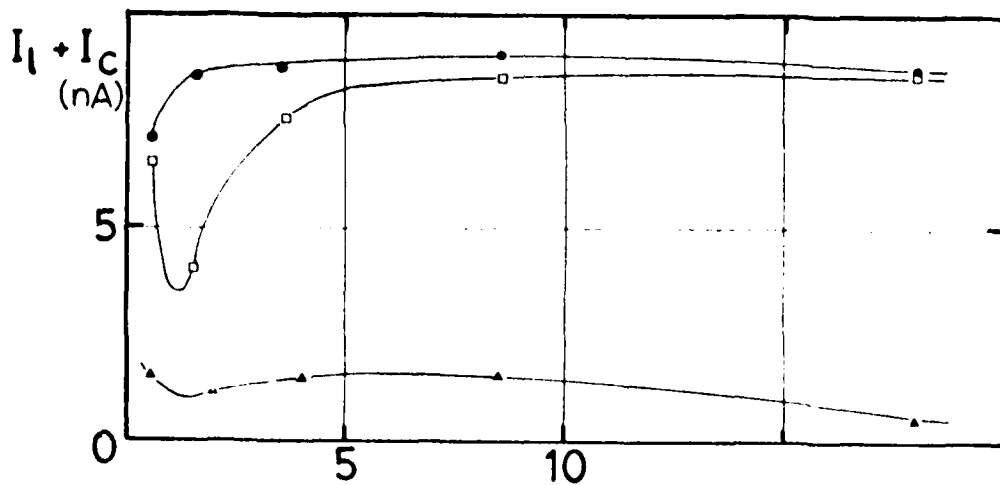
FIGURE 27

15 KEV ELECTRON IRRADIATION (0.5 nA cm^{-2})

- SILICA FABRIC (1 LAYER)
- SILICA FABRIC (3 LAYERS)
- ▲ SILICA FABRIC (1 LAYER) OVER FEP FILM



A



B

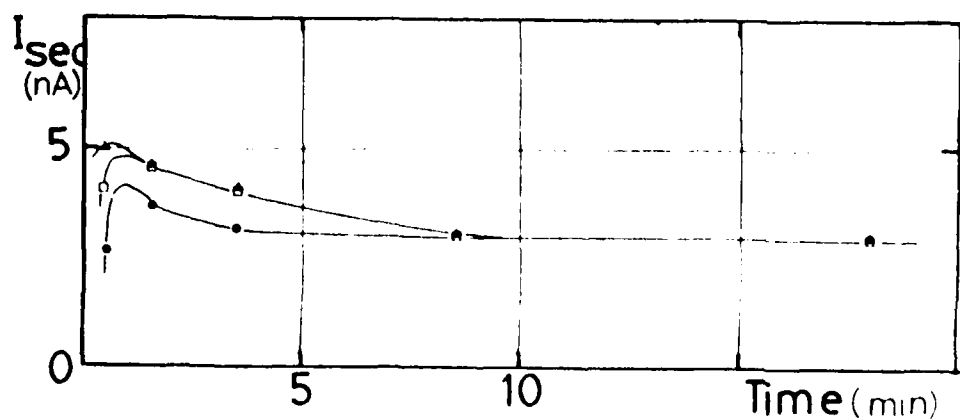


FIGURE 28

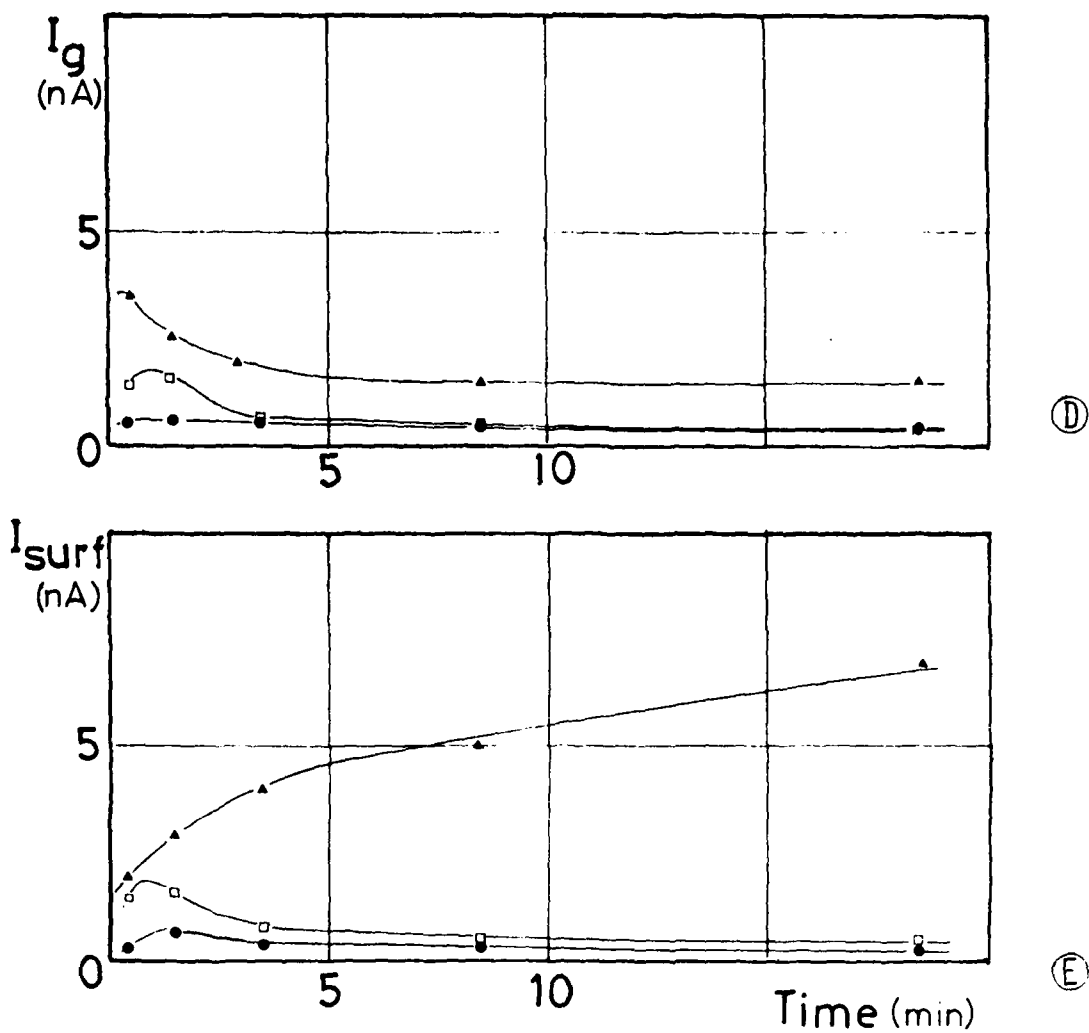


FIGURE 28

20 KEV ELECTRON IRRADIATION (0.5 nA cm^{-2})

- SILICA FABRIC (1 LAYER)
- SILICA FABRIC (3 LAYERS)
- ▲ SILICA FABRIC (1 LAYER) OVER FEP FILM

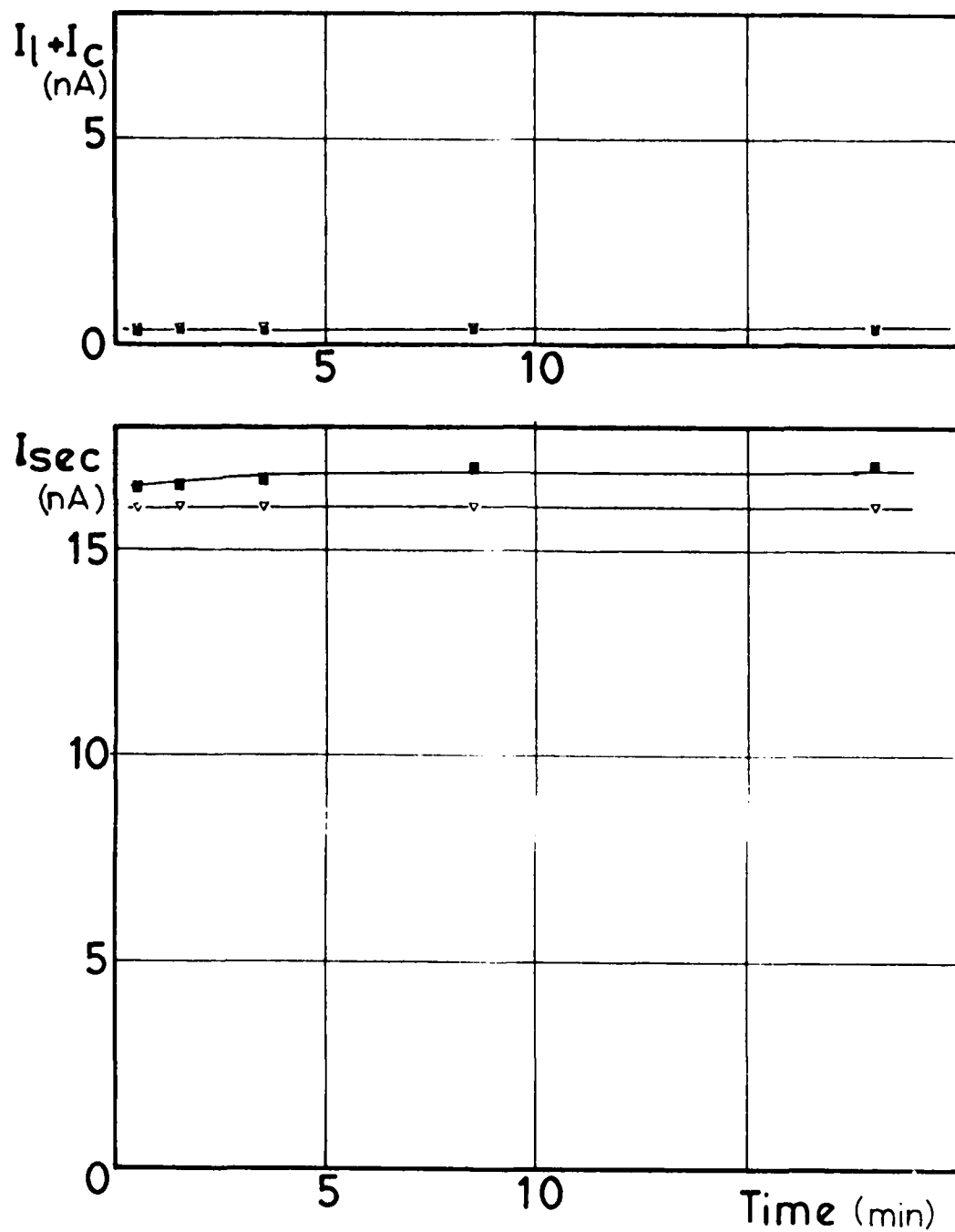
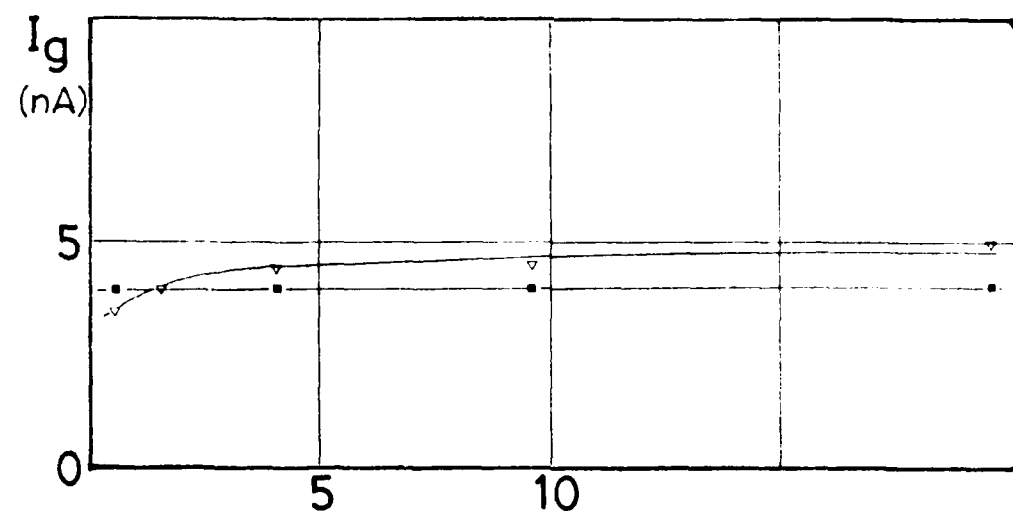
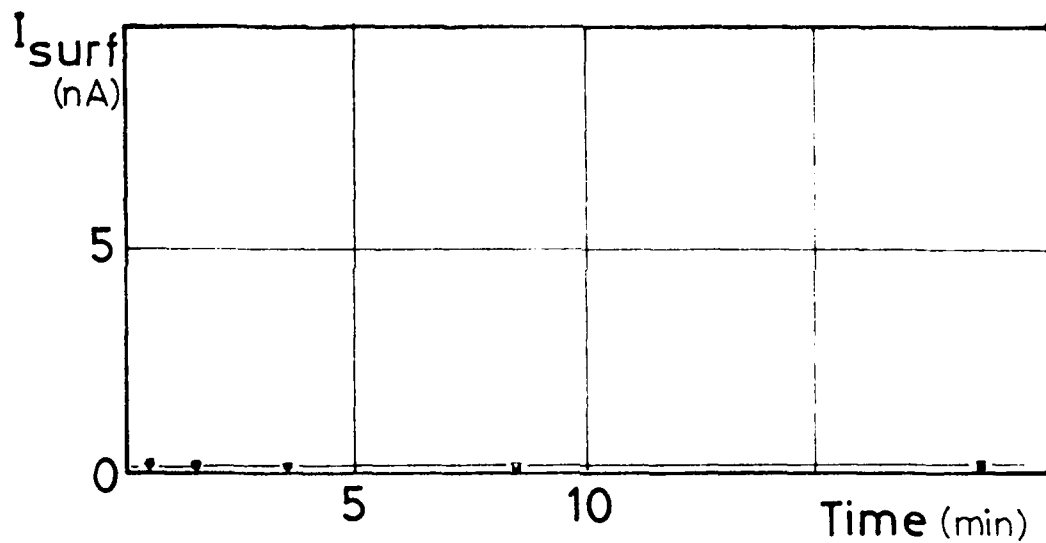


FIGURE 29



D



E

FIGURE 29
5 KEV ELECTRON IRRADIATION (1.25 nA CM^{-2})

- COMPOSITE
- ▽ COMPOSITE OVER FEP FILM

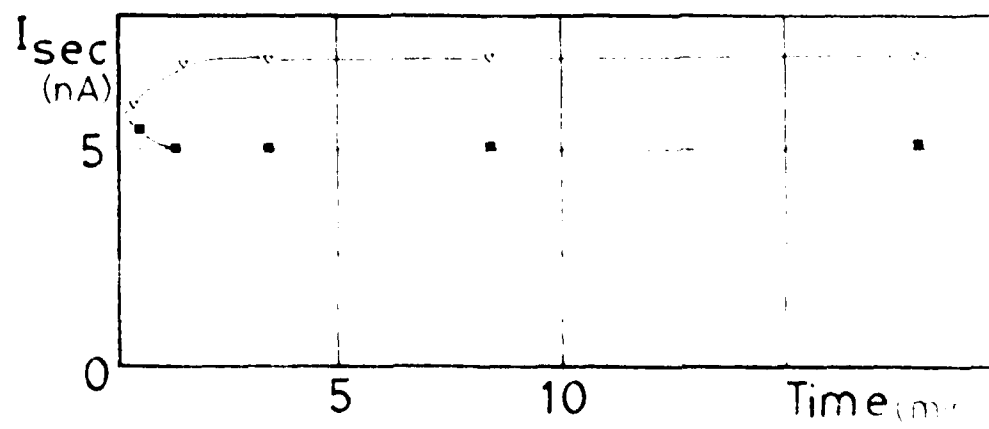
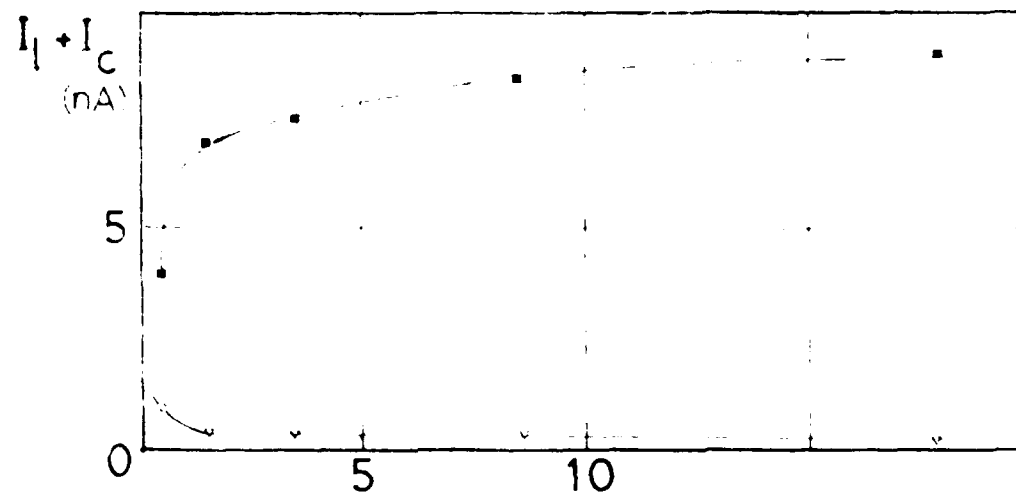
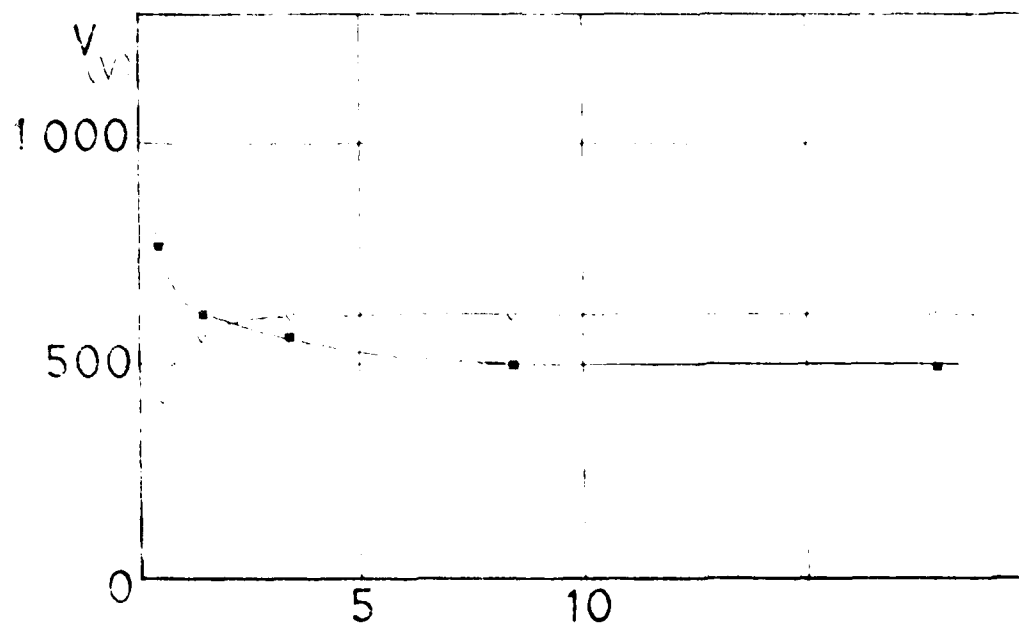


FIGURE 30

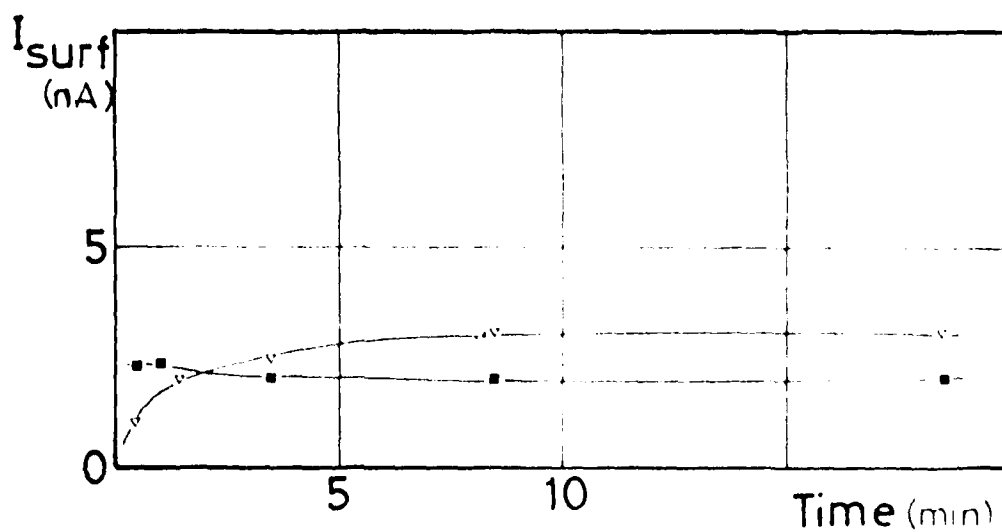
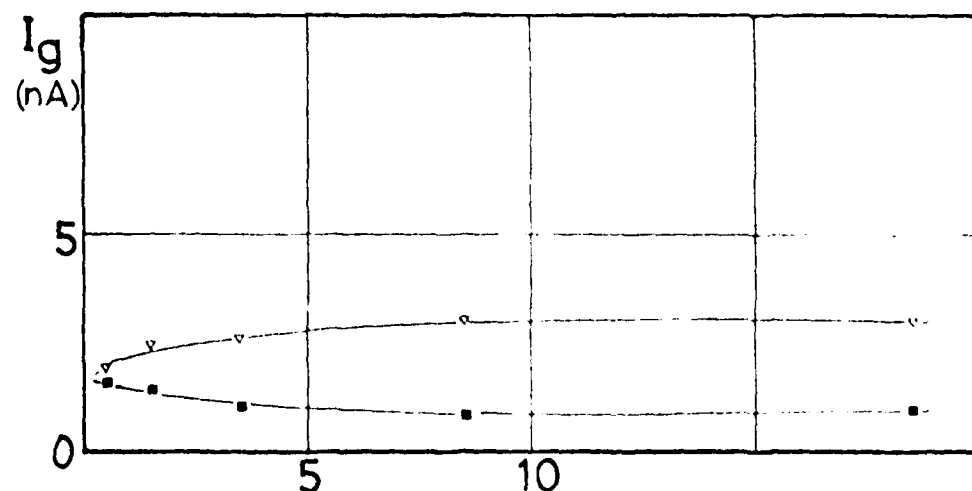


FIGURE 30

10 KEV ELECTRON IRRADIATION (0.7 nA cm^{-2})

- COMPOSITE
- ▽ COMPOSITE OVER FEP FILM

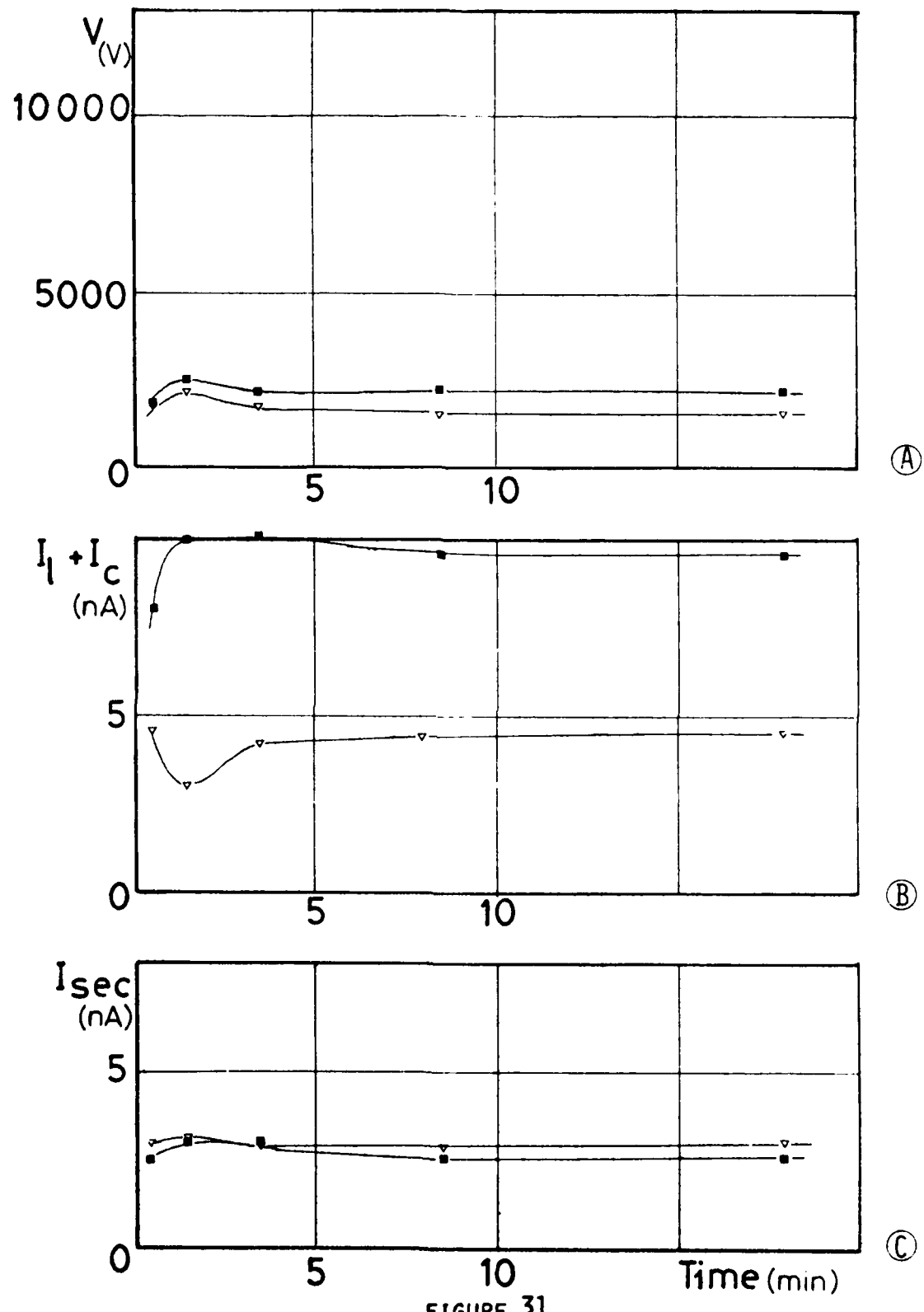
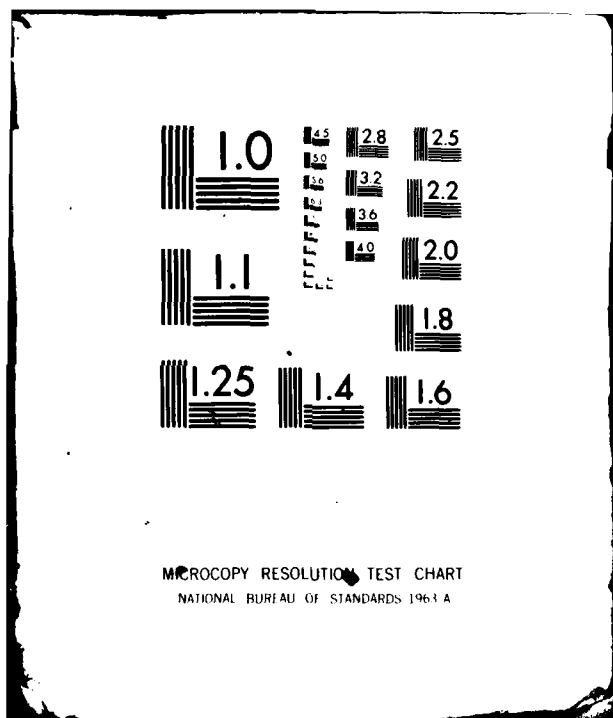


FIGURE 31

AD-A087 675 OFFICE NATIONAL D'ETUDES ET DE RECHERCHES AEROSPATIALE--ETC F/G 22/2
SATELLITE SPACECRAFT CHARGING CONTROL MATERIALS. (U)
APR 80 B BENAISSA, L LEVY, A PAILOUS AFOSR-78-3704
UNCLASSIFIED ONERA/CERT/DERTS-CR-AF-05 AFWAL-TR-80-4029 NL

2 1 2
20-1-2

END
DATE
FILED
9 80
DTIC



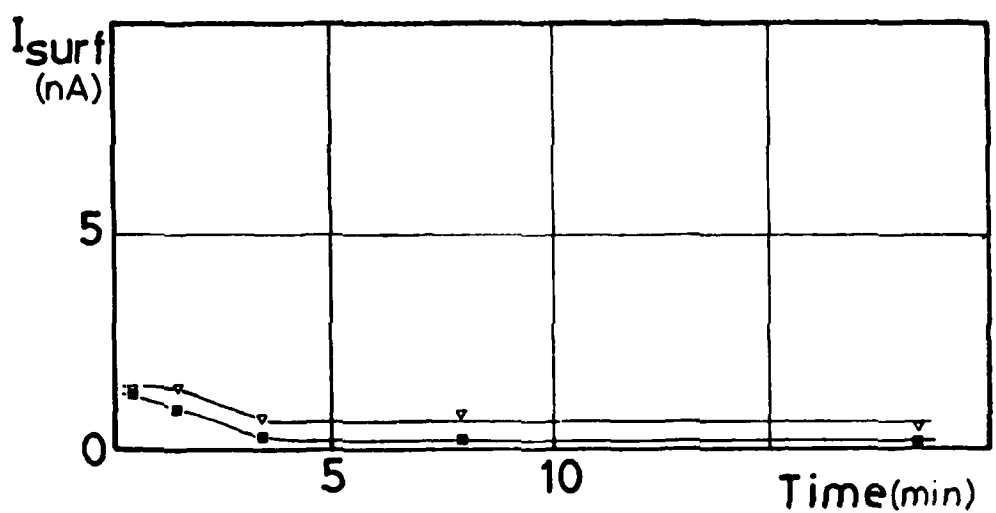
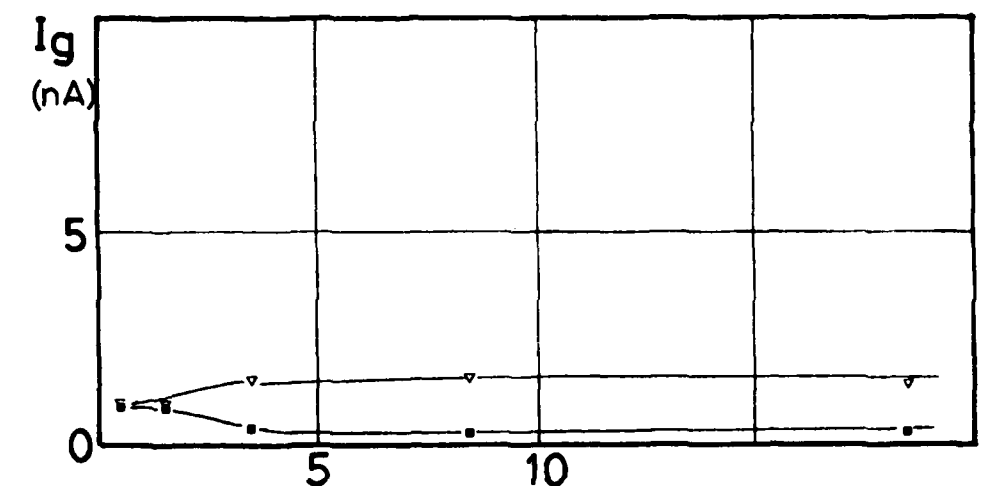
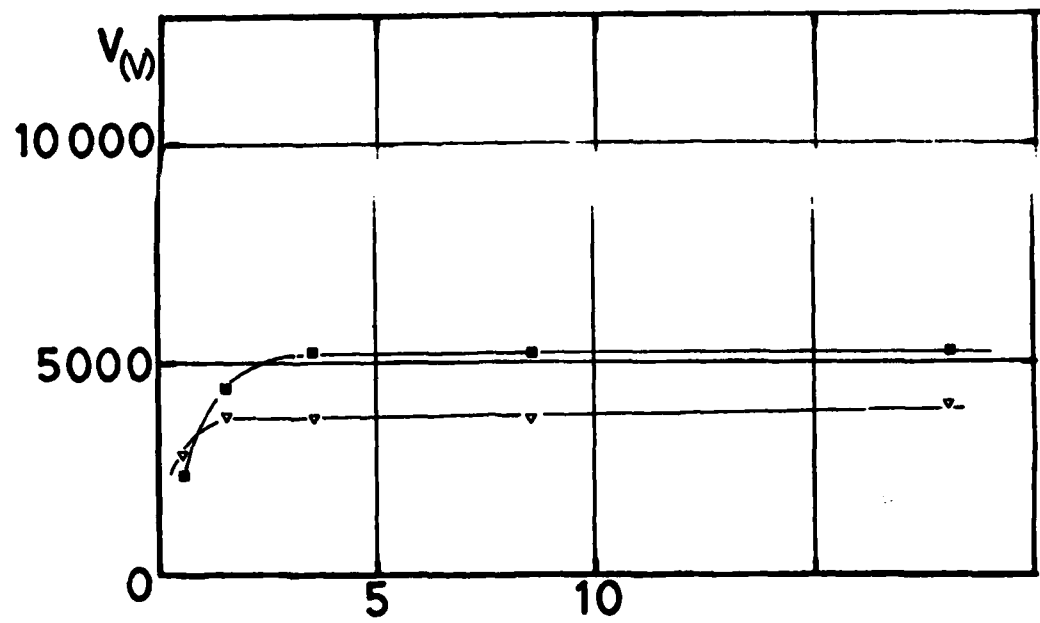


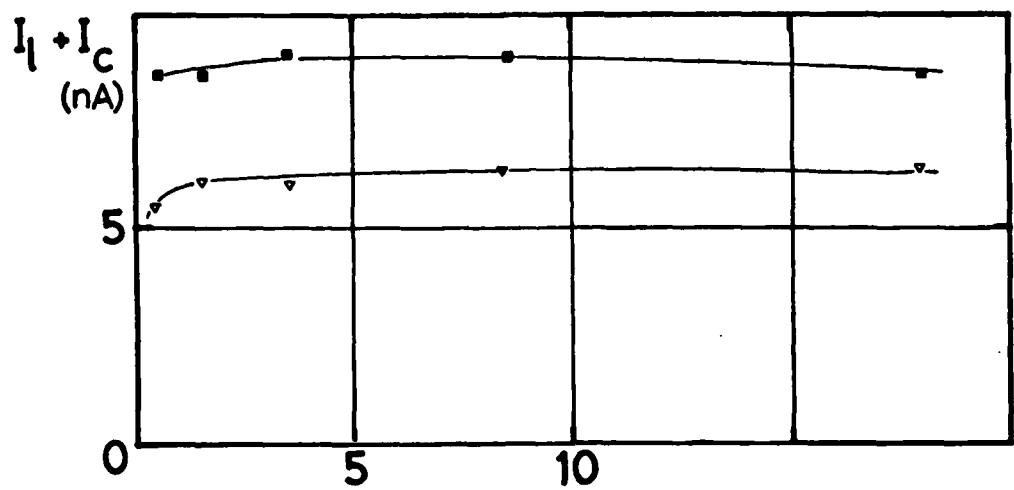
FIGURE 31

15 KEV ELECTRON IRRADIATION (0.5 nA cm^{-2})

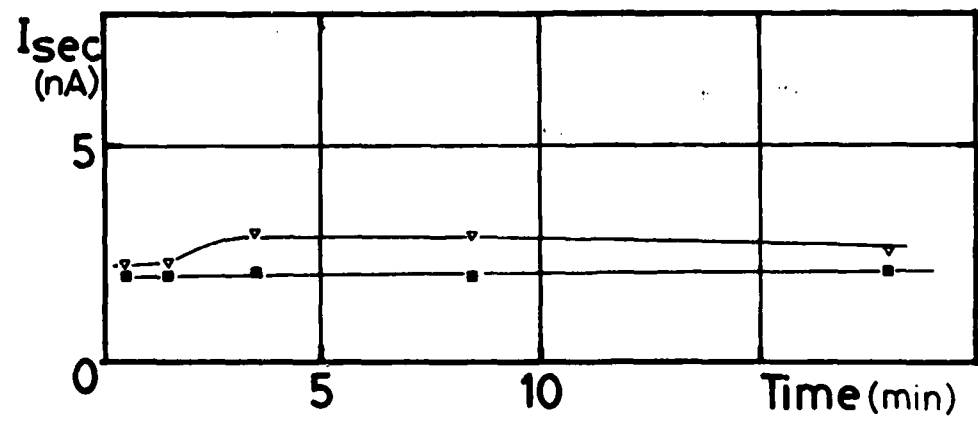
- COMPOSITE
- ▽ COMPOSITE OVER FEP FILM



A



B



C

FIGURE 32

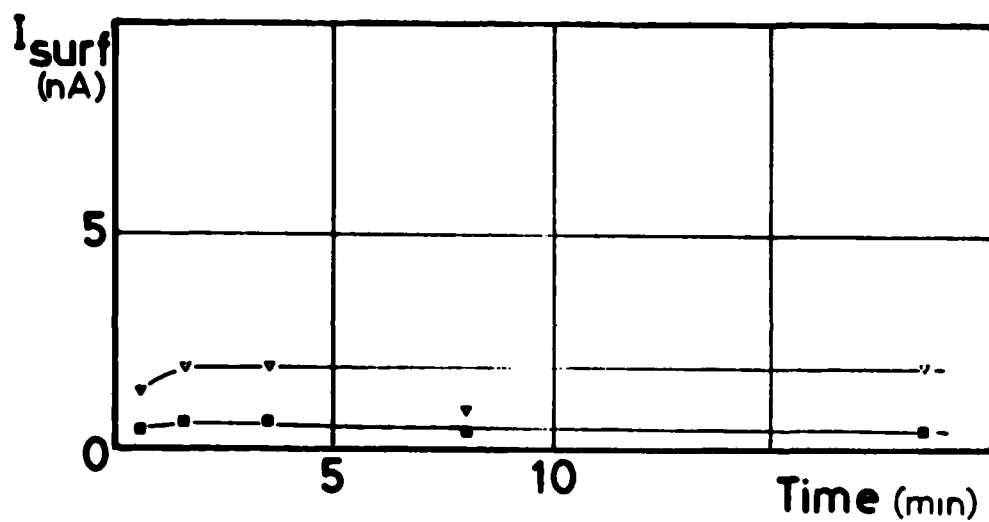
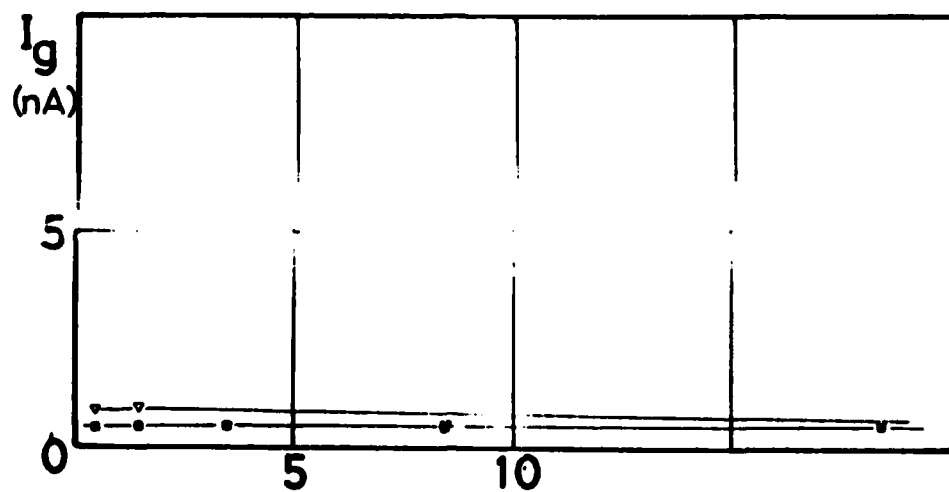


FIGURE 32
20 KEV ELECTRON IRRADIATION ($0.5, \text{nA cm}^{-2}$)

- COMPOSITE
- ▼ COMPOSITE OVER FEP FILM

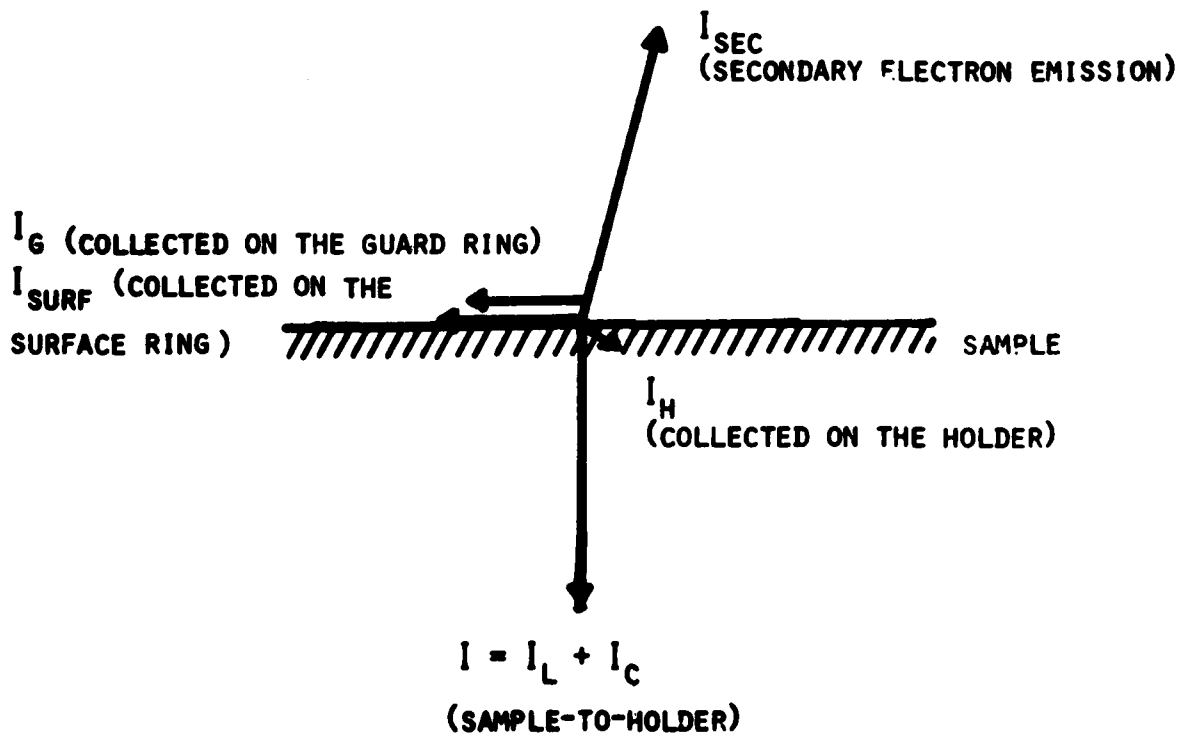
In FIGURES 33 to 37 the results are shown in a schematic presentation that allows to visualize the relative importance of the various measured current components. Each current component is represented by a vector the modulus of which is equal to the direct ratio of this current to the sum ΣI of all the currents.

$$\Sigma I = I_{sec} + (I_L + I_C) + I_{surf} + I_g + I_H$$

The various currents are described at Section 3.2.3

The I_H value (see Section 3.2.3) was not measured for all sample configuration. It has been used where available. (*)

The vector orientation allows to discriminate the various current components as sketched below:



In FIGURES 33 to 37 the surface potential values are also reported.

(*) a dotted vector denotes that the I_H component was not measured

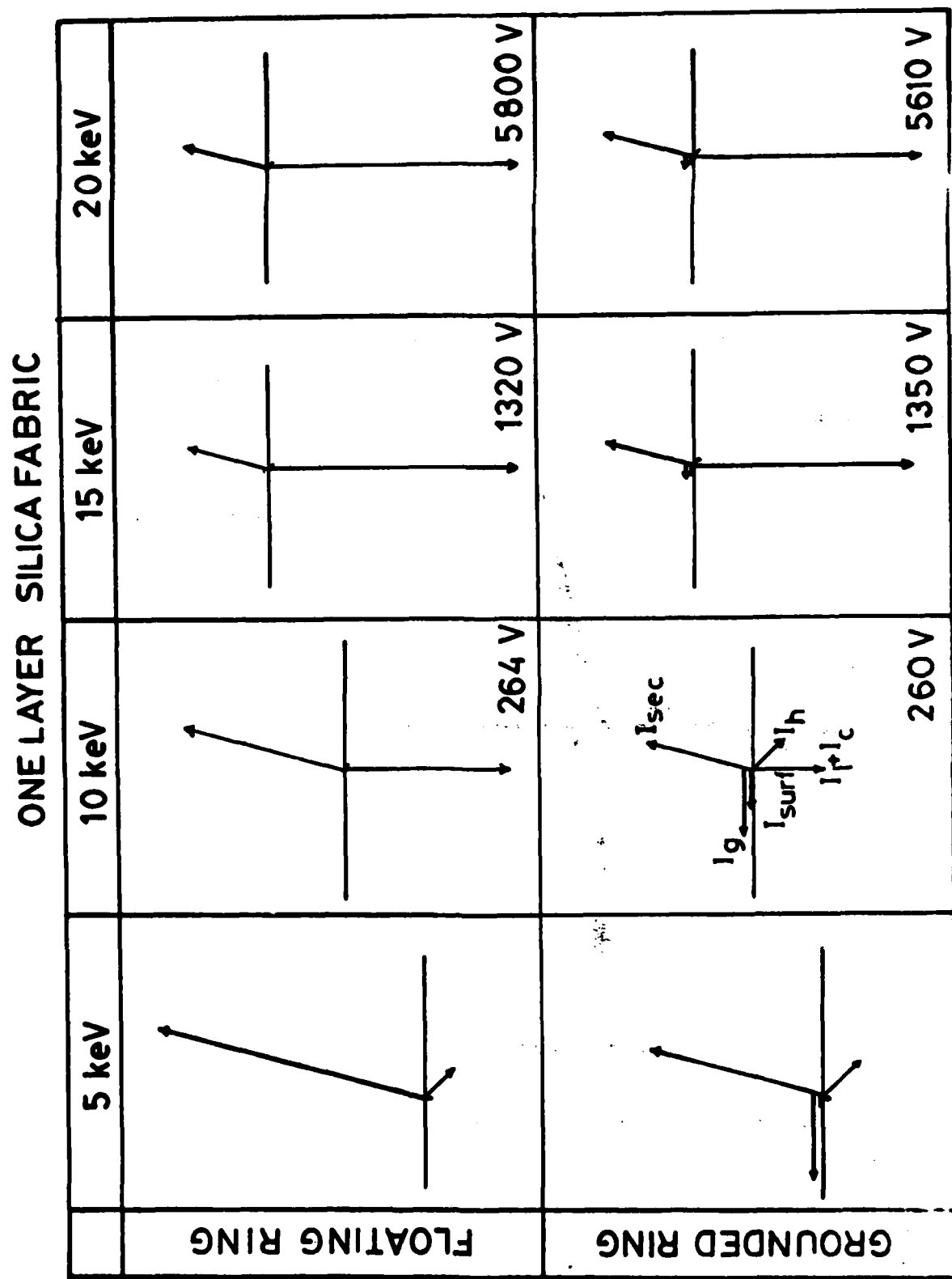


FIGURE 33 - CURRENT COMPONENTS

THREE LAYERS SILICA FABRIC

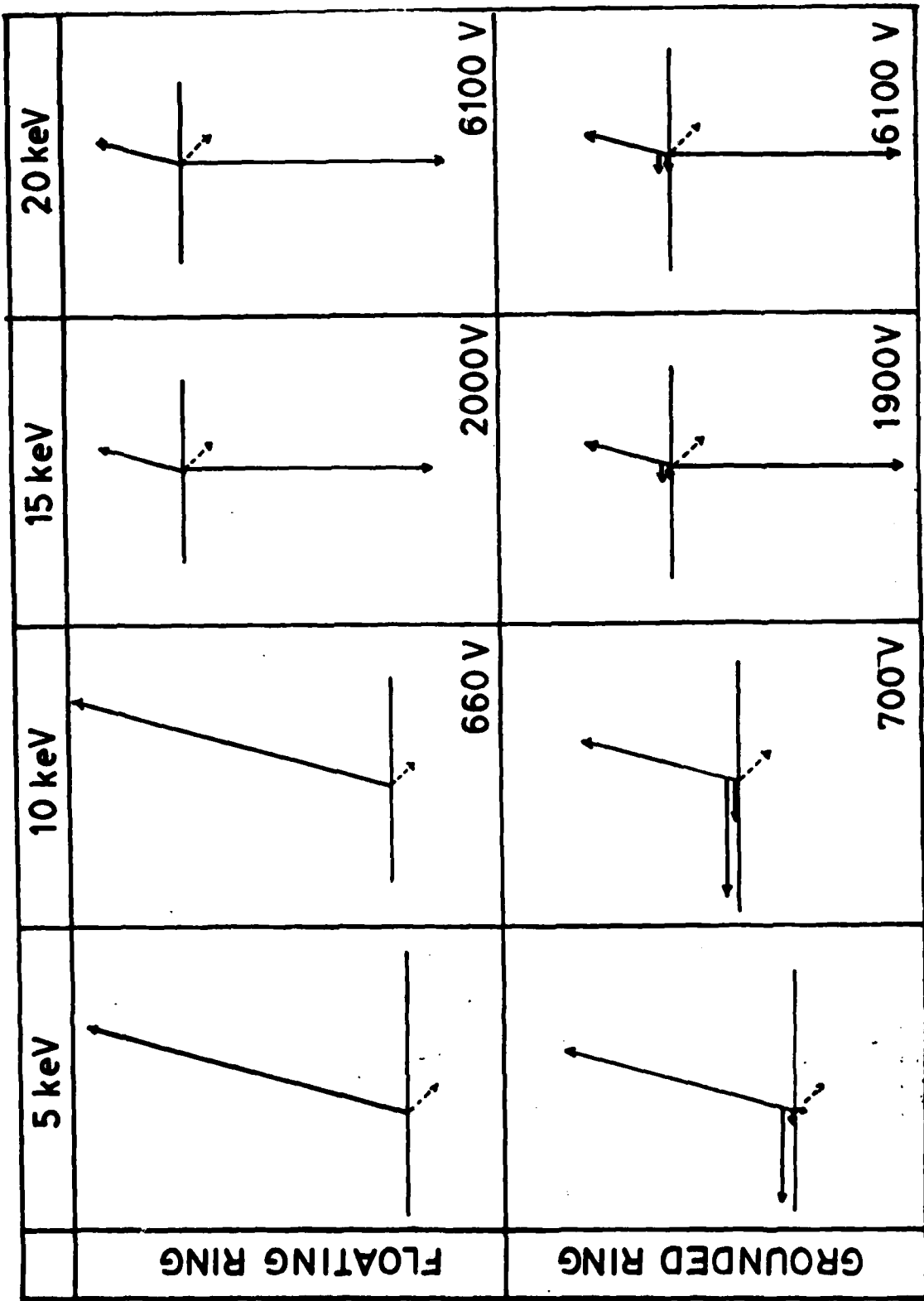


FIGURE 34 - CURRENT COMPONENTS

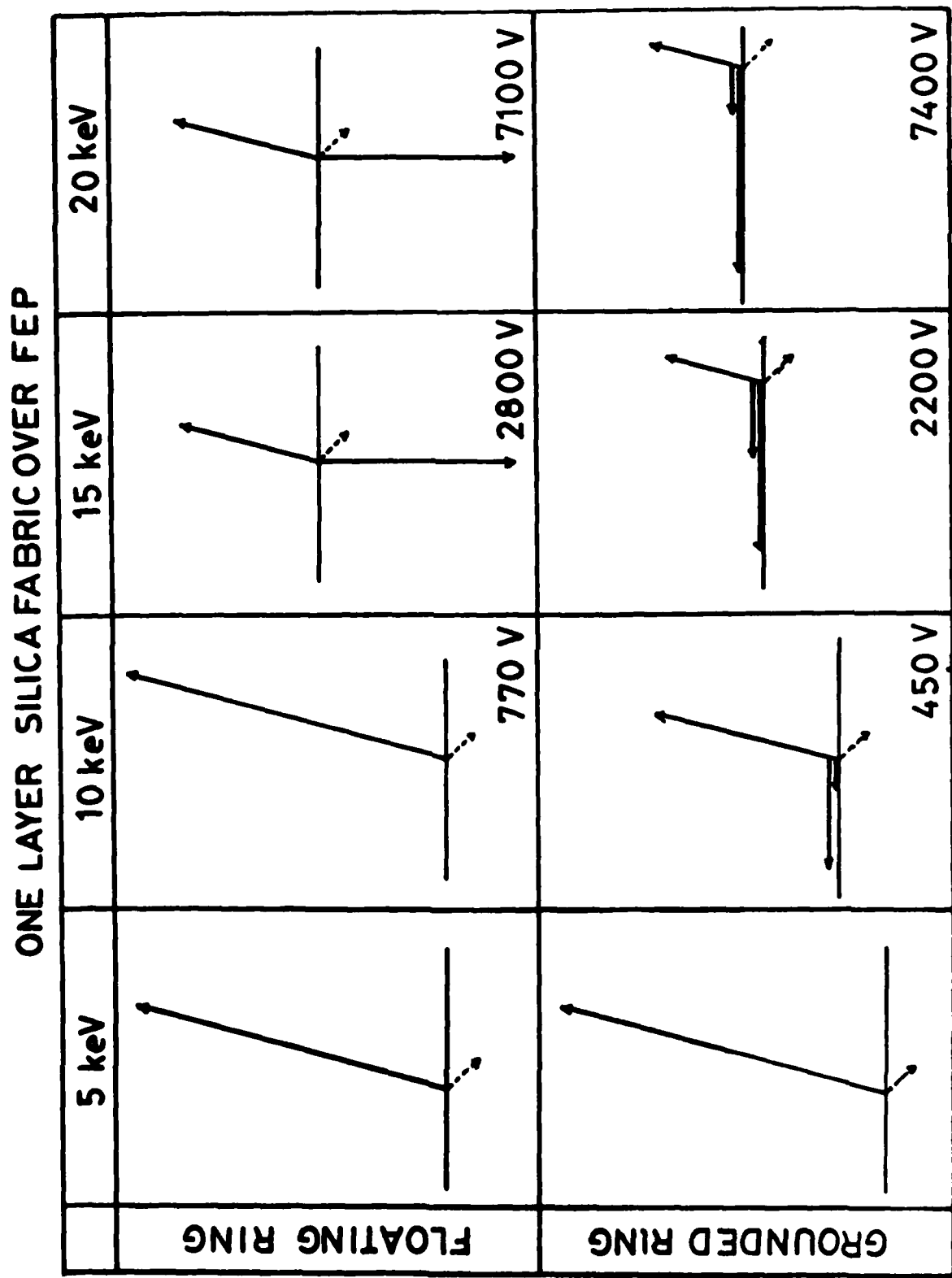


FIGURE 35 - CURRENT COMPONENTS
88

COMPOSITE

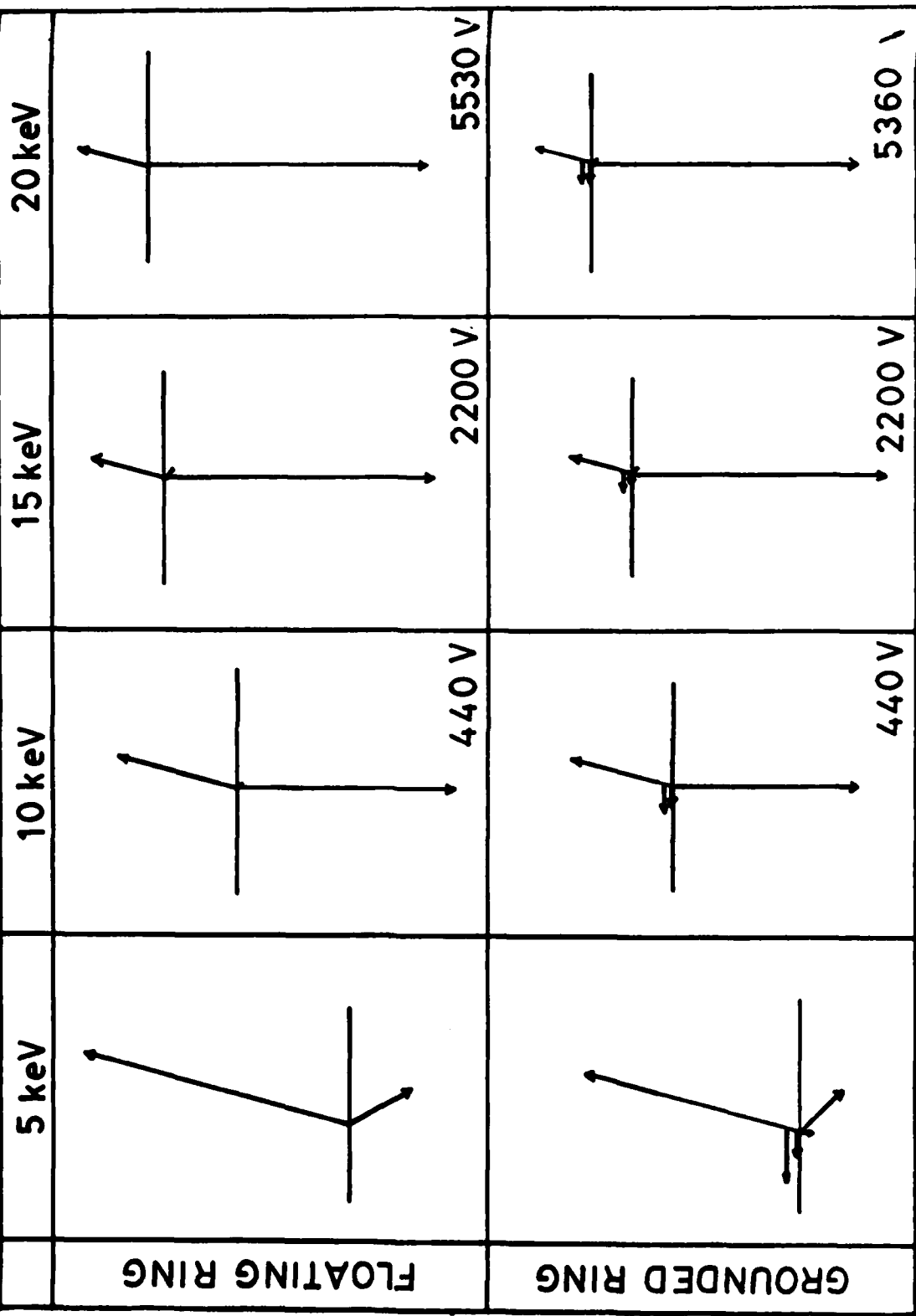


FIGURE 36 - CURRENT COMPONENTS

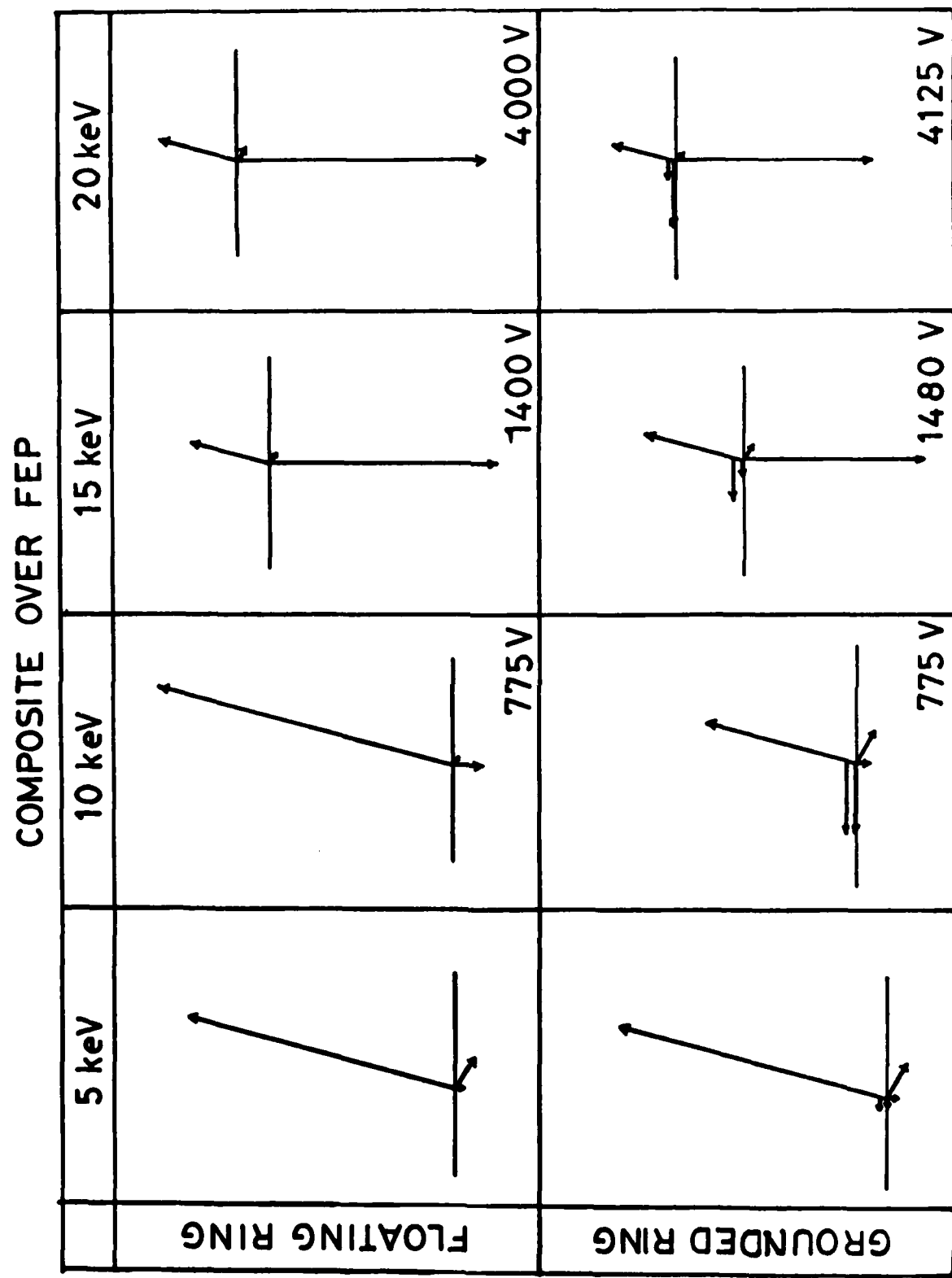


FIGURE 37 - CURRENT COMPONENTS

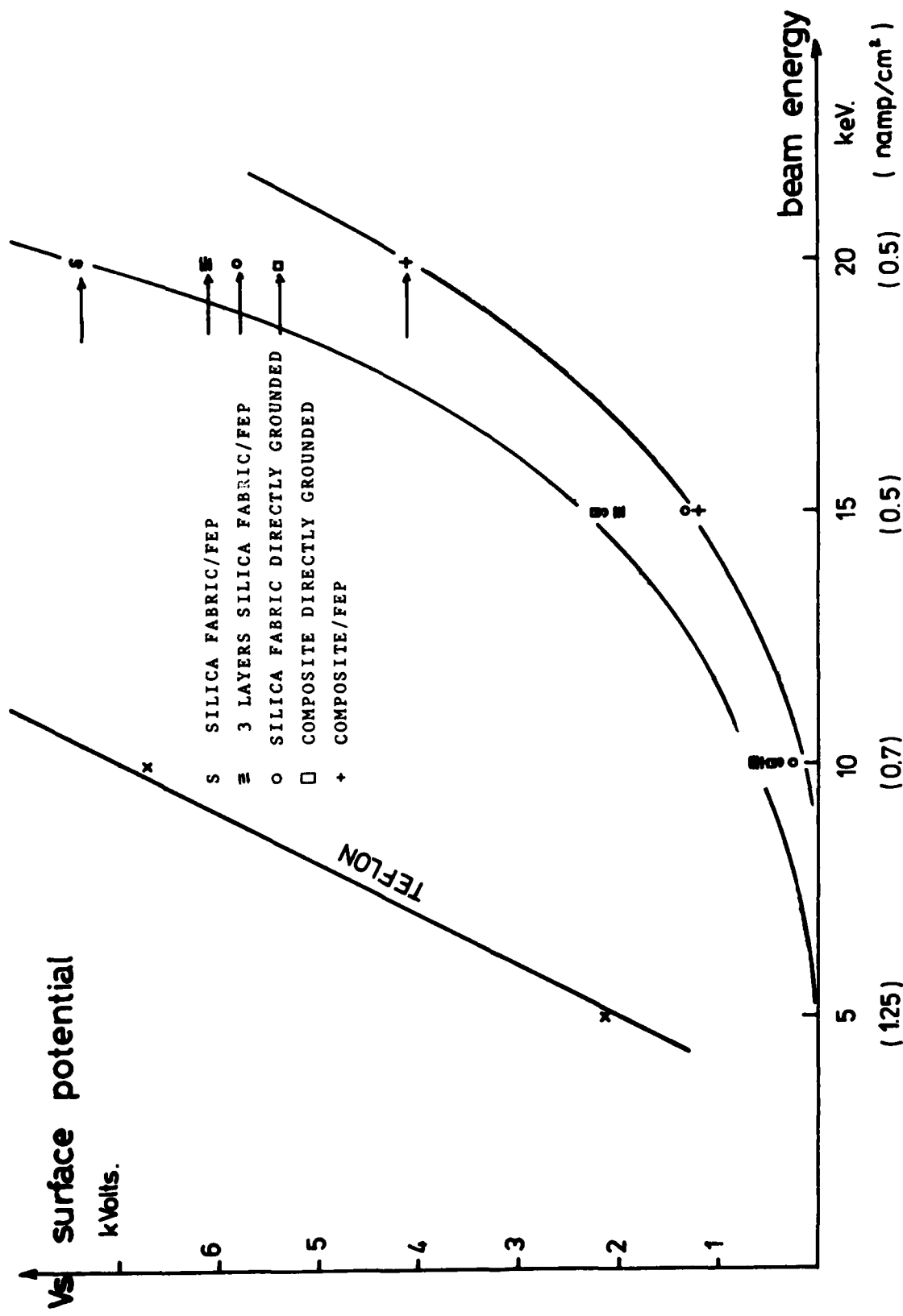


FIGURE 38 - SURFACE POTENTIAL VERSUS BEAM ENERGY

3.4.3 Surface potential in terms of beam energy

In FIGURE 38, one can find the measured values of surface potential that are also reported in TABLE 9.

3.4.4 Typical current recordings

FIGURES 39 to 49 show typical current recordings. With very few exceptions (that are mentionned on the figures), they are related to irradiation times between 12 and 18 minutes (quasi steady state) for the samples with a grounded ring and between 20 and 25 minutes for samples with a floating ring.

TABLES 10 to 14 summarize observations of arcing phenomena that can be got from the current recordings. The current variation as well as the number of events (average value for a 10 minute irradiation duration) are reported.

GROUNDING CONDITIONS	BEAM ENERGY	CONFIGURATIONS			
		LAYER FABRIC	3 LAYERS FABRIC	FABRIC OVER FEP	COMPOSITE OVER FEP
with grounding ring	5 keV	< 10	< 10	< 10	< 10
	10 keV	264	660	450	480
	15 keV	1320	2000	2230 (*)	2210
	20 keV	5800 (*)	6100 (*)	7425 (*)	5350 (*)
with floating ring	5 keV	< 10	< 10	< 10	< 10
	10 keV	231	700	770	440
	15 keV	1452	1900	2230 (*)	2200
	20 keV	5500 (*)	6100	7100 (*)	5530 (*)
(**) arcing (**) not equilibrium conditions					

TABLE 9 - SURFACE POTENTIAL (IN VOLTS) MEASUREMENT AFTER A 18 MINUTES IRRADIATION
THE SAMPLES HAD NOT BEEN EVER IRRADIATED BEFORE THE EXPERIMENT STARTING

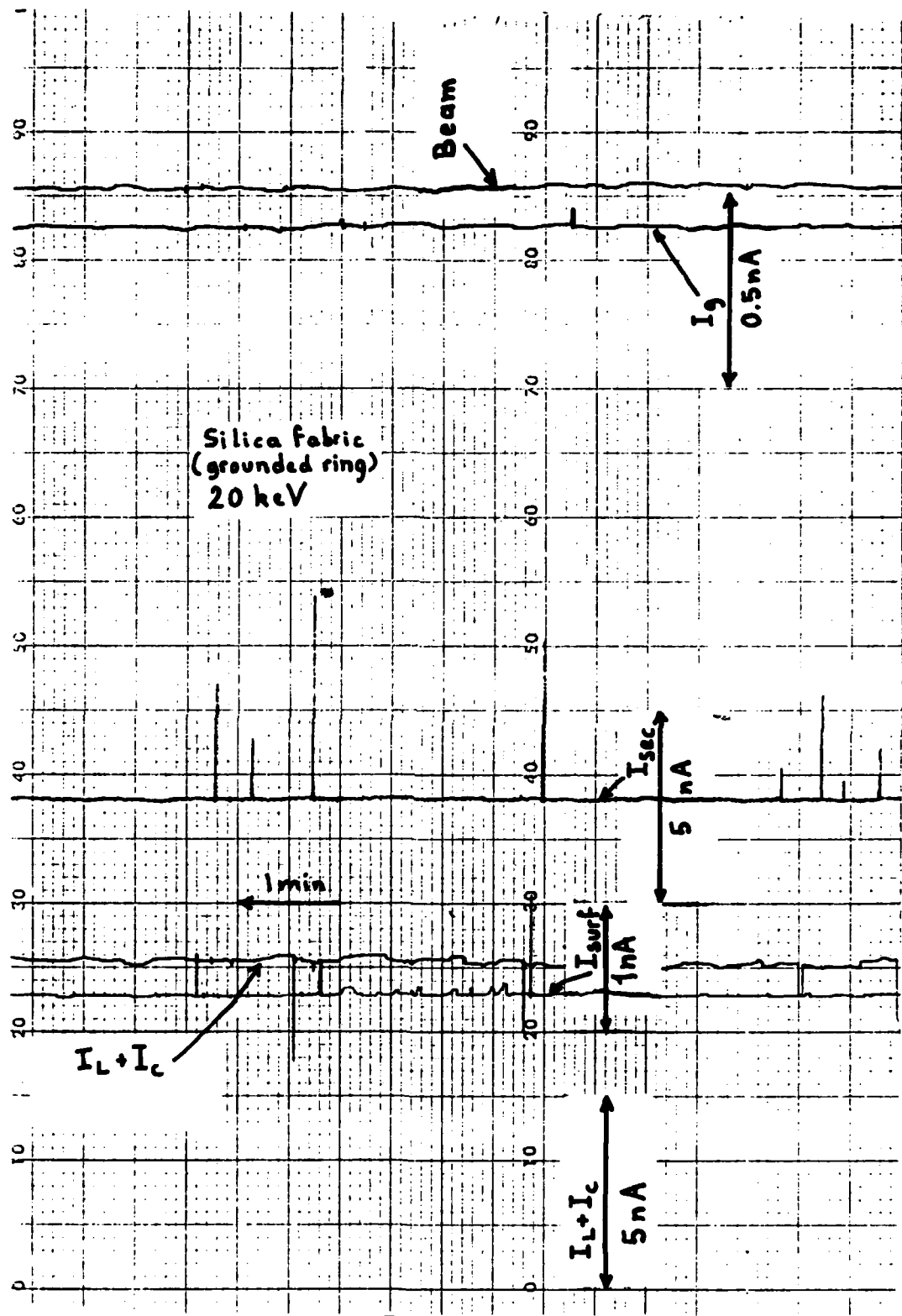


FIGURE 39 - CURRENT RECORDS

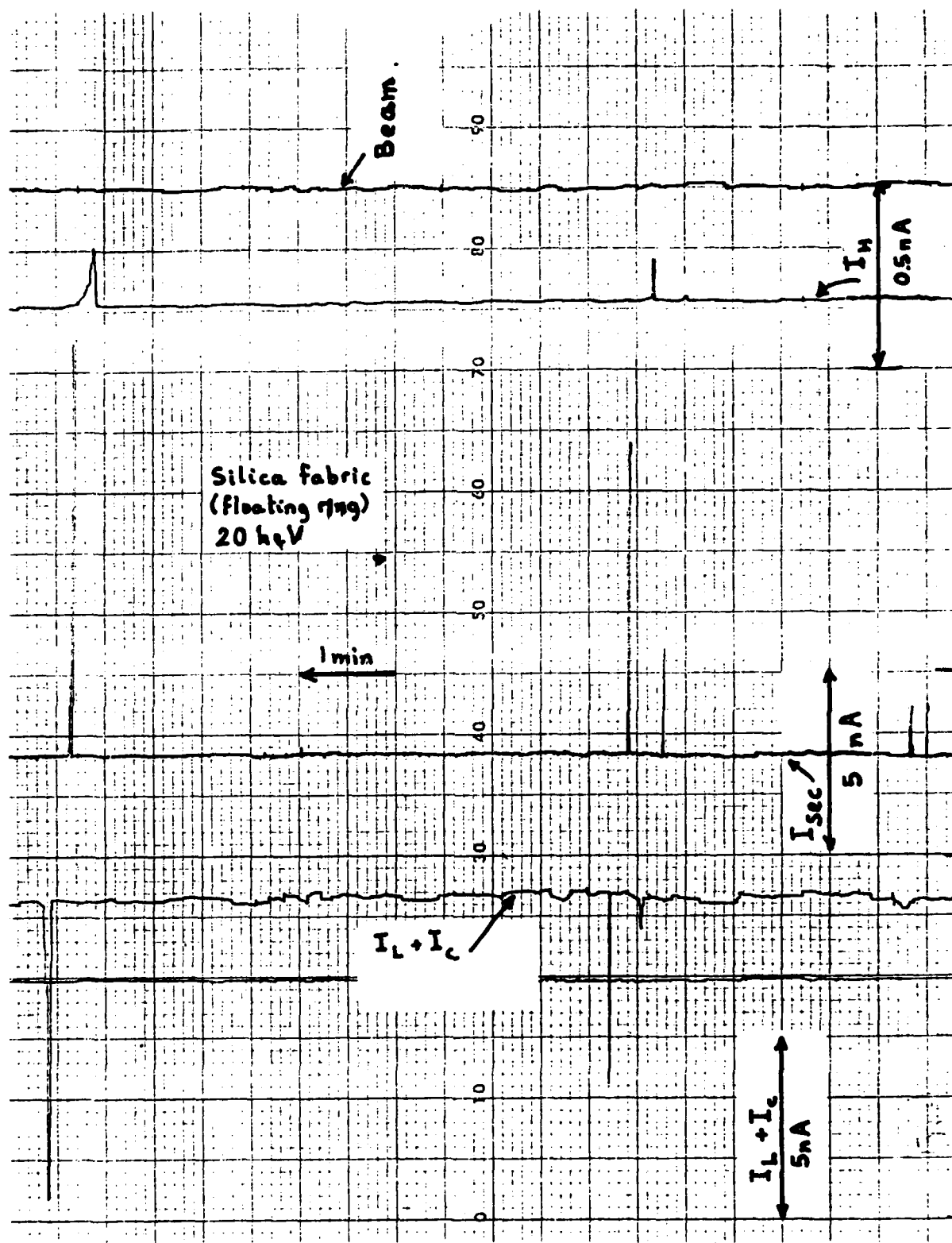


FIGURE 40 - CURRENT RECORDS

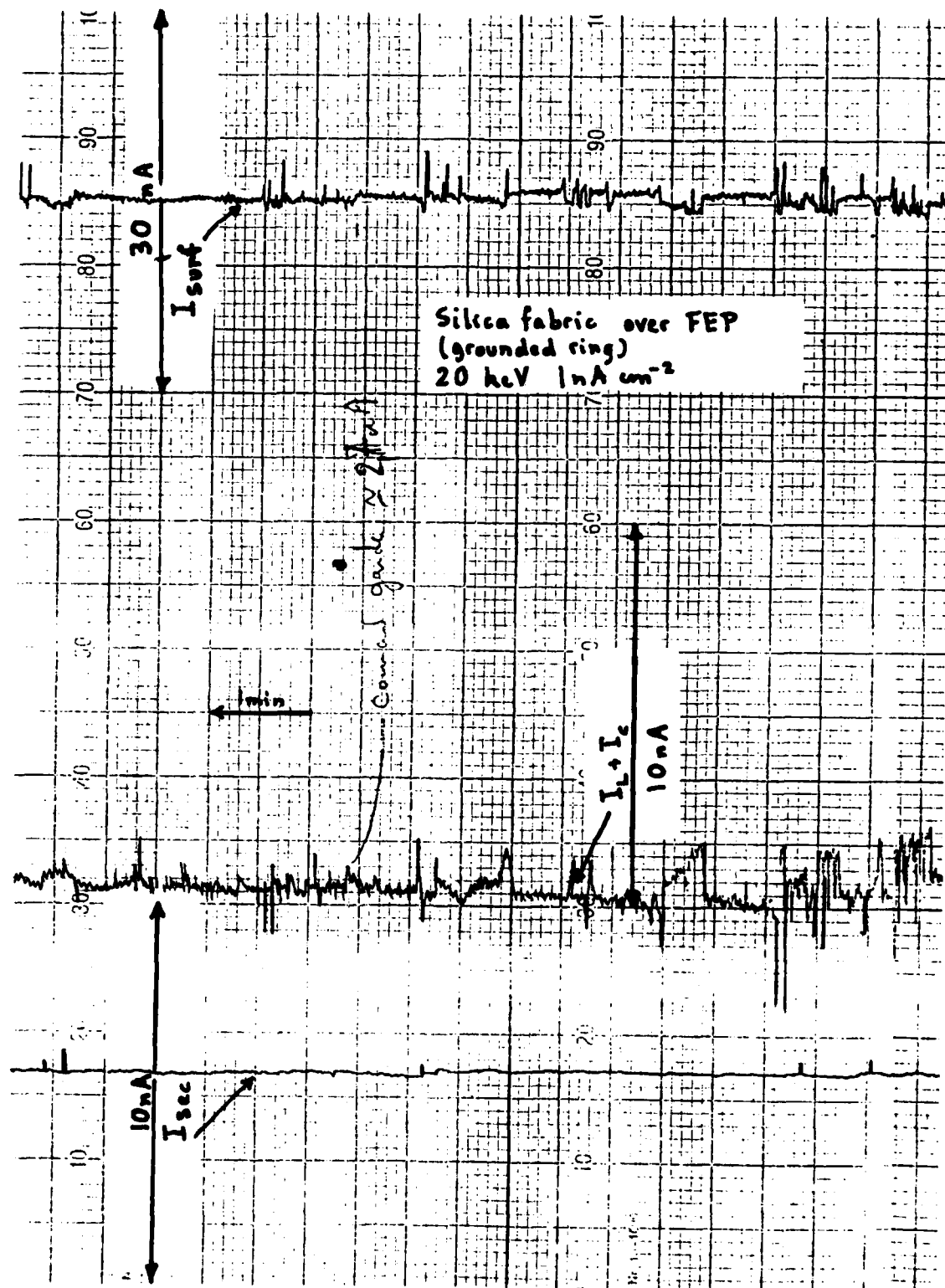


FIGURE 42 - CURRENT RECORDS

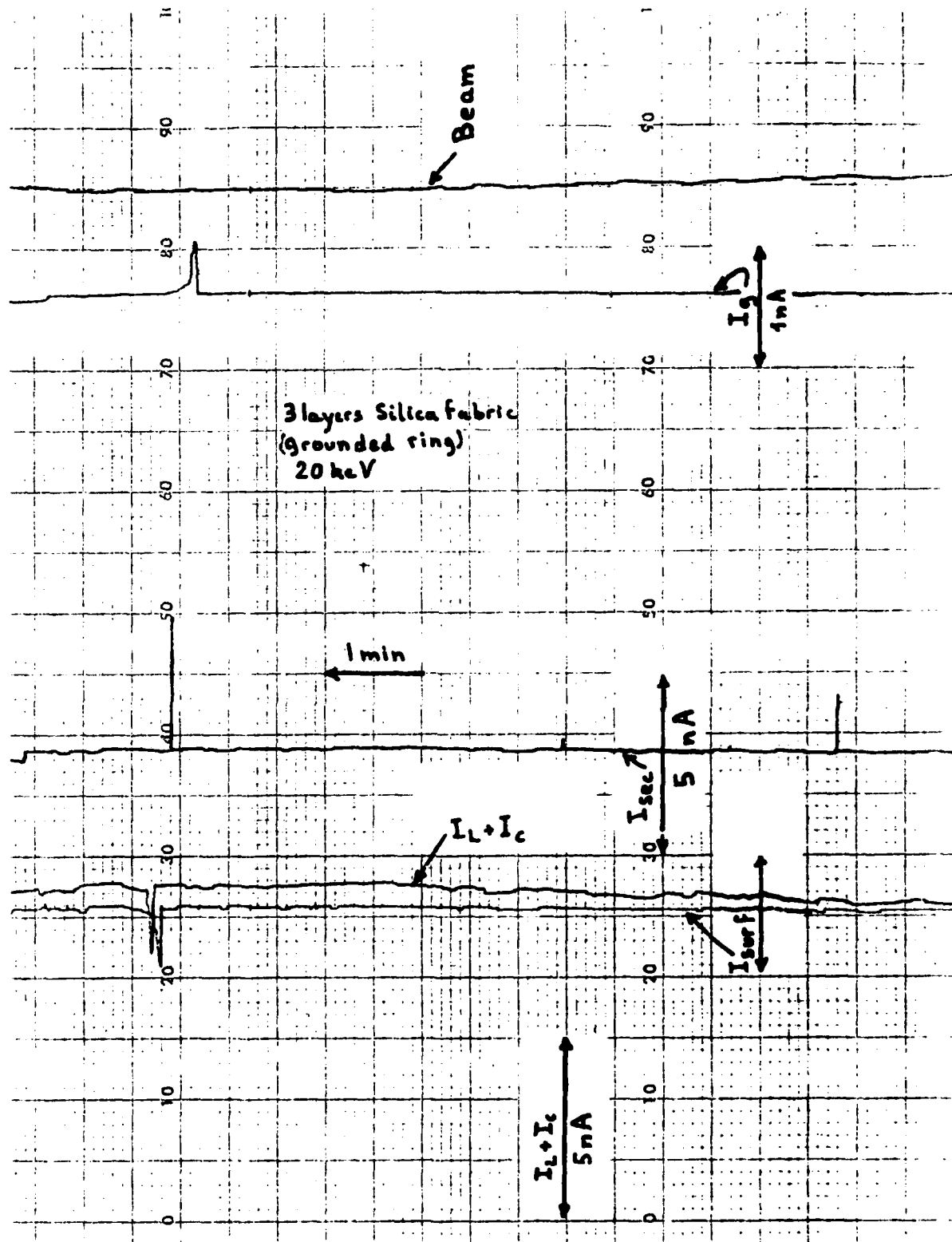


FIGURE 41 - CURRENT RECORDS

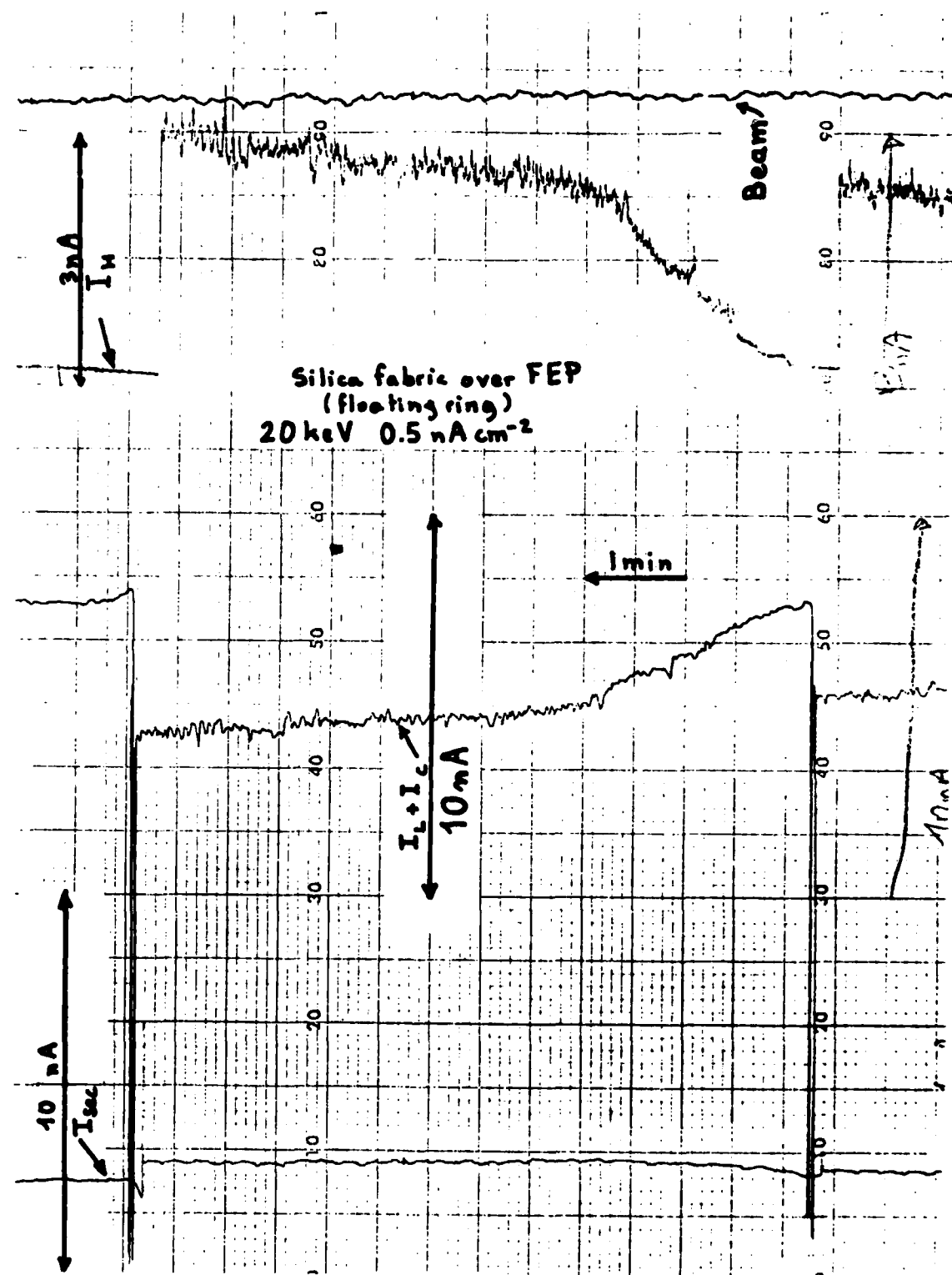


FIGURE 43 - CURRENT RECORDS

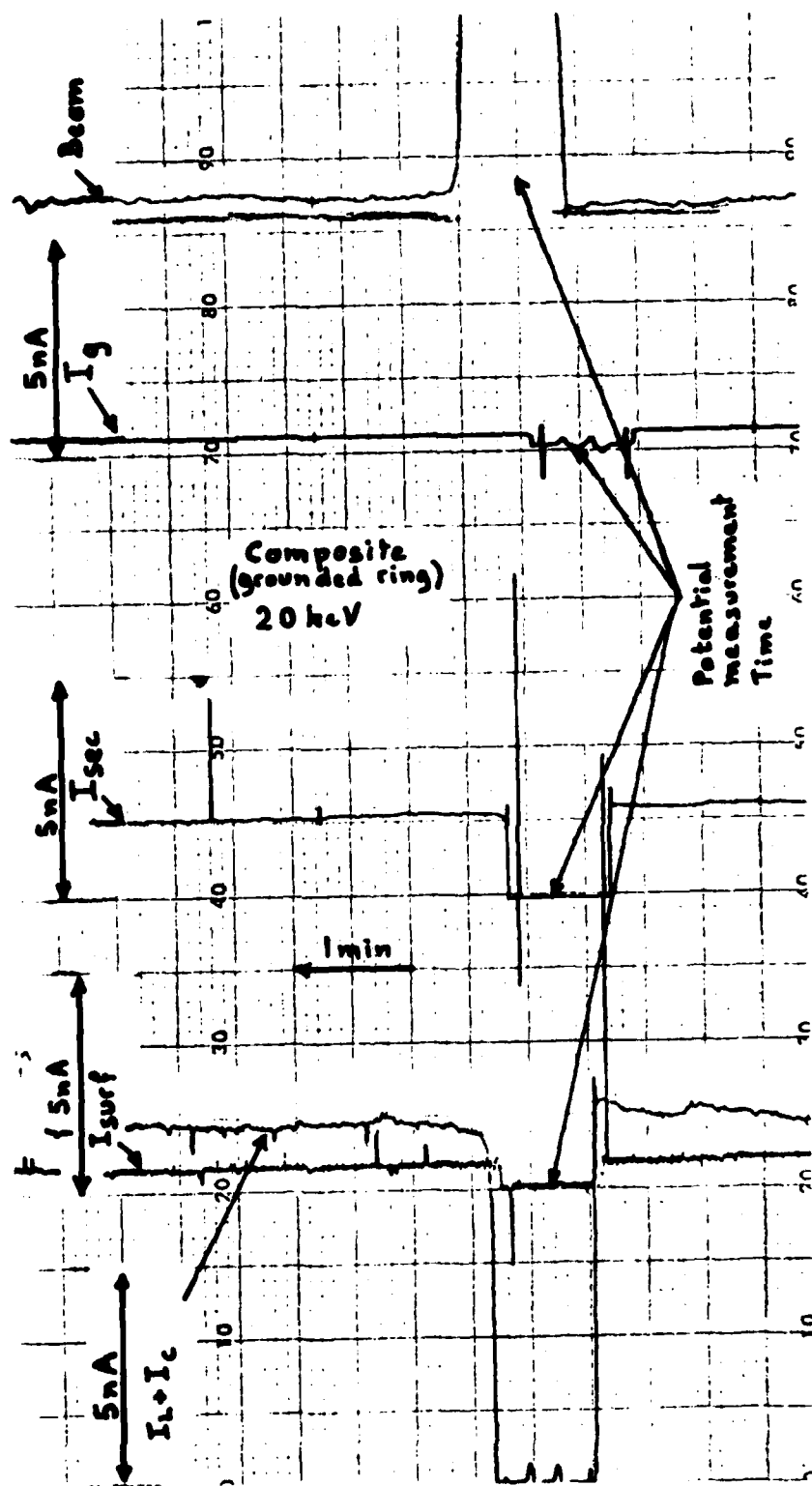


FIGURE 44 - CURRENT RECORDS

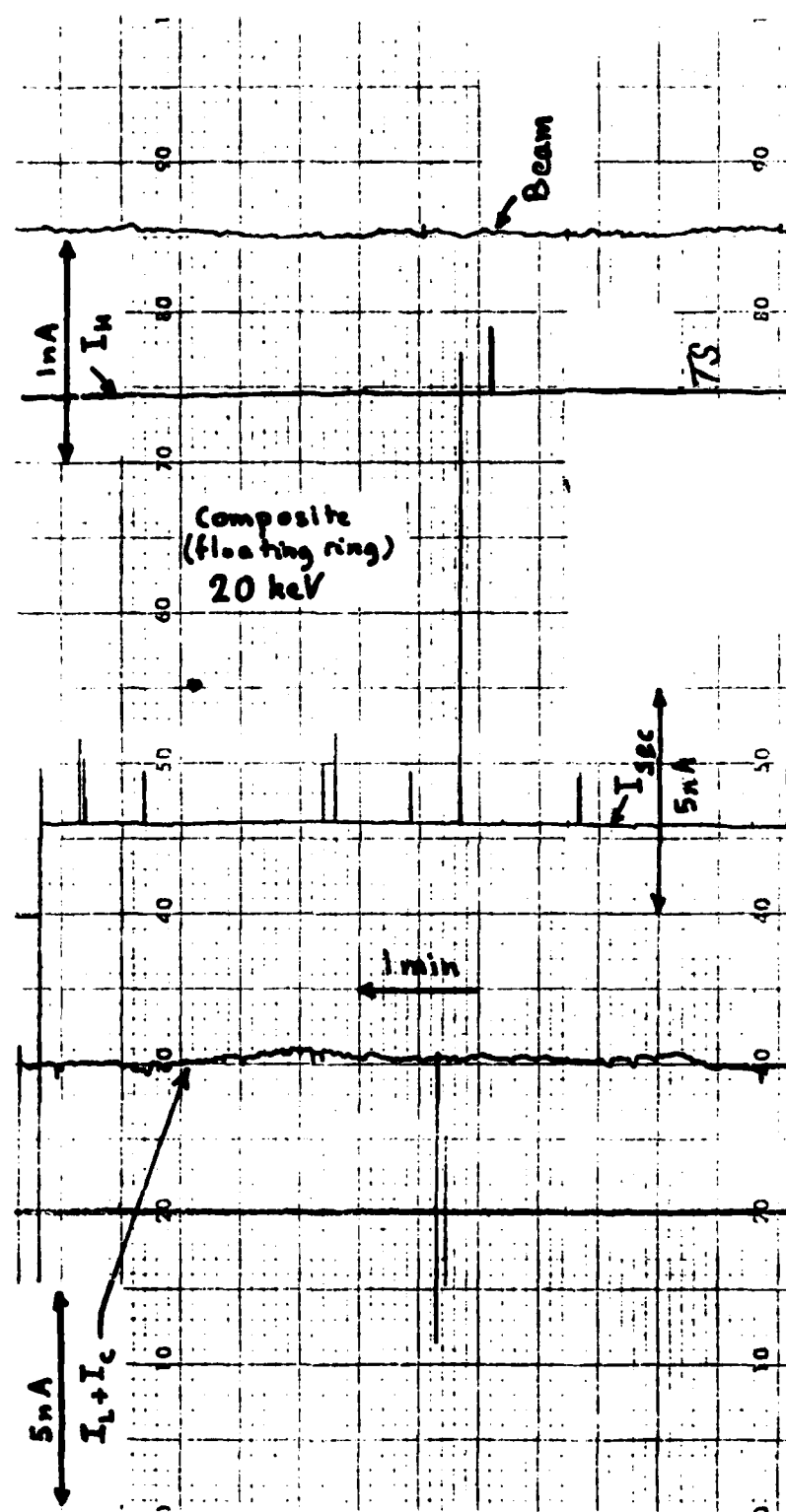


FIGURE 45 - CURRENT RECORDS

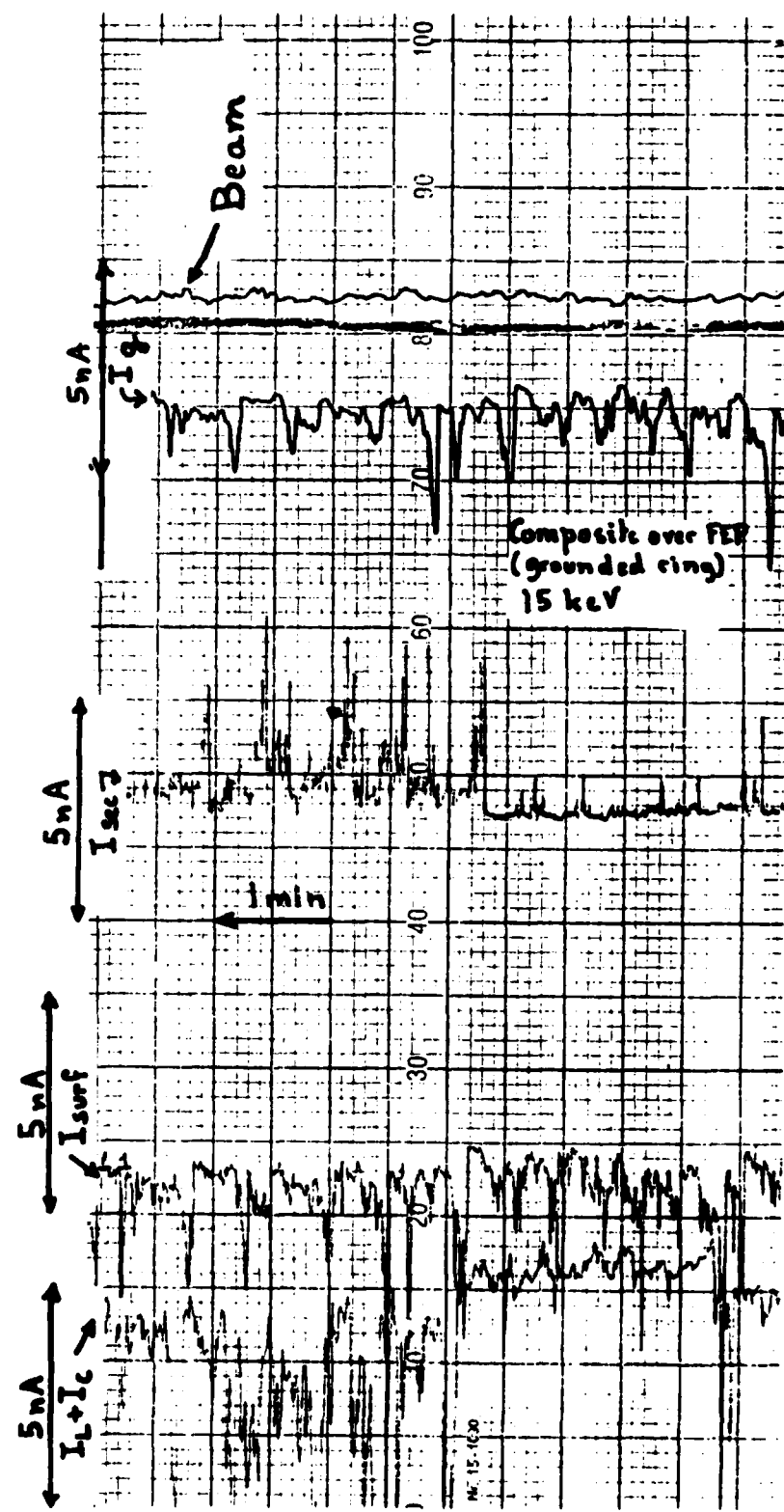


FIGURE 46 - CURRENT RECORDS

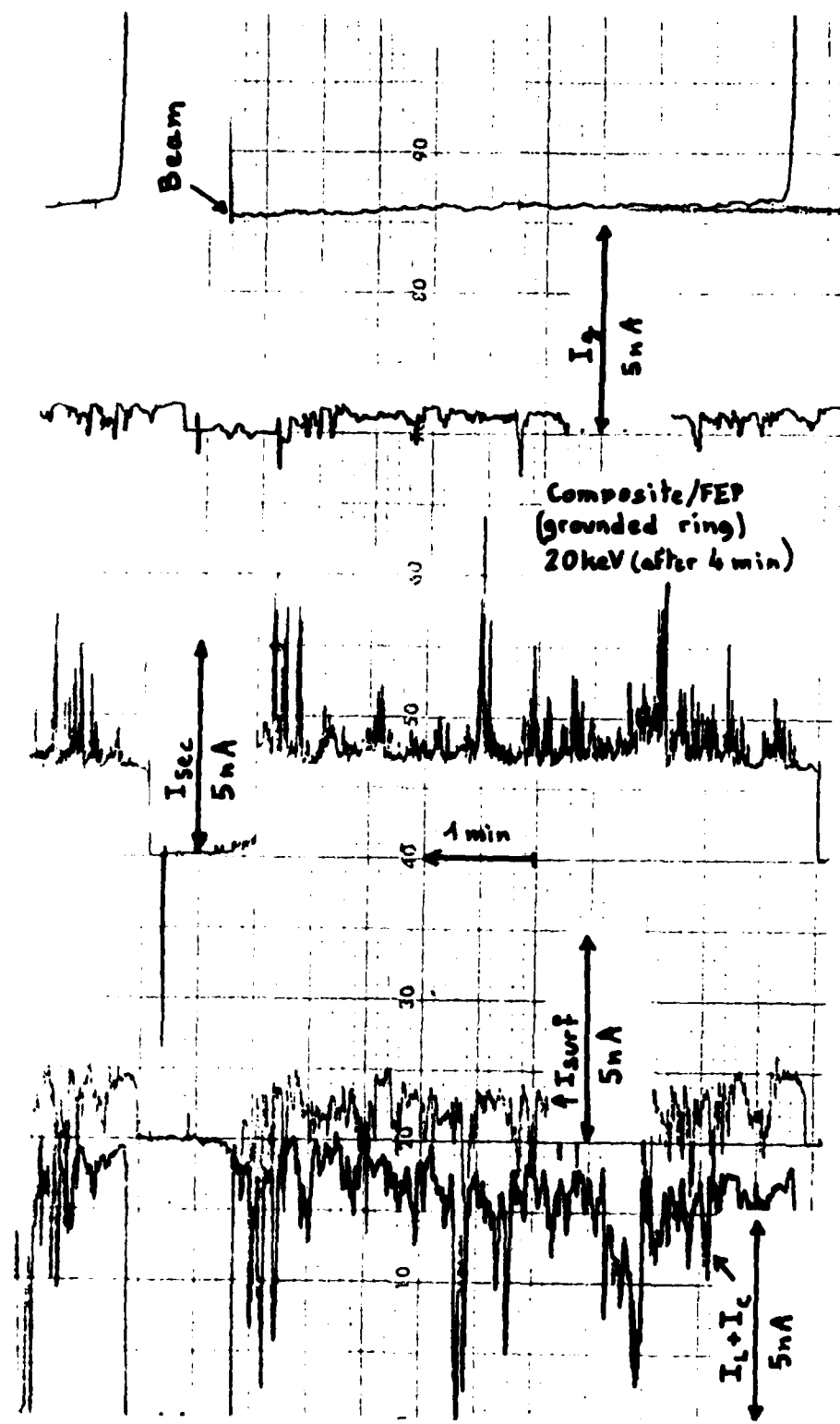


FIGURE 47 - CURRENT RECORDS

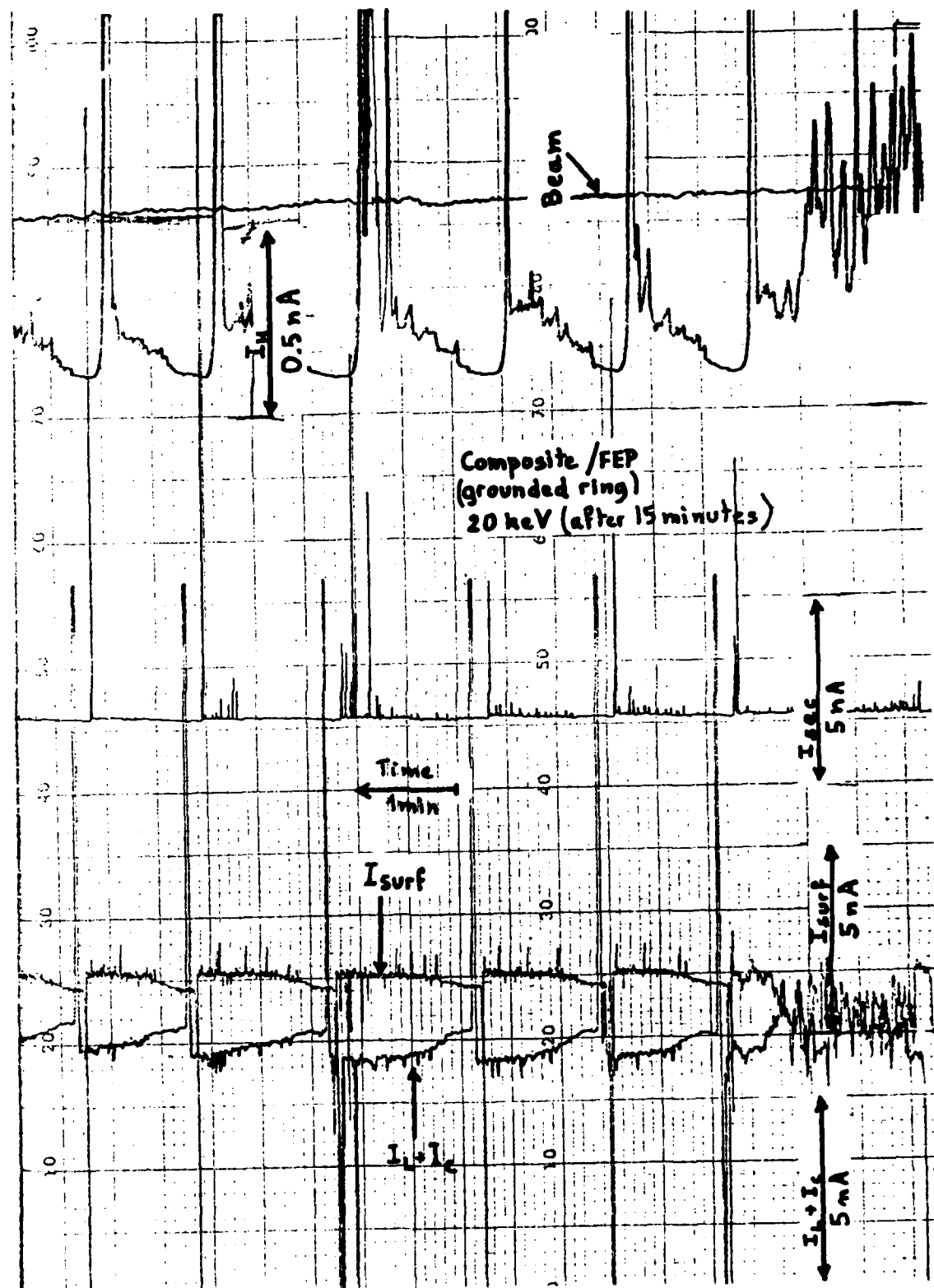


FIGURE 48 - CURRENT RECORDS

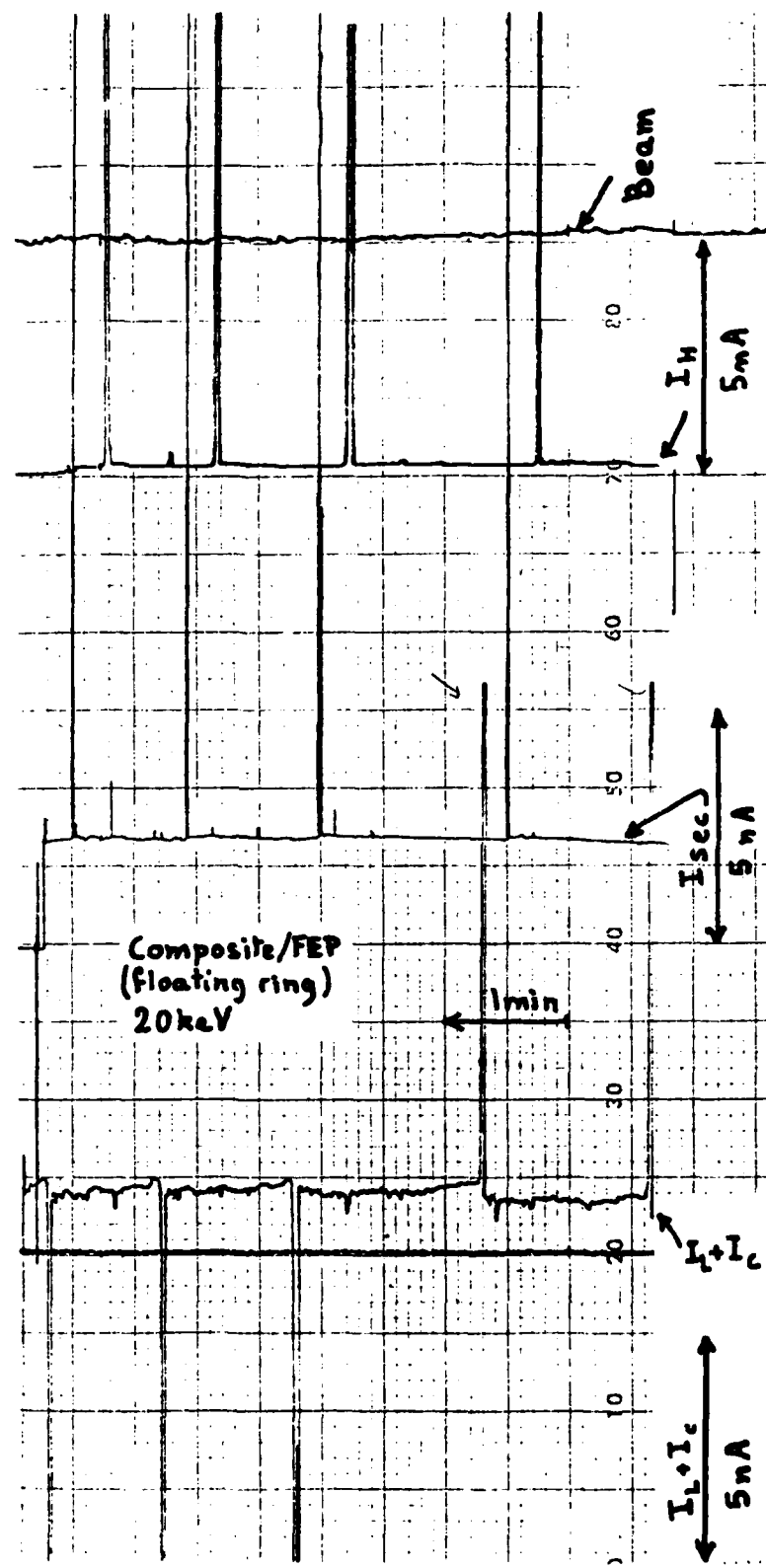


FIGURE 49 - CURRENT RECORDS

ELECTRON ENERGY	GROUNDING CONDITIONS	REMARKS	EVENTS NUMBER (per 10min)	FIGURES
20keV	with grounded ring	small pulses with I_L decreasing I_{surf} , I_{sec} increasing	10	39
	with floating ring	small pulses with I_L decreasing I_{sec} , I_H increasing	5	40
15keV	with grounded ring	no arcing	-	
	with floating ring	no arcing	-	

TABLE 10 - ARCING PHENOMENA FOR THE CONFIGURATION :
1 LAYER SILICA FABRIC ON GROUNDED HOLDER

ELECTRON ENERGY	GROUNDING CONDITIONS	REMARKS	EVENTS NUMBER (per 10min)	FIGURES
20keV	with grounded ring	small pulses generally with I_L decreasing I_{sec} increasing one time with I_{surf} decreasing I_g increasing	4	41
	with floating ring	no-arcing (but total elapsed time less than 5 min)	0(?)	
15keV	with grounded ring	no arcng		
	with floating ring	no arcng		

TABLE 11 - ARCING PHENOMENA FOR THE CONFIGURATION :
3 LAYERS SILICA FABRIC ON GROUNDED HOLDER

ELECTRON ENERGY	GROUNDING CONDITIONS	REMARKS	EVENTS NUMBER (per 10min)	FIGURES
20keV	with grounded ring	<ul style="list-style-type: none"> - small instabilities, I_L current (increasing with time) - many small pulses (decreasing with time) with I_L decreasing not always correlated with I_{sec} increasing - 1 large pulse with I_L decreasing then increasing lastly decreasing and I_{sec} increasing 	100	42
	with floating ring	<ul style="list-style-type: none"> - large current instabilities (increasing with time) - small pulses with I_L decreasing - large pulses with I_L decreasing then increasing lastly decreasing and I_{sec} increasing 	10	
15keV	with grounded ring	<ul style="list-style-type: none"> - very small instabilities mainly in $I_L + I_C$ recording 	60	43
	with floating ring	<ul style="list-style-type: none"> - very small current instabilities - a small pulse 	1	
10keV	with grounded ring	no arcing	0.5	
	with floating ring	no arcing		

TABLE 12 - ARCING PHENOMENA FOR THE CONFIGURATION :
1 LAYER SILICA FABRIC WITH FEP FILM

ELECTRON ENERGY	GROUNDING CONDITIONS	REMARKS	EVENTS NUMBER (per 10min)	FIGURES
20keV	with ground- ed ring	current instabilities and small current pulses with I_{sec} and I_{surf} increasing I_L decreasing I_g decreasing (not always correlative)	15	44
	with float- ing ring	small current pulses with I_L decreasing I_{sec} increasing I_H increasing (not always correlative)	15	45
15keV	with ground- ed ring	no arcing	-	
	with float- ing ring	no arcing	-	

TABLE 13 - ARCING PHENOMENA FOR THE CONFIGURATION :
COMPOSITE SILICA FABRIC/FEP/ALUMINUM ON GROUNDED HOLDER

ELECTRON ENERGY	GROUNDING CONDITIONS	REMARKS	EVENTS NUMBER (per 10min)	FIGURES
20keV	with grounding ring	<p><u>beginning</u>: numerous small and irregular current pulses with I_L, I_{surf}, I_g decreasing I_{sec} increasing</p> <p><u>after</u>: very regular sequences including:</p> <ul style="list-style-type: none"> . <u>small impulses</u>, with I_L, I_{surf} decreasing I_{sec}, I_{surf}, I_H increasing . <u>large pulses type I</u> with I_L, I_{surf} decreasing I_{sec}, I_H, increasing . <u>large pulses type II</u> with I_{surf} decreasing I_L, I_{sec}, I_H increasing 	100	47
	with floating ring	<p><u>beginning</u>: numerous small and irregular pulses with I_L decreasing I_{sec}, I_H increaseing</p> <p><u>intermdediate</u>: small pulses with I_L either decreasing or increasing I_{sec}, I_H increasing</p> <p><u>after</u>: <u>large pulses type I</u> with I_L decreasing I_{sec}, I_H increaseing</p> <p><u>large pulses type II</u> with I_L, I_{sec}, I_H increasing</p>	8 2 9	48 49

TABLE 14 ARCING PHENOMENA FOR THE CONFIGURATION:
 COMPOSITE SILICA FABRIC/FEP/ALUMINUM OVER FEP

ELECTRON ENERGY	GROUNDING CONDITIONS	REMARKS	EVENTS NUMBER (per 10min)	FIGURES
15keV	with grounding ring	numerous small pulses with I_L , I_{surf} , I_g decreasing I_{sec} increasing	80	-
	with floating ring	numerous small pulses with I_L decreasing I_{sec} , I_H increasing	100	46
10keV	with grounding ring	no arcing		
	with floating ring	no arcing		

TABLE 14 (cont'd 1) ARCING PHENOMENA FOR THE CONFIGURATION
COMPOSITE SLICA FABRIC/FEP ALUMINUM OVER FEP

3 - 5 ANALYSIS

3.5.1 Background

A. As a general statement for a dielectric irradiated by electrons and in contact by its back face with a grounded sample holder, an increase with irradiation time of the surface potential is noted.

This increase is correlated with a decreasing sample-to-holder current $I = I_L + I_C$ as shown in FIGURE 50 A and B.

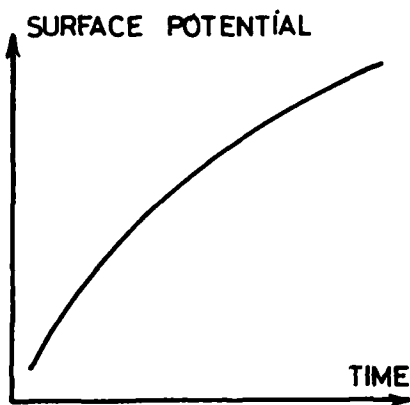


FIGURE 50 A

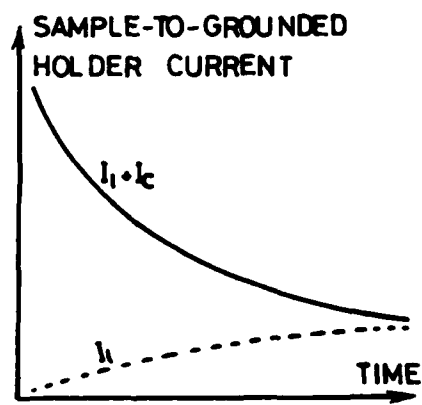


FIGURE 50 B

SURFACE POTENTIAL AND $(I_L + I_C)$ VARIATIONS WITH TIME

A zero value is obtained for the $I = I_L + I_C$ current at steady state for highly resistive samples. The sample-to-holder current is a sum of two components.

I_L is the leakage current through the insulator ; its value increases with the surface potentials V_s .

I_C is the charging current related to the dielectric capacity C :

$$I_C = C \frac{dV_s}{dt}$$

At steady state, the current measured is entirely due to leakage.

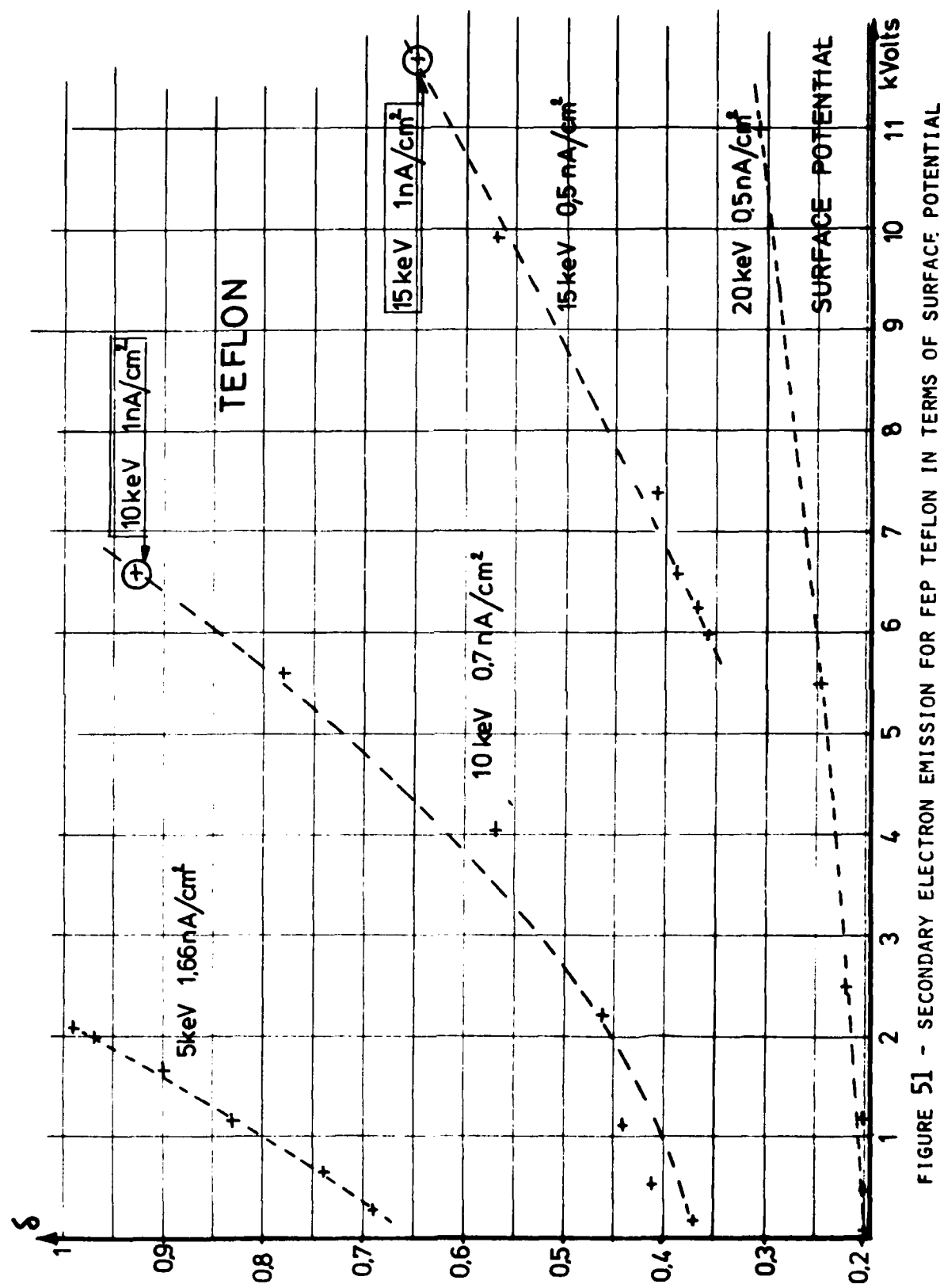


FIGURE 51 - SECONDARY ELECTRON EMISSION FOR FEP TEFLON IN TERMS OF SURFACE POTENTIAL

For a dielectric (e.g. FEP Teflon) the secondary electron emission varies with the surface potential for a given beam energy as shown in FIGURE 51. This secondary emission increases continuously with increasing negative induced potentials. This is a quite expected behaviour for two reasons:

Firstly, the actual energy of the primary electron is lowered due to the decelerating effect of the negatively charged surface and also to the decreasing value of δ when the primary electron energy E_p increases: see FIGURE 52 (δ is the secondary emission ratio)

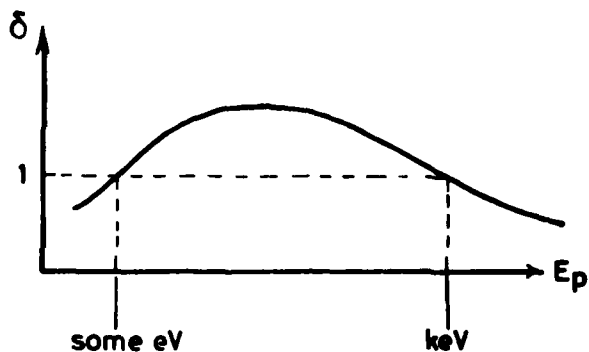


FIGURE 52 - δ VALUE IN TERM OF PRIMARY BEAM ENERGY

Secondly, the electric field resulting from the stored charge at the surface acts as an extracting field for secondary electrons.

B. The behaviour of silica fabric under electron beam has already been found quite different from the one just here above described. The fabric behaves like a conductor under bombardment. This was attributed (7) to a secondary electron emission mechanism, called "secondary emission conductivity." This radiation

induced conductivity is the consequence of the creation of secondary electrons that can be thought as clouds of free charges in the voids between silica fibers.

3.5.2 Silica fabric behaviour

3521 Surface potentials, leakage and secondary electron emission currents

3521-1 Variation with time

The result analysis will be carried out in the next two sections: A and B.

The first one is related to the 5 keV energy for which the interaction of the beam with the sample is shown to take place only at the sample surface. The second is related to the 10, 15 and 20 keV electron beam energies for which the conductivity mechanism arises, indicating the existence of free secondary electrons in the voids between the fibers.

A. 5 keV beam energy

For all the sample configurations (one or three layers silica fabric directly on the sample holder, one layer silica fabric insulated with FEP film, composite grounded by its back face or composite insulated with FEP) the surface potential value is recorded equal to (or very near to) zero.

At 5 keV all the incident electrons are reemitted in the form of secondaries (the current I_g collected on the guard ring is considered to be same in nature as the current I_{sec} collected by the hemispheric electrode).

The sample to holder current $I_L + I_C$ as well as the surface leakage current I_{surf} are very near to zero.

The electrostatic behaviour is here very largely independent of the manner the sample is fixed and finally it does not depend on what is set behind the quartz fabric. Thus the interaction of the beam seems to take place on the very surface of the quartz fabric and secondary electron emission is the only discharging process to be noted.

B. 10, 15 and 20 keV beam energy

Two general behaviours can be differentiated:

The first one BEHAVIOUR "A" is the classical one described at Section 3.5.1 (surface potential continuously increasing while $I = I_L + I_C$ is continuously decreasing). The second one BEHAVIOUR "B" expresses a non monotonic surface potential variation, increasing for the first two minutes of irradiation and then decreasing to a steady state, with a leakage current generally increasing at the same time.

BEHAVIOUR "A"

Such a behaviour is noted in FIGURE 30 a and b concerning the composite insulated with a FEP film irradiated with 10 keV electrons. The same trend is noticed in the first phase of the 15 keV irradiation (FIGURE 31b) and is thought to be counterbalanced by a competitive process in a second phase. This new process could predominate at 20 keV (*).

The three layers sample of silica fabric shows at 10 keV (FIGURES 26 a and b) the BEHAVIOUR "A". The rather large thickness, in this configuration as compared to the penetration depth of 10 keV primary electrons, allows probably to conclude that the two back layers behave like an insulator.

(*) This process could be related to the noisy current recordings (FIGURE 47) which are obviously correlated to arcing phenomena originating probably from the floating aluminum back face of the composite.

BEHAVIOUR "B"

A peak value for the surface potential is in evidence in FIGURES 27a, 28a, 30a, 31a. Its actual occurrence in time cannot exactly be determined due to a lack of continuous surface potential recording.

Associated with these peak values, a maximum secondary electron emission is noted, on the I_{sec} recordings as well as on the I_g recordings. (See FIGURES 27c and d, 28c and d, 30c and d, and also 31c and d for the composite grounded by its back aluminum). The electric field at the sample surface is guessed to determine this secondary emission because it is acting as an extracting field.

An increasing value of the sample-to-holder current ($I = I_L + I_C$) is generally noted. At steady state, its finite measured value shows that this current is a leakage current (see Section 3.5.1).

In the three layers configuration of the silica fabric sample (FIGURES 27b and 28b) it seems that the leakage current is not existing at first and that the behaviour is rather the behaviour "A". Then, after a certain threshold value of electric field inside the material is exceeded, a leakage current arises contributing to the sample discharging. This threshold is not in evidence for all sample configurations: it could happen very soon after the irradiation starts in the case of a single layer directly grounded, this being due to a smaller material thickness with regard to the electron penetration depth. More systematic studies would be needed in order to elucidate that point.

The leakage current is probably originating from the existence of secondary electrons acting as free charges in the voids between fibers creating conducting paths through the material.

3521-2 Variation with the beam energy of steady state values of surface potentials, leakage and secondary electron currents

The FIGURE 38 reports the surface potential V_S in terms of beam energy E_p . The observed general trend is an increase of the surface potential value with increasing beam energy : however, when compared to the surface potential of FEP, this increase is less important (slope $\Delta V_S / \Delta E_p < 1$).

For all sample configurations, it has been noticed that the secondary electron emission decreases when the beam energy increases. At 5 keV all the incident beam is reemitted in the form of secondary electrons for all configurations (see FIGURES 33 to 37). At energy greater than 5 keV, the secondary emission depends on the sample configuration.

It is worth noting that secondary emission at 10 keV for the 3 layers silica fabric sample is the same as the one measured for a single layer fabric insulated with a FEP film, and it is greater than the one measured for the silica fabric directly grounded (see respectively FIGURES 34, 35 and 33). This is directly connected to the existence of a leakage current component since the sum of all the measured currents (which are discharging currents at steady state) is invariant.

3522 Surface leakage current

A surface leakage current I_{surf} is actually collected on the surface electrode, contributing thus together with the volume leakage current and secondary emission to discharge the sample surface (see FIGURES 33 to 37 with grounded ring).

With the presence of a FEP film insulating the silica fabric, or in the case of three layers silica fabric, the leakage (volume) current is less than the one measured in the case of the silica fabric directly in contact with the grounded sample holder. This is particularly noted at 10 keV (FIGURES 33, 34, 35).

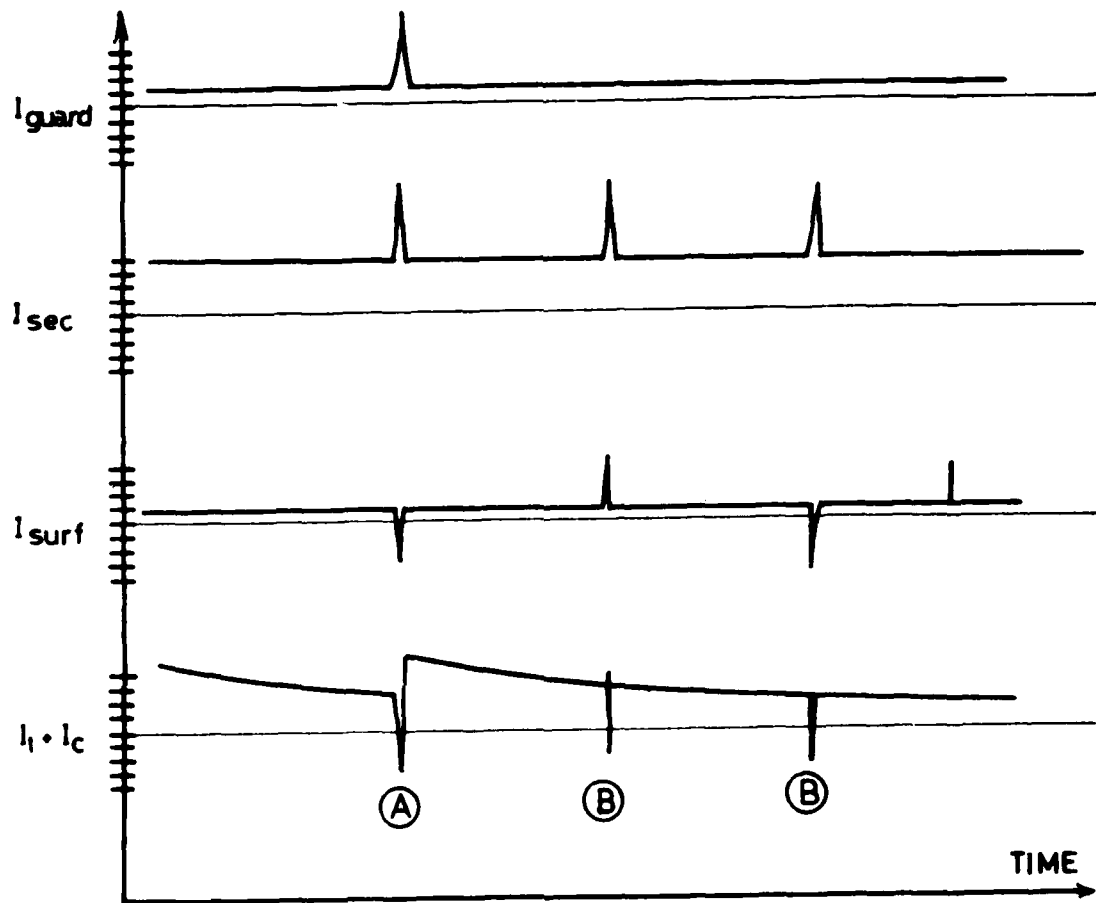


FIGURE 53 - TYPICAL RECORDINGS DURING CHARGING PHENOMENA

At 15 keV and 20 keV the quasi disparition of I_L , in the case of the quartz layer insulated by a FEP film, is balanced by an enhancement of the surface leakage current I_{surf} while the secondary emission I_{sec} and the current collected on the guard ring I_g are not significantly increased (see FIGURES 33c and d, 35c and d). Why the surface leakage current is much more increased than the secondary emission is not clearly understood. An experimental study of the influence of a variable gap between the surface ring and the irradiated area could help to explain this behaviour.

The barrier role played by the FEP insulator film placed under the silica fabric is well illustrated for all the beam energies (FIGURES 35a', b', c', d').

In the case of the composite insulated by an identical FEP film, this barrier role is only observed at 10 keV: at 15 and 20 keV, an important sample to holder current is measured. However current pulses are simultanenously detected.

That observation suggests the possibility that arcing takes place between the aluminized back face of the composite and the neighbouring electrodes (See below sections 3523).

3523 Arcing and discharging

- As a general statement whenever arcing of the irradiated sample was observed pulses were recorded for the various currents. A sudden decrease of the sample-to-holder $I_L + I_C$ current was always correlated to a sudden increase of the I_{sec} current. Other currents showed almost always corresponding pulses the polarity of which were not always the same. The sketch in FIGURE 53 allows to see typical variations. The intensity of these pulses depends on the sample nature as well as the beam conditions. Some very large $I_L + I_C$ variations (as the one reported A in FIGURE 53) are probably due to the total discharging of the surface sample. Others (B in FIGURE 53) are probably corresponding to a local rather small discharge.

- All the sample configurations we tested exhibited a tendency to arc at the 20 keV energy.

Very strong arcing occurring at a very high rate was observed for the samples that were insulated by the FEP film. The samples grounded by their back face (direct contact with the sample holder) showed less pronounced breakdowns.

- The silica fabric when directly in contact with the grounded aluminum holder presents small arcing risks (FIGURES 39 and 40, TABLE 10). There is no arcing at 15 keV.

- When fabric is electrically insulated by a FEP film, arcing is in evidence at 20 keV with very large pulses (FIGURES 42-43, TABLE 12). The grounding of a ring put on the surface does not decrease appreciably the arcing risk. Only very small fluctuations are observed for currents at 15 keV).

- The composite in close contact with the grounded aluminum sample holder by its aluminized surface has the same behaviour as the one of the silica fabric in contact with the grounded aluminum sample holder. The arcing risk exists at 20 keV (FIGURES 44 and 45, TABLE 13) and is only slightly greater than the one for the silica fabric alone. At 15 keV there is neither arcing nor tendency to arcing.

- When the aluminum back face of the composite is insulated by a FEP film, numerous small current pulses are observed at 15 keV (FIGURE 46, TABLE 14). They are irregular in shape and frequency. The same observation can be taken from the first phase of recordings at 20 keV (FIGURE 47). However at 20 keV after 10 to 15 minutes, very regular sequences of pulses are noted (FIGURE 42). Some are very large. These pulses are sometimes recorded as increase of the leakage current $I_C + I_L$, sometimes as decrease of this current. The composite behaviour is not modified when the metallic ring that is in contact with the silica fabric side is not grounded (FIGURE 49).

- From the various data that were gathered, it seems very difficult to localize the breakdown areas of the various configurations. In the case of the composite that is insulated by a FEP film, it is worth noting that some strong and sudden increases of the $I_L + I_C$ occur. Such a behaviour is typical of this sample configuration. It could be a consequence of a field emission at the aluminum edge of the composite since the aluminum layer was let electrically floating. The geometrical disposition of the sample holder, of the rings as well as the actual sample configuration could be of first importance in the arcing initiation. Several competing arcing mechanisms are obvious for some of the samples we tested.

3524 Remarks

3524-1 Contamination_and/or_aging

The results that are reported at Section 3.4 were all obtained with fresh samples (never irradiated until then), after identical exposure time to vacuum.

When a given sample was irradiated again, in the same electron beam conditions, its surface potential value was higher than the one that had been measured in a previous irradiation. Such a behaviour has been noticed for all the samples and all the configurations we tested. However no systematic study of this phenomenon has been performed. It could be related to a contamination layer on the surface under test as well as an ageing effect.

A detailed investigation should be carried out in order to assess the importance of such contamination and/or ageing for the electrostatic behaviour.

3524-2 Visual_inspection_of_the_irradiated_samples

As a general statement, all the samples that were irradiated by electrons, do not exhibit any discoloration or surface defect that could be attributed to discharges or to environment conditions (contamination).

However the composite that was irradiated with its back aluminized face in direct contact with the grounded sample holder clearly exhibits defects in its aluminum layer after irradiation. Small holes are noticed with sizes ranging from 0.1mm to 0.7mm. Bunches of quartz fibers appear through these holes that are located in the irradiated area and may be also outside this zone. This degradation could be of great importance for the practical use of the composite on board a spacecraft. However the exact degradation process is not well understood.

3 - 6 CONCLUSIONS

Some concluding remarks can be made:

the behaviour of the composite under an electron beam simulating the substorm environment is closer to the one of the quartz fabric alone than to the one of the quartz fabric electrically insulated by a FEP film. This observation strongly suggests that the quartz fibers of the composite are in close contact with the back aluminum foil. Therefore the FEP layer does not form a continuous barrier within the laminated composite that we have tested.

The composite behaviour is good only if its aluminum back face is grounded. The use of a conductive adhesive is therefore strongly recommended for bonding the laminate composite to the metallic spacecraft structure or to the next grounding point. However some degradation of the composite aluminum layer seems to occur. It could lessen the optical properties as well as the electrostatic performance .

An arcing phenomenon was observed at 20 keV with the composite we have tested as well as with a silica fabric that was directly grounded by its back face. Previous observations (7) (8) did not indicate this trend.

Localization of arcing points is not evident. The simultaneous recordings of $I_L + I_C$, I_{sec} , I_{surf} , I_g and I_H show that there are several discharge mechanisms.

3 - 7 RECOMMENDATIONS

A few recommendations can be made. They are listed here under.

Recommendations (a) to (d) present technological involvements. The purpose of recommendations (e) to (i) is to obtain a better understanding of some basic physical mechanisms.

- (a) The exact localization of the arcing area should be performed. Edge effect, bulk breakdown, surface streamers and matter blow-out should be studied as related to the immediate vicinity of the sample and to its implementation.
- (b) The degradation of the aluminum back layer in the electron irradiated composite must be confirmed: a long duration electron irradiation ageing test should be carried out on a composite the aluminum back face of which would be grounded by means of a conductive layer. Such a test should lead to a better understanding of the possible damage mechanism. It should also reveal involvements of the attendant optical and electrostatic degradations.
- (c) The impact of low energy electrons (1 to 5 keV range) impinging on a quartz composite simultaneously with high energy electrons (15 to 20 keV range) should be studied having regard to the arcing risk in the actual geomagnetic space environment where a polyenergetic spectrum of electrons is encountered.
- (d) The effects on the electrostatic behaviour of contaminant layers deposited on the surface of quartz fabrics should be studied.
- (e) It would be useful to decide whether the good electrostatic performance of quartz fabrics is due to the chemical nature of the silica or to its physical microscopic state (thin fibers, high surface to volume ratio, curvature radius).

Electron irradiation of various dielectric fabrics or felts (e.g. made of Kevlar, Teflon, FEP) should help to elucidate this point. A technological involvement could be the development of lighter and cheaper temperature control coatings.

(f) The current leakage variation as related to various silica fabric layers (one to five for instance) should help to understand its true nature. This leakage current should be studied for various energies in terms of time together with the surface potential.

(g) The field-dependent resistance of the composite could be evaluated in the same manner as it was by EAGLES (7) on the silica fabric.

(h) The above experiment should also investigate electron irradiation density influence. This could help explaining why breakdowns were not experienced by others at 30 keV, 30 nA/cm^2 (7) and 20 keV, 1 nA/cm^2 while we detected breakdowns at 20 keV, $0,5 \text{ nA/cm}^2$.

(i) The surface electrode proximity to the irradiated area should be studied to elucidate whether the surface current is of same nature as the leakage current. Experiment with several silica fabric layers should also help in that view.

SECTION IV

CONCLUSIONS

As a general conclusion it can be stated that the study reported at Section 2 has confirmed the feasibility, the performance and the durability of "components" combining ITO coated flexible SSM and aluminum straps by means of a conductive adhesive.

The study reported at Section 3 has allowed a better knowledge of the charge dissipation mechanisms for silica fabrics in a geosynchronous magnetic substorm environment. Some recommendations have been given for a better use of the silica fabrics as thermal control coatings in space. However further investigation would be required to assess their practical implementing and durability and to elucidate the physical basic mechanisms that allow them to be considered as very good candidates for future practical use in Space.

DATE
FILMED
0-8